Nonlinear Interactions and Magneto-Thermal Transports in Antiferromagnets

反強磁性体の熱磁気輸送と非線形相互作用

February, 2017

Yurika KUBO

久保　百合香

Nonlinear Interactions and Magneto-Thermal Transports in Antiferromagnets

反強磁性体の熱磁気輸送と非線形相互作用

February, 2017

Waseda University

Graduate School of Advanced Science and Engineering

Department of Pure and Applied Physics,

Research on Theoretical Low Temperature Physics

Yurika KUBO

久保　百合香

Contents

Acknowledgments

Firstly, I would like to thank my supervisor Professor Susumu Kurihara and it was great for me to learn historical background of low temperature physics such as superconductivity, super fluidity, charge density wave and so on. It was also great to give me a chance to search for theme of my doctoral program for myself. I would also like to thank for giving me lots of advice and fruitful discussions.

It is my pleasure to acknowledge Professor Nicolas Shannon in Okinawa Institute for Science and Technology (OIST), giving me a chance to join his group for my last year of doctoral course and for lots of advice and enlighten discussions. It was nice and stimulating for me to join Prof. Shannon's group and interact with many researchers at OIST.

I am very grateful to Professor Keisuke Totsuka and Assistant Professor Ippei Danshita for giving me many advices for the spin wave theory in strong interaction regions during my stay in Yukawa Institute for Theoretical Physics (YITP) of Kyoto University as an atom type researcher for a month. It was also a very stimulating time for me to discuss and interact with group members of Condensed Matter Physics.

I appreciate Professor Hikaru Kawamura for giving me a chance for fruitful discussion of spins and thermal conductivity. I also acknowledge Prof. Kawamura's group members for stimulating discussions.

I appreciate Professor Takuro Katsufuji for giving me many advice on softening of the excitation spectrum from the point of view as an experimentalist.

I acknowledge Professor Kazuya Yuasa and Professor Yoshihiro Yamazaki for giving me a lot of advice on this thesis.

I note that this work was supported in part by Mochizuki Fund of Yukawa Memorial Foundation, Early Bird grant for young researcher at Waseda Research, Institute for Science, Engineering, and Grants for Excellent Graduate Schools, MEXT, Japan, Waseda University Grant for Special Research Projects (Project

number: 2015S-088), and Grant-in-Aid for JSPS Research Fellow (Project number: 16J01331).

I appreciate plenty of financial supports from Charitable trust Hisao Iwai Tokyo Memorial scholarship, which was of great help for me to concentrate on my research.

Lastly I would like to thank my family mental and financial supports for me to study in Waseda University and OIST.

Chapter 1

Introduction

Our daily life relies on the development of electronics which manipulate charge for various devices. Devices using manipulations of spins, which field is called magnetics, are also developed. It is noted that electronics only focus on manipulating charge degrees of freedom while magnetics use only spins, and both of them have been developed independently. However, thanks to the developments of nanofabrications, quantum effects on electric devices have become very important for electronics. Spin electronics (spintronics), which use both charge and spin degrees of freedom, are now studied intensively to improve the efficiency of devices [1, 2].

Spintronics also require manipulating the current of spin (spin current). The spin current flows along a magnetic field gradient, just like charge current flowing along a gradient of the chemical potential [3–5]. It is expected that we need less energy to transport information by spin current than charge current since less Joule heating is expected.

In this thesis, we investigate the low energy excitations of magnets and then we build formalism of magneto-thermal transports. The author believes that these studies are important not only for scientific interests but also for increasing the possibility for spin manipulations.

Magnetic properties are dominated by spins and the Coulomb interactions. Magnets can be divided into two categories. One is a localized spin system, whose spins are localized at specific sites, and its physical properties are explained by focusing only on the spin-spin correlations. The other is an itinerant spin system, whose electrons move around, and its physical properties are explained

by considering the motion of electrons as well as spin-spin correlations. In this thesis, we will consider only the localized spin systems.

A phase transition means that a phase of macroscopic system changes from one to the other having a different nature. In general, systems choose phases with larger entropies at high temperatures while they choose a phase with minimum internal energy at low temperatures.

There are two different types of interactions in localized isotropic spin systems. One is a ferromagnetic interaction, where spins prefer to align parallel. The other is an antiferromagnetic interaction, where spins prefer to align anti-parallel. In the classical limit, a system chooses the state with larger entropy at high temperature, and it chooses the state that minimizes the internal energy at low temperature. Classical ground states can be obtained if spins are treated as vectors.

In ferromagnets, spins align randomly at high temperature with a large entropy, and there is a phase transition at Curie temperature T_{Curie} and the spins align parallel to each other to minimize the internal energy. In a similar way, a collinear (spins align along the same axis) Néel order, where spins align anti-parallel, appears at low temperature for the square lattice Heisenberg antiferromagnets (SLHAFs).

For classical SLHAFs, it is clear that we obtain the Néel order at low temperature. However, it is not obvious whether we get the Néel order at low temperature in the presence of quantum fluctuations, which is caused by a non-commutativity of quantum mechanics. We obtain different states when we apply Heisenberg Hamiltonian to a wave function of the Néel order, where the classical state is hybridized with other states. In other words, the Néel state is not an eigenstate of a wave function because of the non-commutativity. Therefore, it was not clear for quantum spin systems (spin systems with quantum fluctuations) whether the Néel order survives in the presence of quantum fluctuations [6, 7].

In 1949, the Néel order was experimentally confirmed by neutron scattering experiments [8–10]. Though the Néel state itself is not an eigenstate of Hamiltonian, it is now shown that physical properties of SLHAFs in zero field are well-described by the Néel order [7, 11, 12].

A phase transition may occur even at zero temperature in quantum systems when the parameter of system changes. It is suggested that the quantum fluctuations play important roles for these phase transitions and we call them quantum

phase transitions. The author proposes a possibility of quantum phase transition of Heisenberg antiferromagnets in the presence of magnetic fields.

We discuss an existence of quantum phase by the spin wave theory. If you consider a system with ferromagnetic order, where all spins align up-direction, and put a down spin as an excitation. The down spin propagates due to an exchange interaction, and spins start a precession when we distribute a down spin to all spins in whole lattice. We call the precession spin wave, and we call a quantized spin wave a magnon [13]. The same spin wave discussion is true for the antiferromagnetic systems such as one with the Néel structure though the structure is not an eigenstates of a wave function [7].

For the linear spin wave approximation, which is similar to the harmonic approximation of phonon, we take only the leading terms into account and neglect all the multi-magnon interactions. When we go beyond a simple spin wave picture for the noncollinear spin systems, we need to consider a three-magnon interaction, which is a kind of the multi-magnon interactions. The three-magnon interaction appears as a result of hybridyzations of one- and two-magnon states, and the interaction is known to enhance the quantum fluctuations and comes into effects only when the system has noncollinear structures (spins do not align along the same axis). This thesis focuses on effects of three-magnon interactions, expecting to obtain some clues for physics of systems with noncollinear spin structures.

It is known that a noncollinear spin structure, in which spins do not align along the same axis, appears when a system has some interactions which compete with each other. It is also known that quantum fluctuations are enhanced for quantum spin systems when the classical ground state has a noncollinear spin structure.

A magnetic field may compete with the exchange interactions when it is applied. In the classical antiferromagnets, spins form noncollinear canted structures in non-zero fields to minimize a sum of exchange interaction and the Zeeman energy. However, it is less clear if the canted state survives in the presence of quantum fluctuations and there might exist a quantum phase.

Recently, frustrated quantum magnets, where requirements of all the exchange interactions cannot be satisfied simultaneously, draw some attentions since stronger quantum fluctuations are expected due to the competing exchange interactions. To illustrate the notion of frustrated magnets, let us consider the triangular lattice Ising antiferromagnets (TLIAFs). We see from Fig. 1.1 [14] that TLIAFs cannot satisfy all the requirements simultaneously, and they always have

some bonds whose requirements of the exchange interactions are violated [15].

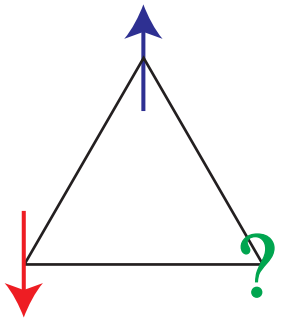

Figure 1.1: An Ising antiferrimagnet on a triangle. The exchange interactions for the bonds cannot be simultaneously satisfied in this model. This figure is taken from Ref. [14].

For frustrated triangular lattice Heisenberg magnets (TLHAFs) in the classical limit, it is known to have a noncollinear 120 degree structure to minimize ground state energy (see Fig. 1.2 [14]). It becomes less clear in the quantum spin case. However, it is now shown that TLHAFs have the 120 degree structure even for $S = 1/2$ quantum magnets [16–19].

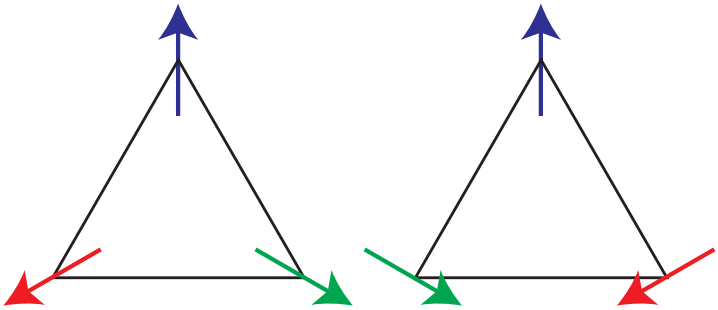

Figure 1.2: Two equivalent noncollinear 120 degree structures, which are both the ground states of the triangular lattice Heisenberg antiferromagnets in the classical limit. The picture is taken from [14].

Large deviations from the linear spin wave spectrum of the 120 degree structure are observed for frustrated TLHAF [20–23] and also in Kagome lattice antiferromagnets [24], which are due to the strong multi-magnon interactions in

noncollinear magnets. We believe that revealing the effects of three-magnon interactions is very important to understand the physics of noncollinear spin systems, which break the SU(2) symmetry.

In this thesis, we focus on Heisenberg antiferromagnets in the presence of magnetic fields h, where h is the fields H normalized by the saturation field $H_{\rm s}$ ($h = H/H_{\rm s}$). The aim of the thesis is to reveal the low energy excitations and clarify whether classical canted states survive in the presence of quantum fluctuations.

We investigate the spin wave spectrum in SLHAFs within the second order perturbation theory. The three-magnon interaction vanishes in zero field and at the saturation field by symmetry. This is because one-magnon states have the odd parity and two-magnon states have the even parity for the spin inversion and hybridizations of them are prohibited for collinear systems with the SU(2) symmetry. The interaction comes into effect in a magnetic field for the noncollinear canted structure in which the SU(2) symmetry is broken [25–28], and the effects become strongest at $h \sim 0.75$. In other words, the strength of three-magnon interaction is tunable by the magnetic field. We focus on the three-magnon interactions to reveal the physical properties of noncollinear spin systems.

Theoretical and experimental studies point out that a quantum phase appears in zero field [29,30] or finite fields [31–40] as a result of enhanced quantum fluctuations due to the competitions between the external field and the exchange interactions. It is not obvious for the magnets with competing interactions whether the classical ground state survives or a quantum phase is induced by quantum fluctuations. Most of the phases in Refs. [31–40] appear in the field region where we obtain noncollinear structures in the classical limits. We speculate that the phases might be related to the enhanced three-magnon interactions in magnetic fields.

In this thesis, we focus on SLHAFs to study the effects of three-magnon interaction. The three-magnon interaction exists for the magnets whose ground state breaks the SU(2) symmetry, such as noncollinear magnets. SLHAFs are one of the best candidates to study the three-magnon interaction since the interaction vanishes in zero field and at the saturation field with collinear structure, and it comes into effect for $0 < h < 1$, and becomes the strongest at $h \sim 0.75$. It means that the strength of three-magnon interaction is tunable by the magnetic field. This system has a special importance to reveal the physics of strong three-

magnon interactions due to the tunability. We expect to obtain some clues for the physics of other noncollinear systems by studying the physics of SLHAFs in fields.

There are several prior numerical works on SLHAFs in an applied field. It is shown that there are no significant anomalies for static properties such as magnetization, susceptibility, and spin stiffness from zero to the saturation field [41, 42]. However, qualitative changes between low and high fields are observed in the dynamical structure factor, and a significant broadening of the excitation spectrum is observed in high fields $h \gtrsim 0.75$ [42, 43].

Nikuni, Zhitomirsky and Chernyshev [25,26] built formalism of spin wave calculations for SLHAFs in fields. Zhitomirsky and Chernyshev [25,26] investigated the spin wave spectrum of SLHAFs within the second order perturbation calculations and found that the leading terms of $1/S$ corrections become comparable at $h \sim 0.75$. We see from the spin wave spectrum of Mourigal *et al.* [27], that an unphysical 'negative excitation energy' appears at a certain wave vector $\mathbf{k}$ in $h = 0.8$. There are two main possible reasons for getting unphysical results:

1. limitations on the approximations that neglect the higher order perturbation corrections,

2. wrong assumptions of the ground state, in other words, the ground state for $h \gtrsim 0.75$ is not a simple canted state.

Zhitomirsky and Chernyshev [26] and Mourigal *et al.* [27] interpreted the problem as 1., and performed self-consistent Born approximations (SCBA) to take higher order perturbation corrections into account [26]. However, the Goldstone boson vanishes because of the procedure. It is clear that their result is unphysical and strongly indicates that SCBA violates a conservation law (the Ward-Takahashi identity (WTI)). Mourigal *et al.* [27] performed SCBA only on the imaginary parts of self-energy corrections (ISCBA) without mentioning 'negative excitation energy' clearly. However, it is clear that ISCBA cannot solve the issue on either 'negative excitation energy' or WTI. Then, Fuhrman *et al.* [28] consider the interlayer interaction to reduce the $1/S$ corrections, but it is clear that their result itself is not a solution for the purely two dimensional SLHAFs. We do not have a clear evidence that support the reason 1.

The author interprets the problem as 2., and investigates the spin wave spectrum within the second order perturbation calculation for SLHAFs on the basis

of Nikuni-Zhitomirsky-Chernyshev formalism [25–27] to obtain the clue of high field phases. We show that a rotonlike minimum (we call roton in this thesis) appears at $h \sim 0.75$ and the energy gap drops rapidly to zero within the 1% increases in h. A complete softening of roton occurs at an incommensurate wave vector $\mathbf{k} = \mathbf{k}_c$ and at $h = h_c$ in SLHAFs due to the strong three-magnon interactions. We obtain a 'negative excitation energy' when we calculate the spin wave spectrum in $h > h_c$ [14, 44, 45].

This is a reminiscent of the Kohn anomaly [46], where a complete softening of the excitation spectrum occurs as a result of the strong electron-phonon interactions at a wave vector of $2k_F$ (k_F is the Fermi wave vector) and a phase characterized by the modulations of $2k_F$ appears after the complete softening. We interpret the softening of roton as a precursor of phase transition, and a new phase characterized by $\mathbf{k}_c$ appears in $h > h_c$. We believe that a high field phase in $h > h_c$ might be similar to the incommensurate phases in high fields, which have been predicted by Refs. [32, 35–40]. We also discuss the possibilities of detecting rotons via specific heat and neutron scattering measurements.

We then turn to focus on the spin mediated magneto-thermal transport in antiferromagnets. Studying magneto-thermal conductivity is important for the developments of spintronics.

A non-obvious question is whether spins can play role for thermal transports. Spin-mediated thermal transports were firstly observed in ferromagnets [47–49] and ferrimagnets [50] but these transports are rather diffusive. Large spin mediated thermal conductivity is observed in one-dimensional antiferromagnets, whose conductivity is quite anisotropic, and it shows much higher thermal conductivity along the chain direction compared to other directions [51–57]. The anisotropic conductivity cannot be explained simply by lattice vibrations (phonon). These results have stimulated much theoretical work on the spin contributions to the spin and thermal conductivity [58–69].

The spin and thermal conductivity in one dimensional XXZ antiferromagnets are theoretically studied in many methods such as the exact diagonalization (ED) [59–61, 63], the Jordan-Wigner (JW) transformation [63], the Bethe-Ansatz (BA) [68], and the quantum Monte Carlo (QMC) method [64, 66]. Ballistic thermal and spin conductivity at finite temperature for a gapless regime of the system are observed in these magnets. Based on theoretical results [59, 60, 63, 64, 66, 68], we attribute the observation of anisotropic thermal conductivity to spins [51–53].

The thermal conductivity of quasi-two dimensional non-frustrated antiferromagnets is studied experimentally in Refs. [70–75]. These magnets also show anisotropic conductivity. These phenomena are also attributed spin contributions to the thermal conductivity.

Recently, thermal conductivity in two to three dimensional frustrated antiferromagnets has been observed in experiment. They show non-monotonic responses to fields and temperature in $R\mathrm{MnO}_3$ (R = rare earth) compound [76,77], $R_2\mathrm{Ti}_2\mathrm{O}_7$ compound [78–83], and organic compounds [84–86]. The origins of non-monotonic behaviors are attributed to some possibilities such as:

- magnon contributions to the thermal transport [70–75],
- a novel quasi-particle of spins such as "monopoles" [78–83] or "spinons" [84–86] contributions to the spin transport,
- spin-phonon or spin-spin scatterings [76, 77].

However, it is not clear which explanation is the best for interpreting experiments since there are few theoretical works on two-to three-dimensional magnets to guide the interpretation [87–90]. In addition, these studies are restricted to collinear antiferromagnets with the Néel structure while we need a theoretical basis for understanding the conductivity in noncollinear systems. It is clear that we should define spin and thermal current operators and build formalism of spin and thermal transports to study the conductivity in noncollinear systems.

One of the goals for this thesis is to build formalism of spin and thermal transports, which is valid for noncollinear as well as collinear magnets. Then, we apply the formalism to the square lattice Heisenberg antiferromagnets with interlayer interactions (qSLHAFs) including the cubic lattice Heisenberg antiferromagnets (CLHAFs) and study the magnto-thermal conductivity.

One of the biggest problems for building the formalism is a difficulty to define spin current operators since spins are not always conserved quantity. To overcome this problem, it is now possible to use macroscopic conserved quantity, which rely on a Kadanoff-Martin hydrodynamical point of view [91]. There are roughly two ways:

1. focus on systems, where magnetization is rigorously conserved, and define an operator using the continuity equation [58–69],

2. focus on systems, where magnetization is approximately conserved, and define the operator [92, 93].

We see that 1. has a stronger restriction on the system than 2. while the approach 1. is more reliable with less ambiguity than that of 2. We consider the approach 1. in this thesis.

Firstly, the spin and thermal current density operators, which are robust for noncollinear as well as collinear antiferromagnets, are defined. These current operators are defined using a conservation of magnetization and energy. Then, formalism of spin and thermal conductivity is proposed on the basis of the linear response theory. This formalism is applied to qSLHAFs in fields using the spin wave theory. It is shown that each conductivity satisfy the sum rules in various fields. This strongly indicates a reliability of our definition and formalism. The author believes that this formalism should also be valid for any other noncollinear as well as collinear systems when the magnetization is conserved [94, 95].

We believe that our definition of spin-and energy-current operators opens possibilities for studying the magneto-thermal conductivity in various magnets with conserved magnetization. In addition, our definition and formalism are valid for noncollinear magnets as well as collinear magnets. We expect that this formalism plays an important role for interpreting the experiments of spin and thermal transports in antiferromagnets. We believe that this formalism contributes to practical realizations of utilizing spin current (spintronics) and enhancements of efficiency in various devices.

This thesis is composed as follows. In chapter 2, the spin wave formalism of Zhitomirsky-Nikuni-Chernyshev is shown [25, 26]. Then, the spin wave spectrum for SLHAFs in fields is investigated focusing on $h \sim 0.75$. The appearance of roton and its rapid softening are studied in detail. Possibilities of detecting the roton and a new phase are discussed [14, 44, 45]. In chapter 3, the formalism of magneto-thermal conductivity, which is valid even for noncollinear magnets, is developed. The spin and thermal current operators are defined. We apply these definitions to both SLHAFs and CLHAFs, and show the conductivity by using the linear response theory. We also show that each conductivity satisfies the sum rules. This fact indicates the reliability of formalism. In chapter 4, we summarize results and discuss conclusions.

Chapter 2

Tunable 'Roton' in Antiferromagnets

In this chapter, we investigate SLHAFs in magnetic field [14, 44, 45] by using formalism of spin wave theory proposed by Zhitomirsky-Nikuni-Chernyshev [25–28, 96, 97]. Then, excitation spectrum which is investigated along the formalism $h \sim 0.75$ is studied in detail. This chapter is along the lines of Refs. [14,44,45,95].

It is well known that classical SLHAFs have a collinear Néel structure in zero magnetic field and have a noncollinear canted structure in finite magnetic fields and spins align toward the field direction at the saturation field. For quantum SLHAFs, it is less clear.

It is pointed out that a three-magnon interaction, which is a kind of magnon-magnon interaction, appears only in noncollinear structure [16, 25–27, 96]. For some frustrated triangular [20–23] and Kagome antiferromagnets [24], the excitation spectrum deviates from the linear spin wave results which should be attributed to strong magnon-magnon interactions.

The strength of three-magnon interactions $\Phi_n\,(n = 1, 2)$ (coupling constant of mixing of one-and two-magnon states in arbitrary scale) of SLHAFs in fields are shown in Fig. 2.1 [14]. We see that SLHAFs are one of the best candidates to study three-magnon interactions since its strength is tunable from zero to sufficiently strong values $\Phi_n \propto h\sqrt{(1-h^2)}$ by varying fields.

We expect to obtain some clues of physical properties in other noncollinear systems, such as frustrated magnets [16, 21–24, 98], by studying SLHAFs since the noncollinear magnets have three-magnon interactions in common.

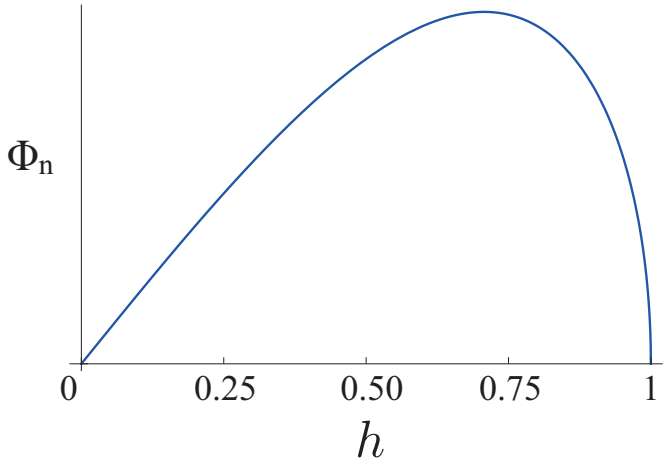

Figure 2.1: A strength of three-magnon interactions changes as a function of fields h. This figure is plotted as arbitrary scale and it is from Ref. [14].

Magnetization curves of SLHAFs are studied previously by the spin wave calculations [25, 97, 99] and numerical calculations [41, 42]. The deviations from linear spin wave results grow around $h \approx 0.75$ but qualitatively the same results, where the magnetization grows monotonically without any anomalies, are obtained [25, 41, 42, 97, 99]. Other static physical properties such as susceptibility and spin stiffness do not show any dramatic change either [42, 97, 99]. However, large deviations from the linear spin wave results and significant broadenings of the excitation spectrum are observed around $h \approx 0.75$ in previous numerical [42, 43] and experimental investigations [100].

SLHAFs in fields have also been studied by the spin wave theory within the second order perturbation calculations [26–28, 96]. There is an issue that the $1/S$ corrections of the excitation spectrum become comparable to that of the leading terms [26, 27, 96]. It is pointed out that there are strong broadenings of the excitation spectrum in $h \gtrapprox 0.75$, and they are attributed to strong hybridizations of one-and two-magnon states. Qualitatively the same argument is discussed previously in quasi-one dimensional magnets [101, 102].

We see from Mourigal *et al.* [27] that an unphysical 'negative excitation energy' appears at $h = 0.8$ at a certain wave vector. This result contradicts to the definition of ground state. It means that something is wrong with the procedure. There are two main possibilities:

1. limitations of the second order perturbation calculations,

2. a wrong assumption on ground state.

Zhitomirsky and Chernyshev [26, 96] attribute an unphysical result to 1., and perform SCBA to take higher order perturbation corrections into account in Ref. [26]. They find a vanishing of Goldstone boson by performing SCBA, which strongly indicates a violation of WTI. Then, Mourigal *et al*. focused only on the imaginary part of the self-energy and perform SCBA only on the imaginary parts of the self-energy and neglected the real parts of the correction [27]. However, their methods did not solve the problem on violations of WTI. Then, Fuhrman *et al*. added interlayer interactions to reduce the $1/S$ corrections [28], which is not the solutions for purely two dimensional models. To sum up, there is no clear evidence which supports the prediction that 'negative excitation energy' is attributed to the limitations of approximations.

We attribute the unphysical results to 2., and studied SLHAFs in fields to obtain some clues for high field phase. We study the spin wave spectrum of SLHAFs in fields [14, 44, 45] within the second order perturbation calculation using Zhitomirsky-Nikuni-Chernyshev formalism [25, 26, 96].

The excitation spectrum is shown in the next section, and a rotonlike minimum appears at $\mathbf{k}_{\rm rot}$, that is at the cross-section of decay threshold and a Γ-M line near a point M ($M = (\pi, \pi)$) at $h \gtrsim 0.75$. This is attributed to especially strong $1/S$ corrections around the decay threshold [44, 45]. The roton softens rapidly and its gap drops to zero with 1% increases of fields at a certain wave vector $\mathbf{k} = \mathbf{k}_{\rm c}$ at $h = h_{\rm c}$. We obtain an unphysical 'negative excitation energy' in $h > h_{\rm c}$.

It is a reminiscent of the Kohn anomaly in one dimensional metals [46], where energy gap of phonon mode closes at $k = 2k_{\rm F}$ ($k_{\rm F}$ is the Fermi wave vector) due to the strong electron-phonon interactions inducing a phase characterized by $2k_{\rm F}$. We interpret the rapid softening of rotons as a precursor of phase transition and predict that a quantum phase, which is characterized by $\mathbf{k}_{\rm c}$, appears in $h > h_{\rm c}$ [14, 44, 45].

This chapter is composed as follows. First, Zhitomirsky-Nikuni-Chernyshv formalism is shown, and the spin wave spectra at $h \sim 0.75$ are studied in detail. Then, the roton wave vector, gap and mass is studied and discussed in detail. Lastly, possibilities for an existence of the new phase and detecting rotons by experiments are discussed.

2.1 Spin Wave Theory

In this section, the non-linear spin wave theory, which is proposed by Zhitomirsky, Nikuni and Chernyshev [25, 26], is discussed.

2.1.1 Linear Spin Wave Theory

Firstly, we start from Hamiltonian of qSLHAF with arbitrary spins S

$$\mathcal{H} = \sum_{<i,j>} J_{i,j} \mathbf{S}_i \cdot \mathbf{S}_j - H \sum_i S_i^{z_0}, \tag{2.1}$$

where $J_{i,j}$ is an exchange constant of the nearest neighbor interaction, z_0 is the field direction and spins align in x_0-z_0 plane. We suppose that the in-plane interaction is J and $J\beta$ is that of the intra-plane, and we obtain:

$$\mathcal{H} = J \sum_{i,\tau_\parallel} \mathbf{S}_i \cdot \mathbf{S}_{i+\tau_\parallel} + J\beta \sum_{i,\tau_\perp} \mathbf{S}_i \cdot \mathbf{S}_{i+\tau_\perp} - H \sum_i S_i^{z_0}. \tag{2.2}$$

It is well-known that Néel structure stabilizes in zero magnetic field and spins cant toward a magnetic field direction in non-zero fields as in Fig. 2.2 [14], where θ denotes the canting angle.

The spin operators in the laboratory frame $S_i^{\mu_0}$ ($\mu_0 = x_0, y_0, z_0$) satisfy the commutation relations of spins

$$[S_i^{\mu_0}, S_j^{\eta_0}] = \mathrm{i}\delta_{i,j}\epsilon_{\mu_0,\eta_0,\lambda_0} S_i^{\lambda_0}. \tag{2.3}$$

We move from the laboratory frame to a rotated frame S_i^{μ} ($\mu = x, y, z$), which satisfy the commutation relations of spins

$$[S_i^{\mu}, S_j^{\eta}] = \mathrm{i}\delta_{i,j}\epsilon_{\mu,\eta,\lambda} S_i^{\lambda}, \tag{2.4}$$

by rotation operation:

$$\begin{pmatrix} S_i^{x_0} \\ S_i^{y_0} \\ S_i^{z_0} \end{pmatrix} = \begin{pmatrix} \sin\theta & 0 & \cos\theta \mathrm{e}^{\mathrm{i}\mathbf{Q}\cdot\mathbf{R}_i} \\ 0 & 1 & 0 \\ -\cos\theta \mathrm{e}^{\mathrm{i}\mathbf{Q}\cdot\mathbf{R}_i} & 0 & \sin\theta \end{pmatrix} \begin{pmatrix} S_i^{x} \\ S_i^{y} \\ S_i^{z} \end{pmatrix}, \tag{2.5}$$

where $\mathbf{Q} = (\pi, \pi)$ for SLHAFs and $\mathbf{Q} = (\pi, \pi, \pi)$ for CLHAFs. It means that $\mathrm{e}^{\mathrm{i}\mathbf{Q}\cdot\mathbf{R}_i} = \pm 1$ for any $\mathbf{R}_i$.

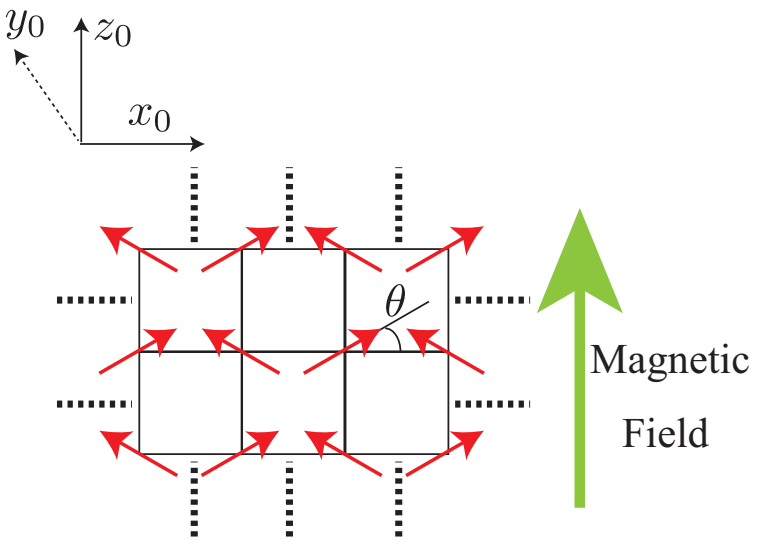

Figure 2.2: We suppose that the spins align in x_0-z_0 plane, and set the field direction z_0. This figure is taken from Ref. [14].

It is shown in Appendix A that the commutation relations are not changed by the rotation of Eq. (2.5). The spin of each sublattice is written by one spin operator since quantum fluctuations of both sublattice are expected to be the same.

Now, we perform the Holstein-Primakoff (HP) transformation to the rotated spin operator

$$\begin{aligned} S_i^+ &= \sqrt{2S}\, f_i a_i, \\ S_i^- &= \sqrt{2S} a_i^\dagger\, f_i, \\ S_i^z &= (S - n_i), \end{aligned} \tag{2.6}$$

where $a_i^\dagger$, a_i are HF bosons, $n_i = a_i^\dagger a_i$, $f_i = \sqrt{1 - n_i/(2S)}$ and

$$\begin{aligned} S_i^+ &= S_i^x + \mathrm{i} S_i^y, \\ S_i^- &= S_i^x - \mathrm{i} S_i^y. \end{aligned} \tag{2.7}$$

We obtain:

$$\mathcal{H} = \sum_{n=0}^{\infty} \mathcal{H}_n, \tag{2.8}$$

where $\mathcal{H}_n$ denotes a section of Hamiltonian $\mathcal{H}$ of $(2-n/2)$-th order of S, and $\mathcal{H}_0$ denotes the classical ground state energy:

$$\mathcal{H}_0 = (2+\beta)JS^2\cos 2\theta - H\sin\theta. \tag{2.9}$$

The canting angle is determined by the variation:

$$\frac{\mathrm{d}\mathcal{H}_0}{\mathrm{d}\theta} = 0. \tag{2.10}$$

The classical canting angle is:

$$\theta = \arcsin h, \tag{2.11}$$

where $H_\mathrm{s} = 4JS(2+\beta)$ denotes the saturation field, and we set

$$h = H/H_\mathrm{s}, \tag{2.12}$$

where h is a field H normalized by H_s.

We see that

$$\mathcal{H}_1 = 4JS\sqrt{\frac{S}{2}}\sum_{<i,j>}(a_j^\dagger + a_j)\cos\theta\,(\sin\theta - h)\,\mathrm{e}^{\mathrm{i}\mathbf{Q}\cdot\mathbf{R}_i}, \tag{2.13}$$

vanishes when the canting angle is correctly determined.

Now, we consider $\mathcal{H}_2$:

$$\begin{aligned}\mathcal{H}_2 =& S\sum_{<i,j>} J_{i,j}[\sin^2\theta(a_i^\dagger a_j + a_i a_j^\dagger) - \cos^2\theta(a_i^\dagger a_j^\dagger + a_i a_j)] \\ &+ S\sum_{<i,j>} J_{i,j}\cos 2\theta(n_i+n_j) + 4JS(2+\beta)h\sum_i n_i\sin\theta.\end{aligned} \tag{2.14}$$

We perform Fourier transformation:

$$a_i = \frac{1}{\sqrt{N}}\sum_{\mathbf{k}} a_\mathbf{k}\mathrm{e}^{\mathrm{i}\mathbf{k}\cdot\mathbf{R}_i}, \tag{2.15}$$

and we obtain:

$$\begin{aligned}\mathcal{H}_2 =& \sum_{\mathbf{k}}\left(A_\mathbf{k}a_\mathbf{k}^\dagger a_\mathbf{k} - \frac{B_\mathbf{k}}{2}\left(a_\mathbf{k}^\dagger a_{-\mathbf{k}}^\dagger + a_{-\mathbf{k}}a_\mathbf{k}\right)\right), \\ \\ A_\mathbf{k} =& 2(2+\beta)JS\left(\cos 2\theta + 2h\sin\theta + \gamma_\mathbf{k}\sin^2\theta\right), \\ B_\mathbf{k} =& 2(2+\beta)JS\gamma_\mathbf{k}\cos^2\theta, \\ \gamma_\mathbf{k} =& \frac{\cos k_x + \cos k_y + \beta\cos k_z}{2+\beta}.\end{aligned} \tag{2.16}$$

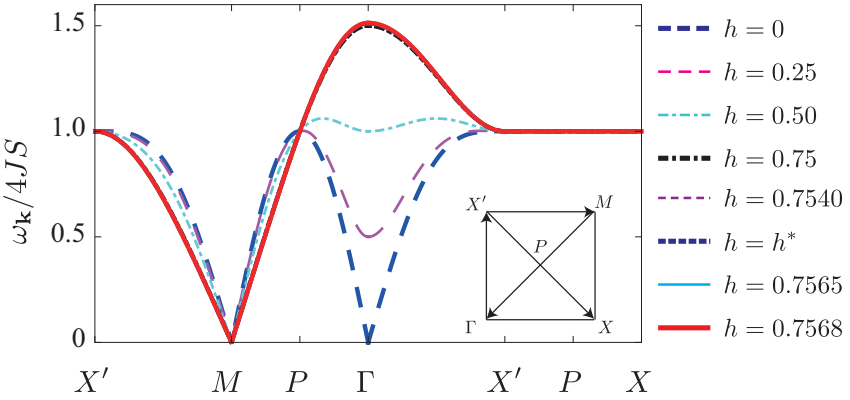

Figure 2.3: The field dependence linear spin wave spectra for $\beta = 0$ for various h is shown. We see that there are two Goldstone bosons at $h = 0$. One is at the Γ point vanishes when $h > 0$ is applied, and the other is at the M point. We see no significant changes by small increases of fields at $h \sim 0.75$. This figure is recited from Ref. [14].

Then, we perform the Bogoliubov transformation with bosons $b_{\mathbf{k}}$:

$$a_{\mathbf{k}} = u_k b_{\mathbf{k}} + v_k b^\dagger_{-\mathbf{k}}. \tag{2.17}$$

Now, we obtain the linear spin wave excitation spectrum $\omega_{\mathbf{k}}$:

$$\begin{aligned} \mathcal{H}_2 =& \sum_{\mathbf{k}} \left[\omega_{\mathbf{k}} b^\dagger_{\mathbf{k}} b_{\mathbf{k}} + \frac{\omega_{\mathbf{k}} - A_{\mathbf{k}}}{2} \right], \\ \omega_{\mathbf{k}} =& \sqrt{A^2_{\mathbf{k}} - B^2_{\mathbf{k}}} \\ u_k^2,\, v_k^2 =& \frac{1}{2} \left(\frac{A_{\mathbf{k}}}{\omega_{\mathbf{k}}} \pm 1 \right), \qquad\qquad u_k v_k = \frac{B_k}{2\omega_k}. \end{aligned} \tag{2.18}$$

The excitation spectra of $\beta = 0$, for various fields are shown in Fig. 2.3 [14]. We see that there are two Goldstone modes appearing at the $\Gamma = (0, 0)$ point and the $M = \pi(1, 1)$ point in zero magnetic field. We name points in the reciprocal space $P = \pi(1/2, 1/2)$ and $X = \pi(1, 0)$. Magnetic fields open a gap on the M point and gap energy is equal to H. We also notice that the spin wave spectra does not change drastically with small amount of field change.

2.1.2 Nonlinear Spin Wave Theory

In this subsection, the spin wave spectrum is investigated within the second order perturbation calculation, and the effects of $1/S$ corrections are discussed.

We consider $\mathcal{H}_4$:

$$\begin{aligned}\hat{\mathcal{H}}_4 = \sum_{<i,j>} J_{i,j} \Bigg[&\cos^2\theta \left(\frac{a_i^\dagger a_j^\dagger (n_i + n_j)}{4} + \text{H.c.} \right) \\ &- \sin^2\theta \left(\frac{a_i^\dagger (n_i + n_j) a_j}{4} + \text{H.c.} \right) - \cos 2\theta n_i n_j \Bigg] .\end{aligned} \tag{2.19}$$

the Hartree-Fock decoupling are:

$$\begin{aligned}
n_i a_i a_j \approx & 2n a_i a_j + 2\Delta_\tau n_i + \delta a_i^\dagger a_j + m_\tau a_i^2 - 2n\Delta_\tau - m_\tau \delta, \\
a_j^\dagger a_i^\dagger n_i \approx & 2n a_i^\dagger a_j^\dagger + 2\Delta_\tau n_i + \delta a_j^\dagger a_i + m_\tau a_i^{\dagger 2} - 2n\Delta_\tau - m_\tau \delta, \\
a_i^\dagger n_i a_j \approx & 2n a_i^\dagger a_j + 2m_\tau n_i + \delta a_i a_j + \Delta_\tau a_i^{\dagger 2} - 2nm_\tau - \Delta_\tau \delta, \\
a_j^\dagger n_i a_i \approx & 2n a_j^\dagger a_i + 2m_\tau n_i + \delta a_i^\dagger a_j^\dagger + \Delta_\tau a_i^2 - 2nm_\tau - \Delta_\tau \delta,
\end{aligned} \tag{2.20}$$

where

$$\begin{aligned}
m_\tau &= \left\langle \frac{1}{2+\beta} \sum_\tau a_i^\dagger a_{i+\tau} \right\rangle , \qquad & n &= \langle n_i \rangle , \\
\Delta_\tau &= \left\langle \frac{1}{2+\beta} \sum_\tau a_i a_{i+\tau} \right\rangle , \qquad & \delta &= \left\langle a_i^2 \right\rangle .
\end{aligned} \tag{2.21}$$

After HF decoupling using Eqs. (2.20) and (2.21), we obtain $\hat{\mathcal{H}}_4^{\text{HF}}$

$$\begin{aligned}
\hat{\mathcal{H}}_4^{\text{HF}} = & \sum_{<i,j>} J_{i,j} [(\Delta_\tau - n)\cos^2\theta + (n - m_\tau)\sin^2\theta](n_i + n_j) \\
& + \sum_{<i,j>} J_{i,j} \left[\left(\frac{\delta}{2} - m_\tau \right) \cos^2\theta + (m_\tau - n)\sin^2\theta \right] (a_i^\dagger a_j + a_i a_j^\dagger) \\
& + \sum_{<i,j>} J_{i,j} \left[(n - \Delta_\tau)\cos^2\theta + (\Delta_\tau - \frac{\delta}{2})\sin^2\theta \right] (a_i^\dagger a_j^\dagger + a_i a_j) \\
& + \sum_{<i,j>} J_{i,j} \left[m_\tau \cos^2\theta - \Delta_\tau \sin^2\theta \right] (a_i^{\dagger 2} + a_i^2).
\end{aligned} \tag{2.22}$$

We perform the Fourier transformation:

$$a_i = \frac{1}{\sqrt{N}} \sum_{\mathbf{k}} a_{\mathbf{k}}, \tag{2.23}$$

and we obtain:

$$\hat{\mathcal{H}}_4^{\mathrm{HF}} = \sum_{\mathbf{k}} \left[\delta A_k^{\mathrm{HF}} a_{\mathbf{k}} a_{\mathbf{k}} - \frac{\delta B_k^{\mathrm{HF}}}{2} \left(a_{\mathbf{k}}^\dagger a_{\mathbf{k}}^\dagger + a_{\mathbf{k}} a_{\mathbf{k}} \right) \right], \tag{2.24}$$

$$\begin{aligned} \delta A_k^{\mathrm{HF}} =& 2J(2+\beta) \left[\{ (\Delta_\tau - n) \cos^2\theta + (n - m_\tau) \sin^2\theta \} \right. \\ & \left. + \left\{ \left(\frac{\delta}{2} - m_\tau \right) \cos^2\theta + (m_\tau - n) \sin^2\theta \right\} \gamma_{\mathbf{k}} \right], \end{aligned} \tag{2.25}$$

$$\begin{aligned} \delta B_k^{\mathrm{HF}} =& 2J(2+\beta) \left[\{ m_\tau \cos^2\theta - \Delta_\tau \sin^2\theta \} \right. \\ & \left. + \left\{ (n - \Delta_\tau) \cos^2\theta + \left(\Delta_\tau - \frac{\delta}{2} \right) \sin^2\theta \right\} \gamma_{\mathbf{k}} \right]. \end{aligned} \tag{2.26}$$

We derive the $1/S$ corrections of the canting angle by considering variational relation:

$$\frac{\mathrm{d}}{\mathrm{d}\theta'} \left(\mathcal{H}_0 + \sum_{\mathbf{k}} \left(\frac{\omega_{\mathbf{k}} - A_{\mathbf{k}}}{2} \right) \right) = 0, \tag{2.27}$$

and we obtain a canting angle θ' which includes the $1/S$ correction:

$$\begin{aligned} \sin\theta' =& h \left(1 + \frac{w}{S} \right), \\ w =& n - m_\tau - \Delta_\tau. \end{aligned} \tag{2.28}$$

The $1/S$ correction to the canting angle in Eq. (2.28) cause corrections of $\mathcal{H}_2$ in Eq. (2.18)

$$\begin{aligned} \delta\mathcal{H}_2 =& 2\sin^2\theta w \sum_{<i,j>} J_{i,j} [(a_i^\dagger a_j + a_i a_j^\dagger) + (a_i^\dagger a_j^\dagger + a_i a_j) - 2(n_i + n_j)] \\ & + \frac{Hw}{S} \sum_i n_i \sin\theta \\ =& \sum_{\mathbf{k}} \left[\delta A_k^\theta a_{\mathbf{k}} a_{\mathbf{k}} - \frac{\delta B_k^\theta}{2} \left(a_{\mathbf{k}}^\dagger a_{\mathbf{k}}^\dagger + a_{\mathbf{k}} a_{\mathbf{k}} \right) \right], \end{aligned}$$

where

$$\begin{aligned} A_k^\theta =& 4w(2+\beta)\sin^2\theta(\gamma_k - 1), \\ B_k^\theta =& -4w(2+\beta)\sin^2\theta\gamma_k. \end{aligned}$$

We now obtain the part of $1/S$ correction to the excitation spectrum

$$\begin{aligned}\delta\epsilon_{\mathbf{k}} =&\frac{A_{\mathbf{k}}}{\omega_{\mathbf{k}}}\left(A_{\mathbf{k}}^{\mathrm{HF}}+A_{\mathbf{k}}^{\theta}\right)-\frac{B_{\mathbf{k}}}{\omega_{\mathbf{k}}}\left(B_{\mathbf{k}}^{\mathrm{HF}}+B_{\mathbf{k}}^{\theta}\right),\\ =&\frac{4J\left(-n+\Delta_\tau+\sin^2\theta(m_\tau+\Delta_\tau)(1-2\gamma_{\mathbf{k}}\cos^2\theta)\right)}{\sqrt{(1+\gamma_{\mathbf{k}})(1-\cos 2\theta\gamma_{\mathbf{k}})}}\\ &+\frac{4J\left(\gamma_{\mathbf{k}}^2\left[n-m_\tau\sin^2\theta(3-2\sin^2\theta)-\Delta_\tau(1-\sin^2\theta+\sin^4\theta)\right]\right)}{\sqrt{(1+\gamma_{\mathbf{k}})(1-\cos 2\theta\gamma_{\mathbf{k}})}}.\end{aligned}$$

We now consider $\mathcal{H}_3$:

$$\begin{aligned}\mathcal{H}_3 =&2\sin 2\theta\sqrt{\frac{S}{2}}\sum_{<i,j>}J_{i,j}\mathrm{e}^{\mathrm{i}\mathbf{Q}\cdot\mathbf{R}_i}\left(n_j a_i^\dagger-n_i a_j^\dagger+\mathrm{H.c.}\right)\\ &+4\cos\theta\left(\sin\theta-h\right)\sqrt{\frac{S}{2}}\sum_{<i,j>}J_{i,j}\mathrm{e}^{\mathrm{i}\mathbf{Q}\cdot\mathbf{R}_i}\left(\frac{a_i^\dagger n_i-a_j^\dagger n_j}{4}+\mathrm{H.c.}\right).\end{aligned}\tag{2.29}$$

We should neglect the latter term when we consider the second order perturbation theory since they are the higher order $1/S$ corrections (see Eq. (2.28)). We see that $\mathcal{H}_3$ vanishes at $H=0$. This is because the three-magnon interaction vanishes in collinear structure with the SU(2) symmetry [96].

We perform HF decoupling to $\mathcal{H}_3$ and we obtain $\mathcal{H}_3^{\mathrm{HF}}$

$$\mathcal{H}_3^{\mathrm{HF}} = -2\sin 2\theta\sqrt{\frac{S}{2}}\sum_{<i,j>}\mathrm{e}^{\mathrm{i}\mathbf{Q}\cdot\mathbf{r}_i}(a_j+a_j^\dagger)w.\tag{2.30}$$

We now see that $\mathcal{H}_1+\mathcal{H}_3^{\mathrm{HF}}$ also vanishes

$$\begin{aligned}\mathcal{H}_1+\mathcal{H}_3^{\mathrm{HF}} =&4S\sqrt{\frac{S}{2}}\sum_{<i,j>}J_{i,j}(a_j^\dagger+a_j)\cos\theta\left(\sin\theta-\frac{H}{4JS(2+\beta)}\right)\mathrm{e}^{\mathrm{i}\mathbf{Q}\cdot\mathbf{R}_i}\\ &-2\sin 2\theta\sqrt{\frac{S}{2}}\sum_{<i,j>}\mathrm{e}^{\mathrm{i}\mathbf{Q}\cdot\mathbf{r}_i}(a_j+a_j^\dagger)w\\ =&4JS(2+\beta)\sqrt{\frac{S}{2}}\sum_i(a_j^\dagger+a_j)\cos\theta\\ &\times\left(\sin\theta-h\left(1+\frac{w}{S}\right)\right)\mathrm{e}^{\mathrm{i}\mathbf{Q}\cdot\mathbf{R}_i},\end{aligned}\tag{2.31}$$

after performing variation (see Eq. (2.27)) correctly.

We then consider $\mathcal{H}_3$ after the Fourier transformation, we obtain:

$$\begin{aligned}\hat{\mathcal{H}}_3 =& \frac{1}{2!}\sum_{\mathbf{k},\mathbf{p}}(b^\dagger_{\mathbf{p}}b^\dagger_{\mathbf{q}}b_{\mathbf{k}} + \text{H.c.})\Phi_1(\mathbf{k},\mathbf{q}=\mathbf{Q}+\mathbf{k}-\mathbf{p},\mathbf{p}) \\ &+ \frac{1}{3!}\sum_{\mathbf{k},\mathbf{p}}(b^\dagger_{\mathbf{k}}b^\dagger_{\mathbf{q}}b^\dagger_{\mathbf{p}} + \text{H.c.})\Phi_2(\mathbf{k},\mathbf{q}=\mathbf{Q}-\mathbf{k}-\mathbf{p},\mathbf{p}),\end{aligned} \tag{2.32}$$

where

$$\begin{aligned}\Phi_1(1,2,3) =& -J(2+\beta)\sin 2\theta\sqrt{\frac{2S}{N}}\left[\gamma_1(u_1+v_1)(u_2v_3+u_3v_2)\right. \\ &\left.+\,\gamma_2(u_2+v_2)(u_1u_3+v_1v_3)+\gamma_3(u_3+v_3)(u_1u_2+v_1v_2)\right],\end{aligned} \tag{2.33}$$

and

$$\begin{aligned}\Phi_2(1,2,3) =& -J(2+\beta)\sin 2\theta\sqrt{\frac{2S}{N}}\left[\gamma_1(u_1+v_1)(u_2v_3+u_3v_2)\right. \\ &\left.+\,\gamma_2(u_2+v_2)(u_1v_3+u_3v_1)+\gamma_3(u_3+v_3)(u_2v_1+u_1v_2)\right].\end{aligned} \tag{2.34}$$

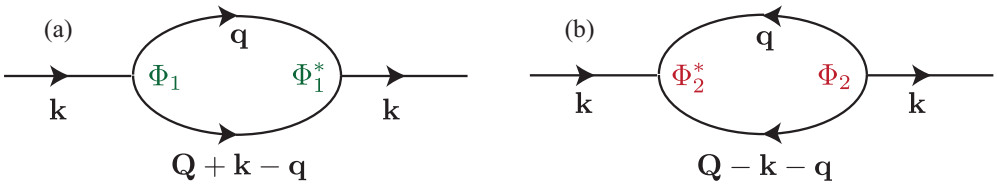

Figure 2.4: Three-magnon interactions which appear by mixing of one-and two-magnon states. This figure is cited from Refs. [14, 44].

We now consider the on-shell self-energy correction in Fig. 2.4 [14, 44]:

$$\Sigma^{(1)}(\mathbf{k},\omega_{\mathbf{k}}) = \frac{1}{2}\sum_{\mathbf{k}}\frac{|\Phi_1(\mathbf{k},\mathbf{Q}+\mathbf{k}-\mathbf{q},\mathbf{q})|^2}{\omega_{\mathbf{k}}-\omega_{\mathbf{Q}+\mathbf{k}-\mathbf{q}}-\omega_{\mathbf{q}}+i0}, \tag{2.35}$$

and

$$\Sigma^{(2)}(\mathbf{k},\omega_{\mathbf{k}}) = -\frac{1}{2}\sum_{\mathbf{k}}\frac{|\Phi_2(\mathbf{k},\mathbf{Q}-\mathbf{k}-\mathbf{q},\mathbf{q})|^2}{\omega_{\mathbf{k}}+\omega_{\mathbf{Q}-\mathbf{k}-\mathbf{q}}+\omega_{\mathbf{q}}-i0}. \tag{2.36}$$

We see from Eq. (2.35) that stronger corrections to the linear spin wave spectrum are expected for smaller energy differences between the one-and two-magnon states.

We now obtain the nonlinear spin wave corrections from the three-magnon interactions:

$$\delta\epsilon_{\mathbf{k}}^{(3)} = \Sigma^{(1)}(\mathbf{k}, \omega_{\mathbf{k}}) + \Sigma^{(2)}(\mathbf{k}, \omega_{\mathbf{k}}). \tag{2.37}$$

We finally obtain the nonlinear spin wave spectrum $\bar{\epsilon}_{\mathbf{k}}$ within the second order perturbation theory

$$\bar{\epsilon}_{\mathbf{k}} = \omega_{\mathbf{k}} + \delta\epsilon_{\mathbf{k}}^{(3)} + \delta\epsilon_{\mathbf{k}}. \tag{2.38}$$

2.1.3 Collinear Néel Structure

We now calculate the spin wave spectrum within the second order perturbation calculation in zero field. According to procedures of the previous subsection, we obtainthe $1/S$ corrected spin wave spectrum:

$$\begin{aligned} \delta\bar{\epsilon}_{\mathbf{k}} =& Z\omega_{\mathbf{k}}, \\ Z =& 1 + \frac{\Delta_{\mathbf{k}} - n}{S}. \end{aligned} \tag{2.39}$$

We see that a hardening of the spin wave spectrum, which is independent of the wave vector, occurs when we take the $1/S$ corrections into account. These results are in good agreements with the previous works: the spin wave calculations [12], the quamtum Monte Carlo method [43] and the exact diagonalization [42] and experiments on SLHAFs :La_2CuO_4 [11, 103], $Sr_2CuO_2Cl_2$ [104] and $Cu(DCOO)_2 \cdot 4(D_2O)$ [105] for the most regions.

Large deviations from the linear spin wave spectrum are observed in high fields, which are attributed to the three-magnon interactions in noncollinear structures. The nonlinear effects become stronger as the field increases and maximum in $h \sim 0.75$ of the saturation field (see Fig. 2.1 [14]) and decrease to zero at the saturation field.

2.1.4 Decay of a Quasiparticle

A decay of quasi-particle in the superfluid Helium is discussed along the lines of Ref. [106] in this subsection.

In this thesis, a spontaneous decay from a quasi-particle to two quasi-particles is discussed. We suppose that a quasi-particle, which has momentum $\mathbf{k}$ and energy $\omega_{0,\mathbf{k}}$, decays into two quasi-particles where a momentum and an energy of one of them is $\mathbf{q}$ and $\omega_{0,\mathbf{q}}$. Using kinematic constraint, we obtain:

$$\omega_{0,\mathbf{k}} - \omega_{0,\mathbf{q}} - \omega_{0,\mathbf{k}-\mathbf{q}} = 0, \tag{2.40}$$

due to the kinematic constraint. We suppose there are more than one linear Goldstone modes.

Now, we expand $\omega_{0,\mathbf{k}}$:

$$\omega_{\mathbf{k}} = c_0 \left(k + \alpha_0 k^3 + \cdots\right), \tag{2.41}$$

where c_0 and α_0 are constants. We approximate the left hand side of Eq. (2.40) using Eq. (2.41):

$$c_0(k - q - |-\mathbf{k} + \mathbf{q}|) + \alpha_0(k^3 - q^3 - |-\mathbf{k} + \mathbf{q}|^3). \tag{2.42}$$

Here, we obtain

$$\begin{aligned} |\mathbf{k} - \mathbf{q}| = \sqrt{|\mathbf{k} - \mathbf{q}|^2} &= \left[(k-q)^2 + 2kq(1 - \cos\psi_0)\right]^{\frac{1}{2}} \\ &= (k-q)\left[1 + \frac{4kq}{(k-q)^2}\sin^2\frac{\psi_0}{2}\right]^{\frac{1}{2}} \\ &\approx k - q + \frac{2kq}{k-q}\psi_0^2, \end{aligned} \tag{2.43}$$

where ψ_0 denotes an azimuthal angle, and we approximate:

$$k^3 - q^3 - |\mathbf{k} - \mathbf{q}|^3 \approx 3kq(k-q), \tag{2.44}$$

where we set

$$|\mathbf{k} - \mathbf{q}|^3 \approx (k-q)^3. \tag{2.45}$$

We now approximate Eq. (2.40):

$$-c_0 \frac{kq}{2(k-q)}\left[\psi_0^2 - 6\alpha_0(k-q)^2\right] \approx 0. \tag{2.46}$$

A constraint of Eq. (2.46) is satisfied only when the curvature is positive: $\alpha_0 > 0$. In other words, the decay of magnon is possible only when the curvature is positive.

The instability of a quasi-particle is discussed since a curvature of liquid helium is positive [106, 107]. However, the curvature is small: $\alpha_0 \gtrapprox 0$ and the problem on perturbation calculation is not serious for the liquid helium.

It is shown that a curvature of magnon: α_0 of qSLHAFs in magnetic fields changes its sign from negative to positive at around 3/4 of the saturation field, and a curvature α_0 can get a big value. This sign change leads to an anomalously strong three-magnon interaction $V(\mathbf{p}_1, \mathbf{p}_2, \mathbf{p}_3)$ to be discussed in the next section.

2.1.5 Decay of a Magnon

In this subsection, we briefly review magnon decays of SLHAFs in fields along the lines of Ref. [106] and Zhitomirsky and Chernyshev *et al.* [16, 26, 27, 96].

We now focus on the Goldstone mode on the M point on qSLHAFs. Firstly, we expand $\gamma_{\mathbf{k}}$ to forth order of k using $\mathbf{k} = k(\cos\phi, \sin\phi)$:

$$\begin{aligned}\gamma_{\mathbf{k}} &= \frac{\cos k_x + \cos k_y}{2} \\ &= \frac{1}{2}\left[1 - \frac{k_x^2}{2!} + \frac{k_x^4}{4!} + 1 - \frac{k_y^2}{2!} + \frac{k_y^4}{4!}\right] + \cdots \\ &\approx 1 + \frac{1}{2}\left[-\frac{k_x^2 + k_y^2}{2!} + \frac{k_x^4 + k_y^4}{4!}\right], \\ &\approx 1 + \frac{1}{2}\left[-\frac{k^2(\cos^2\phi + \sin^2\phi)}{2!} + \frac{k^4(\cos^4\phi + \sin^4\phi)}{4!}\right],\end{aligned} \tag{2.47}$$

where we use

$$\begin{aligned}\cos^4\phi + \sin^4\phi =& 1 - \frac{\sin^2 2\phi}{2} \\ =& \frac{3 + \cos 4\phi}{4},\end{aligned} \tag{2.48}$$

we obtain:

$$\begin{aligned}\gamma_{\mathbf{k}} &= \frac{\cos k_x + \cos k_y}{2} \\ &\approx 1 - \frac{1}{2}\left[\frac{k^2}{2!} + \frac{k^4(3 + \cos 4\phi)}{4 \cdot 4!}\right].\end{aligned} \tag{2.49}$$

The excitation spectrum around the M point is:

$$\omega_{\mathbf{Q}+\mathbf{k}} = 4JS\sqrt{(1 - \gamma_{\mathbf{k}})(1 + \cos 2\theta\gamma_{\mathbf{k}})}, \tag{2.50}$$

we expand the spectrum by using Eq. (2.47):

$$\begin{aligned}\frac{\omega_{\mathbf{Q}+\mathbf{k}}}{4JS} &\approx \left[\frac{1}{2}\left(\frac{k^2}{2!} - \frac{k^4}{4!}\frac{\cos 4\phi + 3}{4}\right)\left(2\cos^2\theta - \frac{\cos 2\theta}{2}\left[\frac{k^2}{2!} + \frac{k^4(3 + \cos 4\phi)}{4 \cdot 4!}\right]\right)\right]^{\frac{1}{2}} \\ &\approx \frac{\cos\theta\, k}{\sqrt{2}}\left[\left(1 - \frac{k^2}{12}\frac{\cos 4\phi + 3}{4}\right)\left(1 - \frac{k^2\cos 2\theta}{8\cos^2\theta}\right)\right]^{\frac{1}{2}}.\end{aligned} \tag{2.51}$$

We then perform the Taylor expansion, and we obtain:

$$\begin{aligned}\frac{\omega_{\mathbf{Q}+\mathbf{k}}}{4JS} &\approx \frac{\cos\theta\, k}{\sqrt{2}}\left[1-\frac{k^2}{12}\frac{\cos 4\phi+3}{8}-(1-\tan^2\theta)\frac{k^2}{16}\right] \\ &= \frac{\cos\theta\, k}{\sqrt{2}}\cos\theta\, k\left[1+\frac{k^2}{16}\left(\tan^2\theta-\frac{\cos 4\phi+9}{6}\right)\right].\end{aligned} \tag{2.52}$$

We now see from Eq. (2.52) that a curvature α_0:

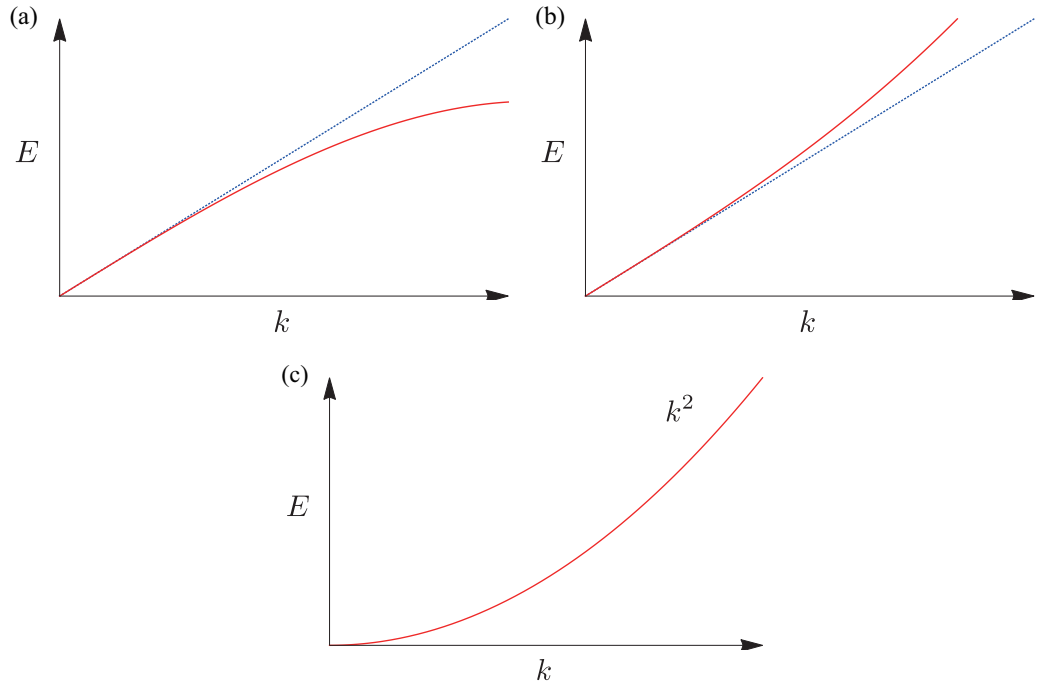

Figure 2.5: (a) A linear mode with a negative curvature $\alpha_0 < 0$ is shown. (b) A linear mode with a positive curvature $\alpha_0 > 0$ is shown. (c) A square mode is shown. These figures are from Ref. [14].

$$\alpha_0 = \frac{1}{16}\left(\tan^2\theta-\frac{\cos 4\phi+9}{6}\right), \tag{2.53}$$

is negative in low fields (see Fig. 2.5 (a) [14]), increases monotonically with an increasing field, changes its sign at $h^* = 2/\sqrt{7} \approx 0.75$ and becomes $\alpha_0 > 0$ in higher fields (see Fig. 2.5 (b) [14]) and the magnon decay become possible in

$h > h^*$. The sign change of the curvature is a precursor of the saturation field, where the spectrum have k^2 modes [96]. Finally, we get a k^2 mode at M point at H_s (see Fig. 2.5 (c) [14]). We also see that α_0 is the highest at the Γ-M line where $\phi = \pi/4 + (n\pi)/2$. In other words, the three-magnon interactions are strongest along the the Γ-M line. It is also seen that the curvature α_0 of SLHAFs is tuned from negative to positive infinity by magnetic fields.

It is pointed out that a decay region, where magnon decay is possible and having a finite lifetime, spreads as a field increases $h > h^*$ [27, 96]. Figure 2.6 shows how the decay region grows as a function of h, where Fig. 2.6 is consistent to Refs. [27, 96], and we denote $\mathbf{k} = \pi(1 - \eta_x, 1 - \eta_y)$. We see that the decay region grows with less than 1% increases of h.

It is also pointed out that the spin wave spectrum become broadened due to the magnon decay [26, 27, 96]. In the previous works, they focused only on the imaginary part of the self-energy corrections and neglected the real parts [27]. However, the real part of the corrections must also be important when the imaginary part plays role since the real and imaginary parts of the corrections are related to each other by the Kramers-Kronig relations. Therefore, we focus on the real part of the corrections in $h \sim h^*$ to be discussed below [14, 44, 45].

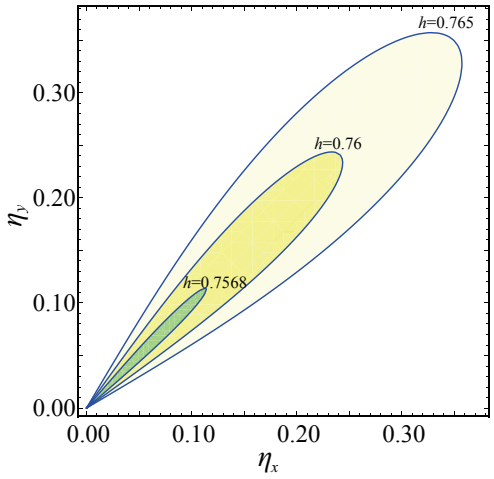

Figure 2.6: Decay threshold as a function of fields $h = 0.7568, 0.76, 0.765$ (h is indicated inside the figures) are shown where wave vectors are $\mathbf{k} = \pi(1 - \eta_x, 1 - \eta_y)$. It is shown that the decay region remarkably grows with small increases of fields. The author note that this figure is consistent to the previous works of Refs. [27, 96].

2.2 Rapid Softening of Rotons

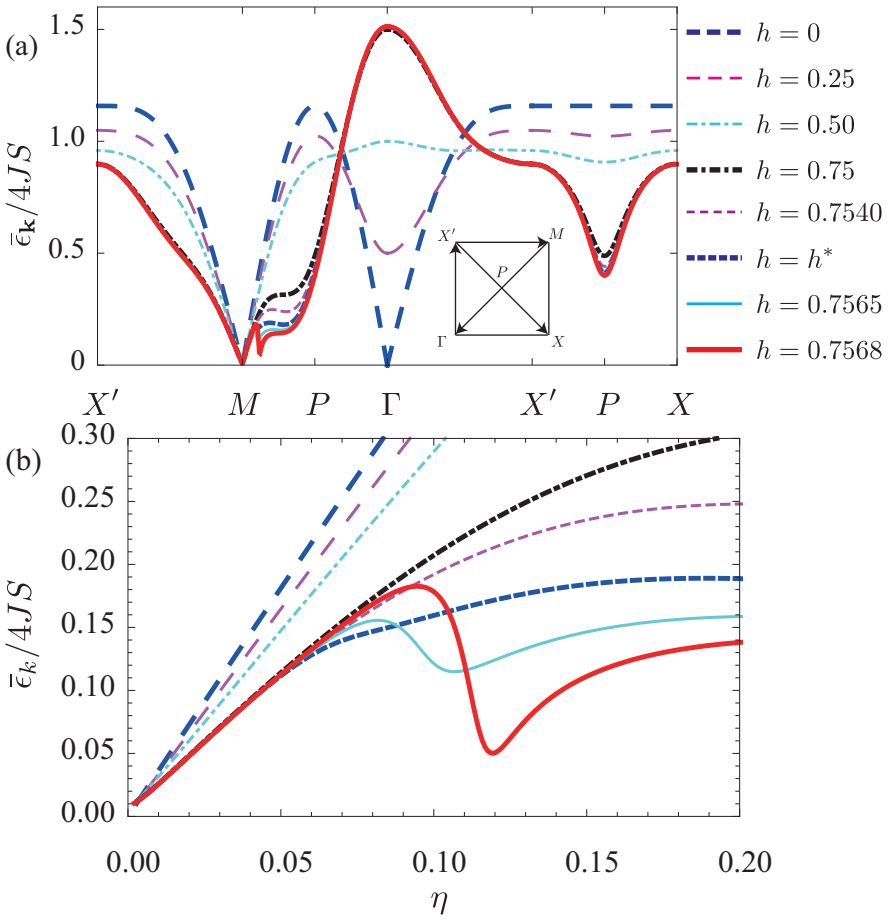

Figure 2.7: (a) Nonlinear spin wave spectra is shown. The plot style for each fields are shown on the right. We see a drastic change in a small increases of fields in $h \sim 0.75$ at around the M point. (b) The enlarged spin wave spectrum around the M point along the Γ-M line, where the wave vector is $\mathbf{k} = \pi(1-\eta, 1-\eta)$, is shown. We now see that rotonlike minimum appears in $h \sim 0.75$ and drops rapidly with an increasing field. These figures are taken from Ref. [14, 44, 45].

In this section, we discuss results of nonlinear spin wave spectra at $h \sim 0.75$ of SLHAFs, and drastic changes of excitation spectra are observed with small increases of fields. A rotonlike minimum appears and its gap drops rapidly to zero. This is a reminiscent of the Kohn anomaly [46], and we suggest that the

complete softening of roton is an indication of a phase transition. This section is along the lines of Refs. [14, 44, 45].

Nonlinear spin wave spectra $\bar{\epsilon}_{\mathbf{k}}$ in various h are shown in Fig. 2.7 (a) [14,44,45]. The plot styles of each field are shown on the right. Enlarged spin wave spectrum around the M point along the Γ-M line is shown in Fig. 2.7 (b) [14, 44, 45].

At $h = 0$, the spin wave spectrum of leading term and with the $1/S$ correction has the same shape with small corrections independent of wave vectors [12, 43, 103]. The wave vector dependent the $1/S$ corrections appears in finite fields. We see the stronger $1/S$ corrections on X points than the $P = \pi/2\,(1, 1)$ point, which is consistent with the previous studies on experiments [108] and [27, 42]. In addition, there is a saddle point at the P point, where it looks like a minimum along the X-X' line but it is on a hill middle along the Γ-M line. Drastic changes of the spin wave spectrum due to strong $1/S$ corrections are observed around the M point along the Γ-M line, where the three-magnon interaction is the strongest, in $h \sim 0.75$. We see from the enlarged spectrum in Fig. 2.7 (b) [14, 44, 45] that there is an energy minimum (we call it roton hereafter) around the M point. This roton is not a saddle point but an energy minimum to be investigated later.

A nonlinear spin wave spectrum $\bar{\epsilon}_{\mathbf{k}}$ at $h = 0.754$ is shown in Fig. 2.8 (a) [14] and linear spin wave spectrum $\omega_{\mathbf{k}}$ in the same field is shown in Fig. 2.8 (b) [14]. Energy for each contour and energy is shown on the right. We see that a very strong $1/S$ corrections appears at $h \sim 0.75$.

A nonlinear spin wave spectrum at $h = 0.7568$ is shown in Fig. 2.8(c) [14,44] for full Brillouin zone and near the point M is shown in Fig. 2.8(d) [14,44]. We now see that the minimum in Figs. 2.7 (a) and (b) [14, 44, 45] is not a saddle point but a minimum. This is in a reminiscent of the roton excitation, which is an excitation around energy minimum of liquid He^4 [107, 109]. We call the excitation around energy minimum roton in this thesis.

Stronger $1/S$ corrections to the spectrum are clearly seen by comparing Fig. 2.8 (a) to (b), and (c) to (d) [14]. It is noted that we see a clear change for shapes of a spectrum by small increases of fields. A spectrum shape perpendicular to the roton wave vector $\mathbf{k}_{\rm rot} = \pi(\eta_{\rm rot}, \eta_{\rm rot})$ is shown in Fig. 2.8 (e) [14, 44] in $h = 0.7568$, where $\mathbf{k} = \pi\,(\eta_{\rm rot}+\eta,\ \eta_{\rm rot}-\eta)$ [14,44]. A valley like structure appears perpendicular to the Γ-M line. We see from the figure that an excitation energy drastically varies by only less than 0.01 changes of η. This is to be discussed later in the following subsection.

The roton appears at $h \gtrsim 0.75$, and there are mainly two reasons:

- $\Phi_n(1,2,3)$ become the strongest around $h = 0.75$ (see Fig. 2.1 [14]),
- Hybridizations of one-and two-magnon states become strong at $h > h^* \sim 0.75$.

It is possible to tune the strengths of three-magnon interactions in SLHAFs from zero to a value strong enough to induce instability by tuning the fields. It means that SLHAFs are ideal materials for studying the physics of three-magnon interactions, and we expect to obtain some clues on understanding physics of three-magnon interactions in other noncollinear magnets by studying SLHAFs.

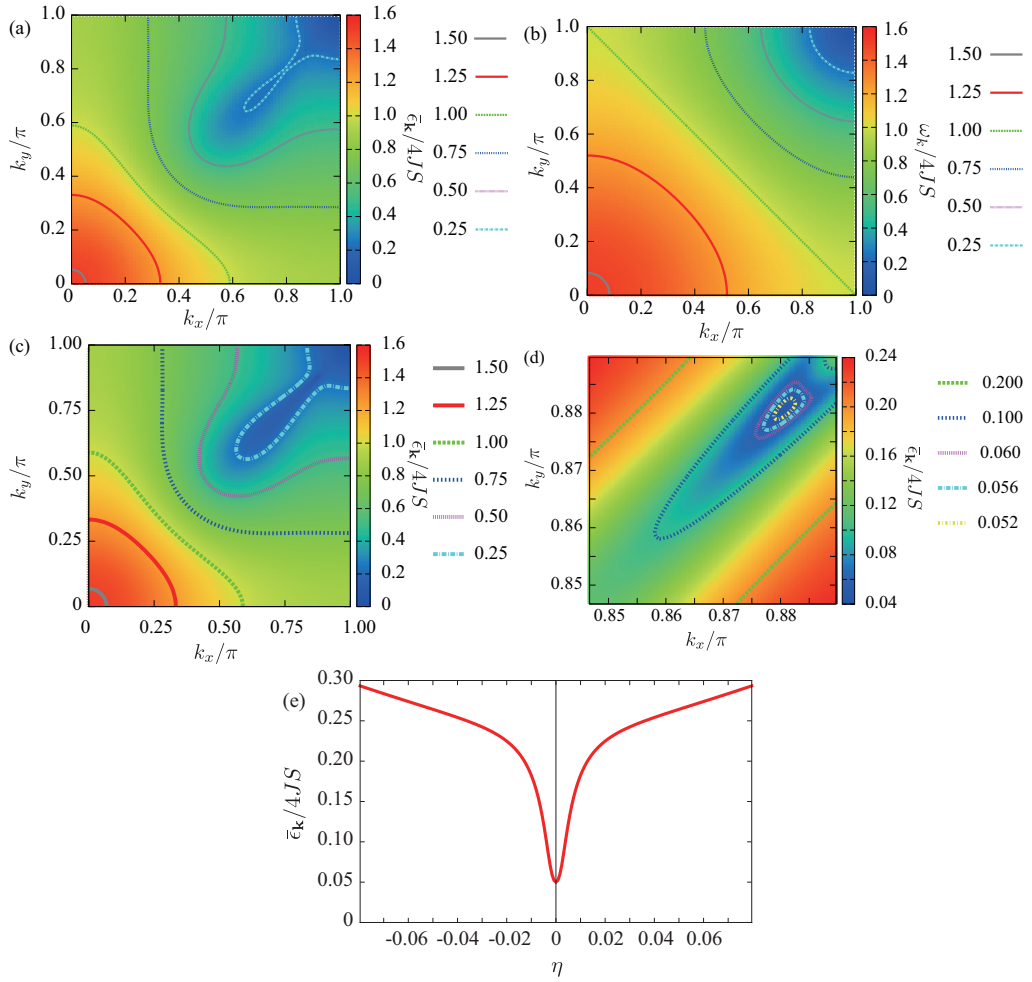

Figure 2.8: (a) Nonlinear spin wave spectrum $\bar{\epsilon}_{\mathbf{k}}$ at $h = 0.754$ is shown by color and contour plots [14]. Energy for each contour and color is shown on the right. We see that there is a minimum near the M point. (b) Linear spin wave spectrum $\omega_{\mathbf{k}}$ at $h = 0.754$ is shown [14] for the comparison. We now see clearly there is a significant $1/S$ corrections around the point M. (c) Nonlinear spin wave spectrum $\bar{\epsilon}_{\mathbf{k}}$ at $h = 0.7568$ is shown [14,44]. The energy for each contour and color are shown on the right. We see that quantum corrections become stronger as a field increases by comparing (a) and (c). (d) Enlarged spectrum of (c) near the M point is shown. We now see clearly that there is a rotonlike minimum (roton) near the M point [14,44]. (e) Nonlinear spin wave spectrum $\bar{\epsilon}_{\mathbf{k}}$ at $h = 0.7568$ perpendicular $\mathbf{k} = \pi(\eta_{\rm rot} + \eta, \eta_{\rm rot} - \eta)$ is shown, where we set roton wave vector $\mathbf{k}_{\rm rot} = \pi(\eta_{\rm rot}, \eta_{\rm rot})$ [14, 44].

2.2.1 Spin Wave Spectrum for Larger S Systems

Strengths of $1/S$ corrections for each S are discussed. Figure 2.9 [14, 44] shows the S dependence ($S = 1/2$, $S = 1$, $S = 3/2$, $S = 3$ and $S = \infty$) at $h = 0.7568$ of the spectrum is shown. We see that the spectra approach to the linear spin wave ($S = \infty$) results, and the smaller $1/S$ corrections are observed for larger S.

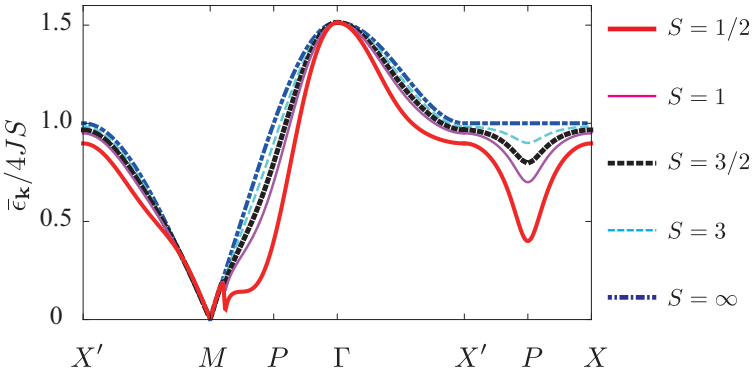

Figure 2.9: Spin wave spectrum for each S are shown. The strength of S is labeled on the right and thick red line is $S = 1/2$ and thin pink line is $S = 1$ and thick dotted line is $S = 3/2$ and dashed cyan line denotes $S = 3$ and dash dotted blue line denoted $S = \infty$ (the linear response results). We see qualitatively the same but stronger $1/S$ corrections for smaller S. This figure is taken from Ref. [14, 44].

2.3 Field Responses of 'Roton'

In this section, the details of roton and its field dependence is discussed. In the previous papers [14,44,45], it is suggested that three-magnon interactions induce

- an appearance of 'roton' and its rapid softening,
- a valley-like structure perpendicular to the Γ-M line,

and interpret the roton as an indications of a new phase.

Figure 2.10 [14,44] shows roton (a) gap $\Delta_{\rm rot}$, (b) wave vector $\mathbf{k}_{\rm rot}$ and (c), (d) masses perpendicular $m_\perp$ and parallel $m_\parallel$ to the Γ-M line ((c) and (d) in different scales) [14,44]. For Fig. 2.10 (a)-(d), green diamonds indicates results of $S = 1/2$ and blue circle indicates results of $S = 1$ and red squares indicate results of a shallow roton $S = 1/2$ which appears only for $S = 1/2$ due to the strong quantum effects. For masses, outlined dots indicates roton masses $m^*_\parallel$ parallel to the Γ-M line, and solid dots indicate perpendicular masses $m^*_\perp$.

We see from Fig. 2.10 (a) [14, 44] that $\Delta_{\rm rot}$ drops to zero as a field increases for both $S = 1/2, 1$. It is now clear that $\Delta_{\rm rot}$ changes its value by less than 1% increases of fields and complete softening occurs at $h_{\rm c} \sim 0.757$ at $\mathbf{k} = \mathbf{k}_{\rm c}$. This complete softening indicates an existence of a phase transition [14, 44, 45] and author expects that the Bose-Eistein condensation (BEC) of the $\mathbf{k}_{\rm c}$ magnons [110–112].

Figure 2.10(b) [14, 44] shows a roton wave vector $\mathbf{k}_{\rm rot} = \pi(1 - \eta_{\rm rot}, 1 - \eta_{\rm rot})$ and we see that $\eta_{\rm rot}$ grows monotonically as the field increases, and almost no change is observed for a shallow roton. It is also shown that $k_{\rm th}$(wave vector of a decay threshold), k_0(approximated value of $k_{\rm th}$) and $k_{\rm rot}$ are in good agreement with each other, which is to be discussed in the next subsection.

We see from Fig. 2.10(c) [14, 44] that $m^*_\parallel$ (outlined dot) of a shallow roton changes non-monotonically. We also see that $m^*_\perp$ (solid dot) is much smaller than that of $m^*_\parallel$.

Figure 2.10 (d) [14, 44] shows that $m^*_\perp$ is smaller than $m^*_\parallel$ for $S = 1/2$ and 1 rotons, and monotonic decrease of $m^*_\perp$ and $m^*_\parallel$ except for $m^*_\parallel$ is observed.

In the subsequent subsections, approximated values of $\mathbf{k}_{\rm rot}$, $\Delta_{\rm rot}$ and m^* is discussed.

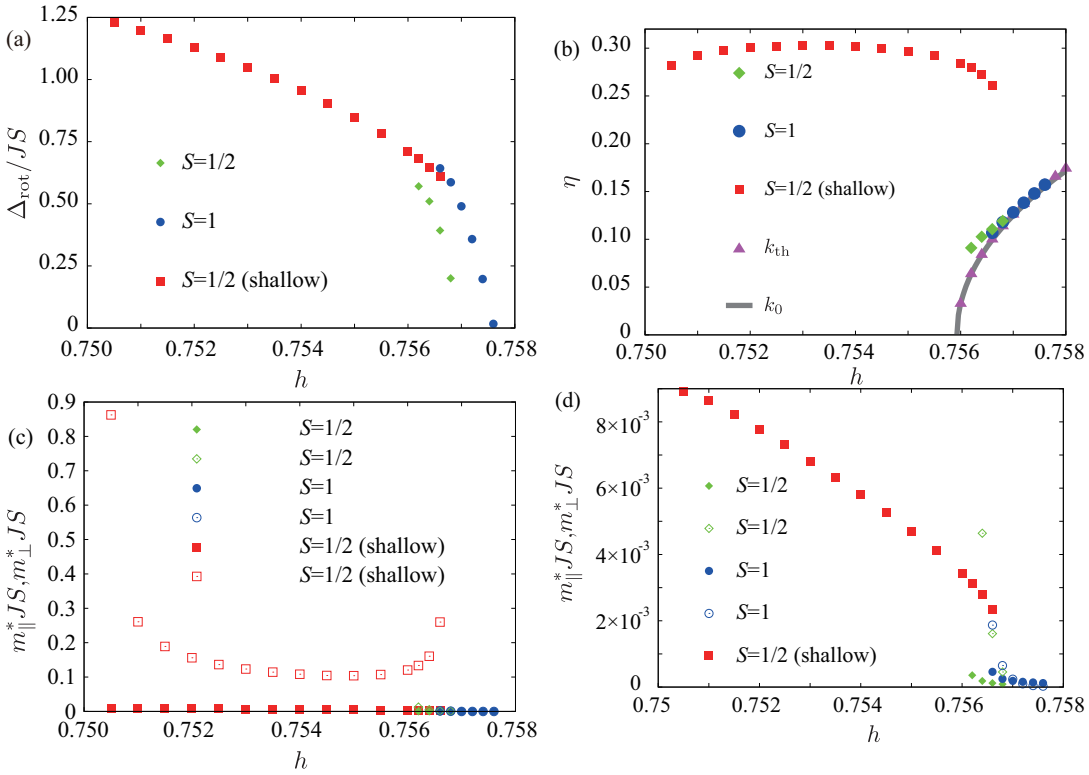

Figure 2.10: (a) Roton gap as a function of field is shown. Red square shows a roton gap $\Delta_{\rm rot}$ of shallow minimum, which appears only for $S = 1/2$ because of a strong quantum effects. Green diamonds and blue circles indicate roton gaps $\Delta_{\rm rot}$ for $S = 1/2$ and $S = 1$. Roton gap drops monotonically and vanish at $h \approx 0.757$ for $S = 1/2$ and $S = 1$. (b) The roton wave vector $k_{\rm rot}$ as functions of h is shown. The point styles are the same as that of (a). The roton wave vector $\mathbf{k}_{\rm rot} = \pi(1 - \eta_{\rm rot}, 1 - \eta_{\rm rot})$ for each S and estimated wave vector decay threshold wave vector $k_{\rm th}$(purple triangle) and k_0 (approximated value of $k_{\rm th}$ and shown in gray line), to be derived later, is shown. We see that $\eta_{\rm rot}$ grows as a field increases and they are in good agreement with the wave vectors $k_{\rm th}$ and k_0 but that of a shallow roton does not change by h. (c) Masses of rotons parallel $m_\parallel$ (outlined dot) and perpendicular $m_\perp$ (solid dot) to the Γ-M line are shown. Green point indicates $S = 1/2$ and blue point is $S = 1$ and red point is the shallow rotons. We see a non-monotonic response of $m_\parallel$ for shallow roton but the others show a monotonic decrease. (d) Enlarged masses $m_\parallel$ and $m_\perp$ are shown. We see a monotonic decrease for $m_\perp$ and $m_\parallel$. It is also observed that $m_\perp$ is much smaller than $m_\parallel$. These figures (a), (b), (c) and (d) are taken from Refs. [14, 44].

2.3.1 Approximate Value of Roton Wave Vector

We estimate the roton wave vector $\mathbf{k}_{\rm rot}$ in this section. We define $\mathbf{k}_{\rm th}$ as a threshold of the two-magnon decay, which is determined by following equation:

$$\omega_{\mathbf{Q}-\mathbf{k}_{\rm th}} = 2\omega_{\mathbf{Q}-\mathbf{k}_{\rm th}/2}. \tag{2.54}$$

We approximate $\mathbf{k}_{\rm th}$ by expansion:

$$\omega_{\mathbf{Q}-\mathbf{k}} \approx ck(1+\alpha k^2+\beta k^4), \tag{2.55}$$

where

$$\begin{aligned} c =& 2JS\sqrt{2}\cos\theta \\ \alpha =& \frac{1}{12\cos\theta}\left[\left(\frac{h}{h^*}\right)^2-1\right] \\ \beta =& \frac{h^4-32h^2+16}{15360\cos^2\theta} \end{aligned} \tag{2.56}$$

for SLHAFs in $h^* \le h \le 1$. By inserting Eq. (2.56) to (2.54), we obtain:

$$\omega_{\mathbf{Q}-\mathbf{k}_{\rm th}} - 2\omega_{\mathbf{Q}-\mathbf{k}_{\rm th}/2} \approx \frac{3}{4}k^3 c\left(\alpha+\frac{5}{4}\beta k^2\right). \tag{2.57}$$

We approximate the left hand side by zero:

$$\alpha+\frac{5}{4}\beta k^2 = 0 \tag{2.58}$$

and we obtain approximated $\mathbf{k}_{\rm th}$ and we call it k_0:

$$k_0 = \sqrt{-\frac{4\alpha}{5\beta}} \propto \left[\left(\frac{h}{h^*}\right)^2-1\right]. \tag{2.59}$$

We see from Fig. 2.10(b) [14,44] that $\mathbf{k}_{\rm th}$ and $\mathbf{k}_0$ are in good agreement with each other in the region where k_0 is small. It is also shown that $\mathbf{k}_{\rm rot}$ appears around the $\mathbf{k}_{\rm th}$, which indicates an appearance of a roton and magnon decays are related to each other.

Figure 2.11 [14, 44] shows a roton gap $\Delta_{\rm rot}$ (a) and mass $m^*_\perp$ (b) and $m^*_\parallel$ (c) as a function of k_0. We see $\Delta_{\rm rot} \propto k_0^4$ from Fig. 2.11 (a) [14, 44], $m^*_\perp \propto k_0^{-2}$ from Fig. 2.11 (b) [14,44] and $m^*_\parallel = \mathcal{A}+\mathcal{B}k_0$, where $\mathcal{A}, \mathcal{B}$ are constants, from Fig. 2.11 (c) [14, 44].Details of approximations are discussed in subsequent subsection, and these figures are recited from Refs. [14, 44].

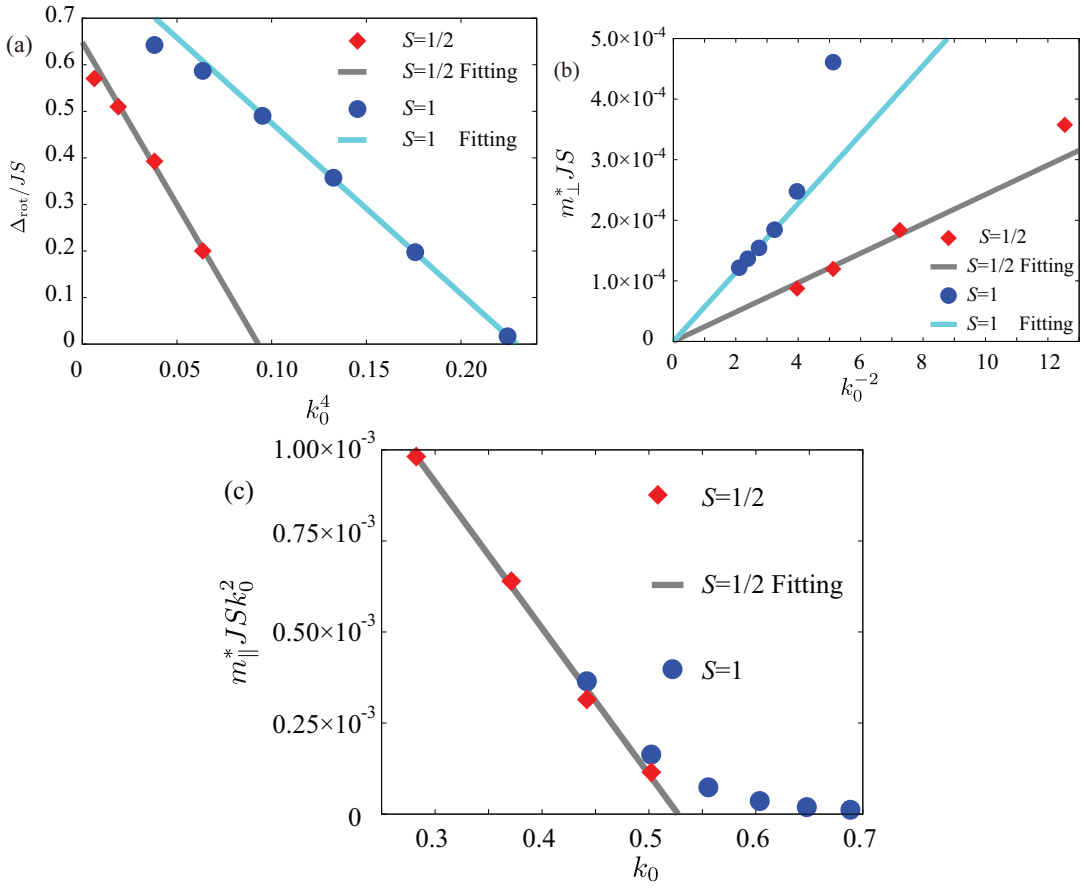

Figure 2.11: (a) Roton gap $\Delta_{\rm rot}$ as a function of k_0^4 is shown. Red diamonds denote one for $S = 1/2$ and blue circles denote $S = 1$, and lines are fittings for these plots. We see that $\Delta_{\rm rot}$ follows k_0^4 fairly well, and this behavior is discussed in this thesis. (b) Roton mass $m_\perp^*$ as a function of k_0^{-2} is shown. The same styles of dots as (a) are used and lines are fittings of these dots. We also see a fairly well agreement to fittings and plots. (c) Roton mass $m_\parallel^*$ as a function of k_0 is shown, using the same styles of dot and line as (a) and (b), and it also shows fairly well agreements. All the figures (a), (b) and (c) are taken from Refs. [14, 44].

2.3.2 Approximate Value of Roton Gap

We approximate the self-energy of Eq. (2.35) using $\mathbf{k}_0$ in Eq. (2.59). Firstly, we approximate

$$\frac{A_{\tilde{\mathbf{k}}}+B_{\tilde{\mathbf{k}}}}{\omega_{\tilde{\mathbf{k}}}}=\left(\frac{A_{\tilde{\mathbf{k}}}-B_{\tilde{\mathbf{k}}}}{\omega_{\tilde{\mathbf{k}}}}\right)^{-1}=\sqrt{\frac{1-\gamma_{\mathbf{k}}}{1+\cos 2\theta\gamma_{\mathbf{k}}}}\approx\frac{k}{2\sqrt{2}\cos\theta}, \tag{2.60}$$

where $\tilde{\mathbf{k}}=\mathbf{Q}-\mathbf{k}$ and we use the approximation which is valid only for the small k:

$$\gamma_{\tilde{\mathbf{k}}}\approx -1. \tag{2.61}$$

The matrix elements of the small $\mathbf{q}$ becomes

$$\begin{aligned}\frac{2NS\left|\Phi_1(\tilde{\mathbf{k}},\tilde{\mathbf{q}},\tilde{\mathbf{p}})\right|^2}{(8JSh\cos\theta)^2}\approx&\frac{9}{4}\frac{kqp}{(2\sqrt{2}\cos\theta)^3}+\frac{3}{2}\frac{p+q-k}{2\sqrt{2}\cos\theta}\\&+\frac{2\sqrt{2}\cos\theta}{4}\left(\frac{p}{kq}+\frac{k}{pq}+\frac{q}{kp}+\frac{2}{k}-\frac{2}{q}-\frac{2}{p}\right)\\\approx&\frac{9}{4}\frac{kqp}{(2\sqrt{2}\cos\theta)^3}.\end{aligned} \tag{2.62}$$

Here, we see that

$$\Phi_1(\tilde{\mathbf{k}},\tilde{\mathbf{q}},\tilde{\mathbf{p}})\propto\sqrt{kqp}, \tag{2.63}$$

which result is also discussed in the problem of liquid helium [106, 107]. We see from Fig. 2.10 (b) [14, 44] that the strongest $1/S$ corrections are expected on the decay threshold $\mathbf{k}_0$, which self-energy is Fig. 2.12 [14, 44]. The approximated matrix elements are:

$$\left|\Phi_1(\tilde{\mathbf{k}}_0,\mathbf{q})\right|^2|_{\mathbf{q}\to 0}\approx J^2S(\sin 2\theta)^2\frac{9k_0^3}{(2\sqrt{2}\cos\theta)^3}, \tag{2.64}$$

which means that the matrix elements diverges as k_0 increases. In liquid Helium case, the curvature α is small and matrix elements are small enough, where perturbation calculations are still reliable. However, for magnets, the curvature α changes from minus to plus infinity and it induces one-magnon decays [27, 96]. Moreover, $\alpha\gg 0$ results in large decay region and large k_0 for Eq. (2.64). This means the perturbation calculations are less reliable in the high field region.

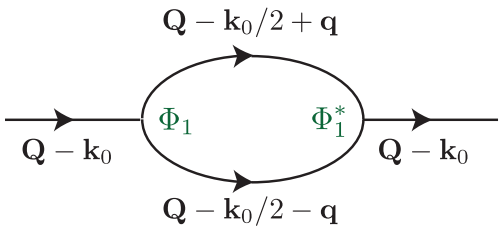

Figure 2.12: The self-energy, which cause strongest corrections is shown. This figure is taken from [14, 44].

We denote a denominator of the self-energy in Eq. (2.35) as $W[\tilde{\mathbf{k}}_0, \mathbf{q}]$;

$$\begin{aligned}\Sigma^{(1)}(\tilde{\mathbf{k}}_0, \omega_{\tilde{\mathbf{k}}_0}) &\approx \frac{1}{2}\sum_{\mathbf{p}} \frac{\left|\Phi_1(\tilde{\mathbf{k}}_0, \tilde{\mathbf{k}}_0/2+\mathbf{q}, \tilde{\mathbf{k}}_0/2-\mathbf{q})\right|^2}{\epsilon_{\tilde{\mathbf{k}}_0} - \epsilon_{\tilde{\mathbf{k}}_0/2+\mathbf{q}} - \epsilon_{\tilde{\mathbf{k}}_0/2-\mathbf{q}}} \\ &= \frac{1}{2}\sum_{\mathbf{p}} \frac{\left|\Phi_1(\tilde{\mathbf{k}}_0, \mathbf{q})\right|^2}{W[\tilde{\mathbf{k}}_0, \mathbf{q}]},\end{aligned} \tag{2.65}$$

where

$$W[\tilde{\mathbf{k}}_0, \mathbf{q}] = \omega_{\tilde{\mathbf{k}}_0} - \omega_{\tilde{\mathbf{k}}_0/2+\mathbf{q}} - \omega_{\tilde{\mathbf{k}}_0/2-\mathbf{q}} \tag{2.66}$$

$$\approx c\,(k_0 - |\mathbf{k}_0+\mathbf{q}| - |\mathbf{k}_0-\mathbf{q}|) \tag{2.67}$$

$$+ \alpha[k_0^3 - (k_0/2+q)^3 - (k_0/2-q)^3]). \tag{2.68}$$

We approximate the above equation by using

$$|\mathbf{k}/2+\mathbf{q}| = k/2 + q - \frac{1}{4}\frac{kq}{(k/2+q)^2}\psi^2, \tag{2.69}$$

where ψ is an azimuthal angle. By inserting Eq. (2.69), we obtain

$$\begin{aligned}W[\tilde{\mathbf{k}}_0, \mathbf{q}] &\approx -\frac{ck_0}{2}\frac{q^2}{(k_0/2)^2-q^2}[\psi^2 - 6\alpha\frac{((k_0/2)^2-q^2)^2}{q^2}] \\ &\approx -\frac{ck_0}{2}\frac{q^2}{(k_0/2)^2-q^2}[\psi^2 - \psi_0^2],\end{aligned} \tag{2.70}$$

where

$$\psi_0 = \sqrt{6\alpha}\frac{(k_0/2)^2-q^2}{q}. \tag{2.71}$$

We now see that Eq. (2.35) is approximated to

$$\Sigma^{(1)}(\tilde{\mathbf{k}}_0, \omega_{\tilde{\mathbf{k}}_0}) \propto -Jk_0^4 \tan^2\theta \int \frac{q^{\mathrm{D}-1}\mathrm{d}q}{q^2}, \tag{2.72}$$

where D denotes the dimension. It is clear that we obtain

$$\Sigma^{(1)}(\tilde{\mathbf{k}}_0, \omega_{\tilde{\mathbf{k}}_0}) \propto Jk_0^4 \tan^2\theta \ln\left[\frac{\Lambda}{k_0}\right], \tag{2.73}$$

where we set Λ a cut off wave vector for two dimensional magnets. It is noted that $k_0^4 \ln\left[\frac{\Lambda}{k_0}\right]$ goes to zero for the limit of $k_0 \to 0$ and there is no singularity though $\ln[k_0]$ diverges for the limit [14, 44]. We now see that roton appears as a result of logarithmic singularity in the $1/S$ corrections.

For three dimensional magnets, we obtain

$$\Sigma^{(1)}(\tilde{\mathbf{k}}_0, \omega_{\tilde{\mathbf{k}}_0}) \propto -Jk_0^4 \tan^2\theta. \tag{2.74}$$

It is clear that the self-energy correction is reduced, which means the perturbation calculations are more reliable than that of the two dimensional one, by adding interlayer interactions as already discussed in Ref. [28,96]. However, this solution cannot solve the problems on two-dimensional magnets.

Now, we obtain Δ_{rot} for SLHAFs

$$\Delta_{\mathrm{rot}} \approx ck_0 + \mathcal{A}_0\, Jk_0^4 \tan^2\theta \ln\left[\frac{\Lambda}{k_0}\right], \tag{2.75}$$

where we set $\mathcal{A}_0$ as a constant. It means that the roton gap drops as a function of k_0^4. Roton gap as a function of k_0^4 is shown in Fig. 2.11(a) [14, 44]. Red diamonds and blue circles are results of $S = 1/2$ and $S = 1$ and lines are fitting. Fittings capture the phenomena well and it means the self-energy corrections of Fig. 2.12 [14, 44] plays an important role though approximations are rough.

2.3.3 Approximate Value of Roton Mass

We estimate the approximated value of roton mass by differentiation perpendicular to the Γ-M line

$$\begin{aligned}\frac{1}{m_{\perp}^{*}} \approx & \frac{1}{2\,k_0}\frac{\partial\Sigma^{(1)}(\tilde{\mathbf{k}}_0,\omega_{\tilde{\mathbf{k}}_0})}{\partial k_0} \\ = & \frac{1}{2k_0}\sum_{\mathbf{q}}\left[\frac{\left|\Phi_1(\tilde{\mathbf{k}}_0,\mathbf{q})\right|}{k_0}\frac{\partial}{\partial k_0}\left(\frac{1}{W[\tilde{\mathbf{k}}_0,\mathbf{q}]}\right)+\frac{1}{W[\tilde{\mathbf{k}}_0,\mathbf{q}]}\frac{\partial\left|\Phi_1(\tilde{\mathbf{k}}_0,\mathbf{q})\right|^2}{\partial k_0}\right],\end{aligned} \tag{2.76}$$

and we obtain

$$\begin{aligned}\frac{1}{m_{\parallel}^{*}} \approx & \frac{\partial^2\bar{\epsilon}_{\mathbf{k_0}}}{\partial k_0^2} \\ = & b_0 k_0^3 \\ & +\frac{1}{2}\sum_{\mathbf{q}}\left[\frac{\partial}{\partial k_0}\left(\frac{2}{W[\tilde{\mathbf{k}}_0,\mathbf{q}]}\right)\frac{\partial\left|\Phi_1(\tilde{\mathbf{k}}_0,\mathbf{q})\right|^2}{\partial k_0}\right. \\ & \qquad +\frac{1}{W[\tilde{\mathbf{k}}_0,\mathbf{q}]}\frac{\partial^2\left|\Phi_1(\tilde{\mathbf{k}}_0,\mathbf{q})\right|^2}{\partial k_0^2} \\ & \qquad \left.+\left|\Phi_1(\tilde{\mathbf{k}}_0,\mathbf{q})\right|^2\frac{\partial^2}{\partial k_0^2}\left(\frac{1}{W[\tilde{\mathbf{k}}_0,\mathbf{q}]}\right)\right],\end{aligned} \tag{2.77}$$

by differentiation parallel to the Γ-M line. We solve Eqs. (2.76) and (2.77) by differentiating

$$\begin{aligned}\frac{\partial}{\partial k_0}\left(\frac{1}{W[\tilde{\mathbf{k}}_0,\mathbf{q}]}\right) = & -\frac{1}{W[\tilde{\mathbf{k}}_0,\mathbf{q}]^2}\frac{\partial W[\tilde{\mathbf{k}}_0,\mathbf{q}]}{\partial k_0}, \\ \frac{\partial^2}{\partial^2 k_0}\left(\frac{1}{W[\tilde{\mathbf{k}}_0,\mathbf{q}]}\right) = & -\frac{1}{W[\tilde{\mathbf{k}}_0,\mathbf{q}]^2}\frac{\partial^2 W[\tilde{\mathbf{k}}_0,\mathbf{q}]}{\partial k_0^2} \\ & +\frac{2}{W[\tilde{\mathbf{k}}_0,\mathbf{q}]^3}\left(\frac{\partial W[\tilde{\mathbf{k}}_0,\mathbf{q}]}{\partial k_0}\right)^2.\end{aligned} \tag{2.78}$$

We also obtain

$$\begin{aligned}\frac{\partial w[\tilde{\mathbf{k}}_0,\mathbf{q}]}{\partial k_0}\approx&\frac{2cq^2}{k_0^2}(\phi^2+3\phi_0^2),\\ \frac{\partial^2 w[\tilde{\mathbf{k}}_0,\mathbf{q}]}{\partial k_0^2}\approx&-\frac{4cq^2}{k_0^3}(\phi^2-3\phi_0^2).\end{aligned} \tag{2.79}$$

We obtain

$$m_\perp^* \propto k_0^{-2}, \tag{2.80}$$

$$m_\parallel^* \propto (1-\mathcal{D}_0 k_0), \tag{2.81}$$

by inserting Eqs. (2.78) and (2.79) to Eqs. (2.76) and (2.77), where $\mathcal{D}_0$ denotes a constant.

We now see that $m_\perp^*$ changes as a function of k_0^{-2} and $m_\parallel^*$ does as a function of k_0 as in Figs. 2.12 (b) and (c) [14, 44].

2.3.4 Valley Like Structure Perpendicular to the Γ-M Line

In this subsection, we discuss the valley like structure which appears perpendicular to the Γ-M line. This discussion is along the lines of Refs. [14, 44].

Using Eq. (2.70), we obtain angular integral

$$\begin{aligned}\int \mathrm{d}\phi \frac{1}{W[\tilde{\mathbf{k}}_0,\mathbf{q}]} \approx& -\frac{1}{cqk_0^2}\int \mathrm{d}\phi\left(\frac{1}{\phi-\phi_0}-\frac{1}{\phi+\phi_0}\right)\\ \propto& \ln\left[|\phi/\phi_0-1|+\delta\right],\end{aligned} \tag{2.82}$$

where δ is a cut off

$$\delta \propto k_{\mathrm{rot}}/k_{\mathrm{th}}-1. \tag{2.83}$$

It is noted that $|\phi/\phi_0-1|$ changes perpendicular to the Γ-M line, and therefore we see a sharp valley perpendicular to the line. This is seen in Fig. 2.8(e) [14, 44].

2.3.5 Line Broadenings

We have focused on the real part of self-energy. Now, we discuss the imaginary parts of the spectrum and line broadenings of spin wave spectrum. We set the

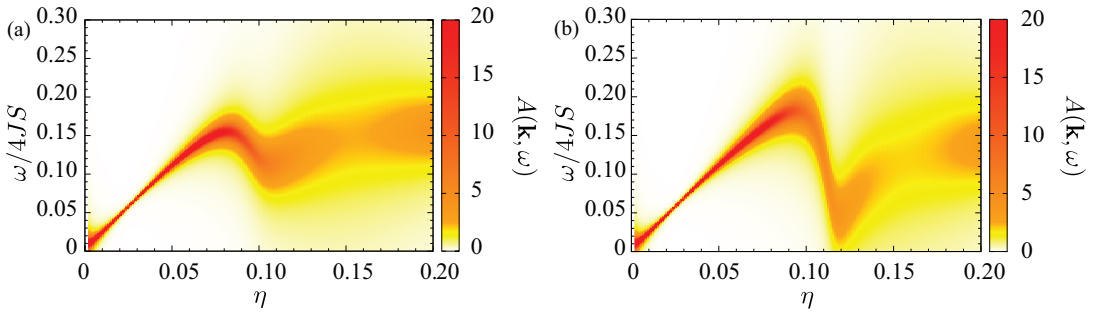

Figure 2.13: (a) Spectral weights $A(\mathbf{k},\omega)$ along the Γ-M line ($\mathbf{k} = \pi(1-\eta, 1-\eta)$) at $h = 0.7565$ is shown. This figure is taken from Ref. [45]. The value of $A(\mathbf{k},\omega)$ for each color is shown on the right. (b) Spectral weights $A(\mathbf{k},\omega)$ along the Γ-M line at $h = 0.7568$ is shown. This figure is taken from Refs. [44, 45].

imaginary parts of self-energy by $\Gamma_{\mathbf{k}}$ and spectral weights are written by

$$A(\mathbf{k},\omega) = \frac{1}{\pi}\frac{\Gamma_{\mathbf{k}}}{(\bar{\epsilon}_{\mathbf{k}} - \omega)^2 + \Gamma_{\mathbf{k}}^2} \tag{2.84}$$

and $A(\mathbf{k},\omega)$ for $h = 0.7565$ is shown in Fig. 2.13(a) [45] and $A(\mathbf{k},\omega)$ for $h = 0.7565$ is in Fig. 2.13(b) [44, 45]. Each color indicates values of $A(\mathbf{k},\omega)$ and the color is shown on the right.

(2.85)

We see broadened spectral weights due to the magnon decay, and its effects grow as the field increases. It is noted that we still see a roton shape tough there are strong spectrum broadening.

In experiments, a broadened excitation spectrum in SLHAFs is observed in this field regions $h \sim 0.75$ [100]. Now, we discuss the two possibilities of a broadening

1. spontaneous magnon decays as discussed on Refs. [26, 27, 42, 43, 96, 100]. As the previous works pointed out, an emergence of imaginary part of the self-energy induce a large broadenings ΔE_1

$$\Delta E_1 = \mathrm{Im}[\Sigma^{(1)}(\tilde{\mathbf{k}}_0, \omega_{\tilde{\mathbf{k}}_0})], \tag{2.86}$$

and this effect become especially strong around the decay threshold [26, 27, 96].

2. There are another possibilities, which is attributed to resolutions of experiments or calculations: ΔE_2 [14, 44]. We set Δk as a resolution of wave vector, which varies dependent to size of the numerical calculations or environments of experiments. We obtain

$$\Delta E_2 \sim \frac{\partial \mathrm{Re}[\Sigma^{(1)}(\mathbf{Q}-\mathbf{k}_0, \omega_{\mathbf{Q}-\mathbf{k}_0})]}{\partial k} \Delta k. \tag{2.87}$$

It is possible to reduce ΔE_2 by doing measurements in higher resolutions.

Basically, it is expected that $\Delta E_2 \ll \Delta E_1$. However, we believe that ΔE_2 is not negligible since SLHAFs has a valley like structure perpendicular to the Γ-M line as discussed in Section 2.3.4.

2.4 Discussions

In this section, we compare results between the previous studies on numerical [41–43] and spin wave results [25–28, 97, 99] and author's works [14, 44, 45]. We would like to discuss some issues:

1. a possibility to detect rotons,
2. what is it like a new phase,
3. a comparison of the previous and our research,
4. a reliability of perturbation calculation in high fields.

2.4.1 Possibility to Detect Rotons

The possibilities for detecting rotons are discussed in this subsection [14, 44]. We expect to observe the heat capacity $C \propto \mathrm{Exp}[-\Delta_{\mathrm{rot}}/T]$ just like the heat capacity observed for a roton in liquid helium [109]. In the helium case, the roton gap changes slightly by pressure [109] but we expect to observe much more drastic responses of Δ_{rot} by small increases of uniform fields. We also expect to detect the excitation spectrum by the neutron scattering measurements.

To detect the roton, careful measurements are desired. 1% accuracy for the uniformity of fields is desirable to detect the roton since Δ_{rot} changes dramatically with 1% increases of fields. In other words, we expect to see a broadening of the spectrum due to the inhomogeneity of external fields. High momentum accuracy to capture 1% changes of the wave vector is desired since valley like structure is predicted perpendicular to the Γ-M line. It is known that the neutron scattering measurements needs larger single crystals than the specific heat measurements. It means that specific heat measurements are less difficult to detect roton than neutron scattering since it is easier generate homogeneous field for smaller samples.

Now, we discuss the candidate materials to detect rotons. As we have discussed in Eqs. (2.72) and (2.73), the strong corrections are attributed to a logarithmic singularity of two dimensionality. It means that strong interlayer interactions might smear out the roton shape. We have shown that the effects becomes weaker for larger S and the $1/S$ correction vanishes for $S = \infty$. It means that the smaller S is more desirable for detecting rotons. The materials for $S = 1/2$ and

$S = 1$ are desirable for detecting rotons since the complete softening is observed in $S = 1/2$ and $S = 1$. We note that the saturation field should be low enough to reach $h \approx 0.75$. Recently, generating uniform magnetic field up to ~ 10 T is now possible using a superconducting magnet. We suggest that a pyrazine family is a good candidate material [113] since its magnetic systems are qSLHAFs with small interlayer interactions [114] and low saturation field (up to $\sim 10T$).

2.4.2 Quantum Phase in High Fields

In this chapter, we discuss a rotonlike minimum, which softens rapidly to zero at $h = h_c$ and $\mathbf{k} = \mathbf{k}_c$ [14, 44, 45]. We predict that there is a new phase in $h > h_c$. In this subsection, we discuss how it is like the new phase.

We believe that the new phase is a slightly modulated simple canted state since no significant anomaly is observed for static physical properties such as magnetization and spin stiffness [41, 42]. If the phase is much differ from the simple canted state, we expect to see much stronger anomalies on static properties because of the strong fluctuations. It is expected that a freezing of $\mathbf{k}_c$ magnon (BEC) occurs at $h = h_c$ and it should have a $\pi/\mathbf{k}_c$ periodic structure. We expect that the phase might be similar to the spiral phase, which is suggested to appear in some frustrated magnets below the saturation field [32,35–40]. Though we need more investigations, the softening might be the clues for understanding physics of high field phase in other antiferromagnets.

2.4.3 Comparison with the Previous Research

Firstly, we summarize the previous works and our results.

Static physical quantity such as a spin wave velocity, spin stiffness, susceptibility [42,99], magnetization [25,41,42,97] and static structure factor [43] show no strong anomalies from zero field to the saturation field. However, it is observed that dynamical structure factors in high fields are qualitatively different from that of low fields [42,43]. The qualitative change of an excitation spectrum is also suggested in experiments [100]. Lüscher and Läuchli [42] and Syljuåsen [43] claimed that the broadening of excitation spectrum is attributed to a huge imaginary part of the self-energy corrections of spin wave calculations [26–28]. However, real parts of the self-energy corrections must also play an important role, when that of an imaginary part is important. The previous studies [26, 27] lack this

points of discussions and they claim that the simple canted state is stable from zero to the saturation field [27].

We have focused on the real part of the self-energy corrections [14, 44, 45] and investigated the spin wave spectrum within the second order perturbation calculations. It is found out that a roton appears and its gap drops rapidly to zero at $h = h_c$, $\mathbf{k} = \mathbf{k}_c$, and finally we obtain an unphysical 'negative excitation spectrum', if we apply even higher fields. We take a problem on complete softening of roton seriously and interpret it as a precursor of phase transition. We see from the above discussions that an interpretation of a result is qualitatively different.

The broadening of magnon in high fields are observed in the Honeycomb lattice antiferromagnets [115] and quasi-one dimensional magnets [101, 102] in fields, and its cause is the same as SLHAFs in fields. We believe that the softening of magnon mode is observed by other magnets in fields since the origin of softening is attributed to a positive curvature of the Goldstone mode near the saturation field. In other words, the rapid softening and high field phase are expected in other magnets as well as SLHAFs and this study must help to understand these phases.

2.4.4 Reliability of Perturbation Calculations and Future Works

In this section, we discuss results of the spin wave spectrum within the second order perturbation calculations on the basis of Refs. [14, 44, 45]. We believe that the rapid softening of roton is a precursor of phase transition referring to the Kohn anomaly [46].

However, there is a point to be concerned: a reliability of the second order perturbation calculation in this field region. As discussed in many of textbooks, the perturbation calculation is a powerful tool at a weakly interacting region. For SLHAFs in a zero field, the magnon-magnon interaction is small and the linear spin wave spectra [43] are in good agreements with that of experimental results with small quantitative corrections [11, 105]. However, perturbation calculations are less reliable in a strongly interacting region. We focus on the region $h \sim 0.75$, where the leading terms of the excitation energy and the $1/S$ corrections compete each other, and perturbation calculations are less reliable.

The softening of a roton is investigated on a belief that the wave vector $\mathbf{k}_c \approx$

$\mathbf{k}_{\rm th}$ might characterize a new phase in the same way as the Kohn anomaly [46]. We note that the Kohn anomaly is firstly pointed out by a complete softening and an unphysical 'negative excitation spectrum' due to strong electron-phonon interactions by a perturbation calculation [46]. It is expected that the softening in SLHAFs indicates an existence of a new phase. However, the results are not conclusive since perturbation calculations are less reliable in the region and we need careful numerical investigations to clarify whether there is a phase.

As we have already discussed, numerical calculations on static properties such as magnetization or spin stiffness [41–43] does not show any evidence for existence of a new phase. However, there is a qualitative change between low and high field region of the dynamical properties [42, 43]. It is important to study the region $h \sim 0.75$ in detail by numerical calculations and clarify whether there is a phase.

The authors have pointed out [14, 44, 45] that the rapid softening of roton occurs at $h \sim 0.75$ and it is caused by a positive curvature for Goldstone bosons. The positive curvature is expected for various magnets near the saturation field. Therefore, we believe that understanding SLHAFs in fields is important for revealing physics of the various noncollinear magnets focusing on the three-magnon interactions.

2.5 Summary

In this chapter, we have focused on the effects of three-magnon interactions, which plays a role in noncollinear magnets. SLHAFs, which is one of the best candidate for studying the interactions, are focused in this thesis. The three-magnon interaction is known to become extremely strong when the spin wave spectrum has a linear mode with positive curvature. SLHAFs have a linear mode with positive curvature in $h \gtrsim 0.75$.

The spin wave spectrum, which are calculated within the second order perturbation theory has been shown. Strong $1/S$ corrections due to the strong three-magnon interaction have been observed along the Γ-M line at $h \approx 0.75$. The strong $1/S$ corrections cause a roton like minimum and it softens rapidly to zero at $h = h_{\rm c}$ and $\mathbf{k} = \mathbf{k}_{\rm c}$. In $h > h_{\rm c}$, we obtain an unphysical 'negative excitation spectrum' [27].

This is a reminiscent of the Kohn anomaly [46], and we have interpreted roton's softening as a precursor of phase transition [14, 44, 45]. Roton gaps $\Delta_{\rm rot}$ and masses m^* as functions of field has been studied in detail expecting to obtain some clues for a phase in $h > h_{\rm c}$. We have found out that extremely strong $1/S$ corrections along the intersection of Γ-M line and decay threshold $\mathbf{k}_{\rm th}$ cause a roton. It has been shown that the roton gap $\Delta_{\rm rot}$ and mass m^* drop as a function of k_0, which have been in good agreements with roughly approximated results from $\Sigma_1(\mathbf{k}, \omega)$.

We believe that it is possible detect rotons by the specific heat and neutron scattering measurements under uniform fields. Recently, highly uniform magnetic field up to ~ 10 T becomes reachable by using superconducting magnets. To detect rotons, we recommend pyrazine family materials [113, 114], which are almost ideal qSLHAFs with small interlayer interactions and its saturation fields are around 10T.

We guess that a freezing of roton mode occurs at $h = h_{\rm c}$ and $\mathbf{k} = \mathbf{k}_{\rm c}$. We believe that modulated canted states, which has $\pi/k_{\rm c}$ periodic structure, appears in $h > h_{\rm c}$ after the complete softening.

The softening of roton infers a phase transition referring to the Kohn anomaly. However, we need more numerical investigations to clarify an existence of a phase because the second order perturbation calculation itself is less reliable in a strongly interacting region.

We believe that an appearance of new phase and a softening of roton also hap-

pen in other noncollinear magnets since the cause of softening is the extremely strong three-magnon interaction. It is discussed that linear modes with positive curvatures cause strong three-magnon interactions, and the positive curvature might appear in any antiferromagnets near the saturation field. This means that extremely strong three-magnon interactions might also appear in other antiferromagnets near the saturation field. We hope that more investigations on noncollinear magnets including SLHAFs reveal the physics of three-magnon interactions, and these investigations become guides for understanding antiferromagnets in high fields.

Chapter 3

Formalism of Magneto-Thermal Conductivity

In this chapter, we discuss magnon mediated spin and thermal conductivity in antiferromagnets. The contents of this chapter are based on Refs. [14, 45, 94, 95].

It is well known that charge current flows when we apply a chemical potential gradient to metal [3]. In the same way, spin current flows when a magnetic field gradient is applied along a magnet [14, 60, 69, 88].

The spin mediated thermal transports are suggested in one dimensional ferromagnets [47–49] and ferrimagnets [50], but they are rather diffusive. Spin contributions to large thermal conductivity due to spins are suggested in one dimensional antiferromagnets [51–57]. Much larger thermal conductivity only along the spin chain direction than other directions is observed. These experiments have stimulated theoretical works on spin and thermal transports one-dimensional magnets in various methods such as the exact diagonalizations and the exact solutions [58–69]. These studies are developed along the lines of electrical and thermal conductivity [3–5]. These theoretical works support the existence of spin mediated thermal transports. The anisotropic thermal conductivities [51–57] are now interpreted as spin contributions.

Spin mediated thermal conductivity is also suggested in non-frustrated two-dimensional magnets [70–75], and the conductivity shows roughly T^2 dependency when the gradient is along a magnetic layer. However, there are only a few theoretical studies on the conductivity in high dimensional magnets [87–90] and we need a guide to interpret these experiments.

Recently, the thermal conductivity of frustrated systems are studied and non-monotonic responses to fields and temperatures are observed for frustrated magnets such as $R\mathrm{MnO}_3$ [76, 77], $R_2\mathrm{Ti}_2\mathrm{O}_7$ [78–83] and organic compounds [83–86]. One of the aims for these experiments is to detect low energy elementary excitations of spins [83–86]. However, there might be some other contributions for the conductivity such as spin-phonon scatterings, which is expected be strong in frustrated magnets [116, 117], or spin-spin scatterings [118]. Therefore, it is not clear whether non-monotonic behavior is attributed to the elementary excitation of spins or effects of spin-phonon interactions. It is clear that a theoretical basis which can guide the interpretation for experiments is important and necessary to interpret experiments.

Thanks to developments of nanofabrications for devices, efficiency for electric device are improving incredibly. However, sizes of devices are getting so tiny and devices now experience quantum effects. They have started projects to manipulate the spin degrees of freedom for electrons as a carrier of an information: spintronics. They try to control a spin current, which flows along the magnetic field gradient just like charge current flows along the chemical potential gradients [119, 120]. Spintronics focus firstly on magnetic metals but magnetic insulators draw some attentions since it is expected to reduce energy costs of the Joule heat and to have a longer mean free path for spin current flow [119–123].

One of the biggest problems on the spintronics is a difficulty to define a spin current operator [92]. This is because spins are not always conserved quantities. In general, they restrict themselves to the system, where magnetization is conserved, and spins and fields are collinear, to derive a current operator using a conservations of magnetization. They define spin current operators by considering only longitudinal fluctuations for align direction of spins [87–90].

However, there had not been a reliable definition, to author's knowledge, for noncollinear magnets. We need to define a spin current operator which is valid for noncollinear systems to spread the possibilities for investigations. To define a spin current operator in noncollinear systems, we need to consider the transverse fluctuations as well as the longitudinal ones for align direction of spins. One of the main goals of this chapter is to define spin and energy current operators, which are valid even for noncollinear systems, and derive reliable formalism of the spin and thermal conductivity using the linear response theory.

We develop formalism of spin and thermal conductivity in magnets which

is valid as far as the magnetization is conserved. We calculate spin and thermal conductivity in non-frustrated quasi-two-dimensional magnets of magnons. We believe that this is a first step for establishing a theoretical background for interpreting experiments on noncollinear systems [76–86].

This chapter is composed as follows. Firstly, a definition of spin current operator for collinear magnets is reviewed referring to Refs. [58–69]. Then, we define a spin and energy current operator, which are valid even for noncollinear magnets as well as collinear magnets [14, 45, 94]. The calculation of conductivity is done by the linear response theory, which is studied along the lines of electric conductivity [3,5] and one dimensional magnets [58–69]. Then, the conductivity of qSLHAFs in fields are studied using the spin wave theory of Zhitomirsky-Nikuni-Chernyshev formalism, which has been shown in the previous chapter [26, 28, 96]. A reliability of the definition is shown by a satisfaction of sum rule for each conductivity [14, 45, 94].

We believe that the definition becomes a reliable basis to study the spin and thermal transports to noncollinear as well as collinear systems and it broadens possibilities to research the transports in various magnets. We believe that revealing spin contributions of the conductivity contribute to developments of spintronics as well as interpreting experiments on thermal conductivity.

3.1 Spin and Energy Current in Collinear Magnets

The main purpose of this study is to build formalism of spin and thermal conductivity in non-collinear antiferromagnets [14, 94]. There are previous works on magneto-thermal conductivity in magnets, which restricted themselves to one-dimensional systems [58–69] or the system where spins and fields are collinear [87–90]. These studies are on the basis of previous works on metals [3–5]. The spin and thermal conductivity in collinear magnets is reviewed in this section.

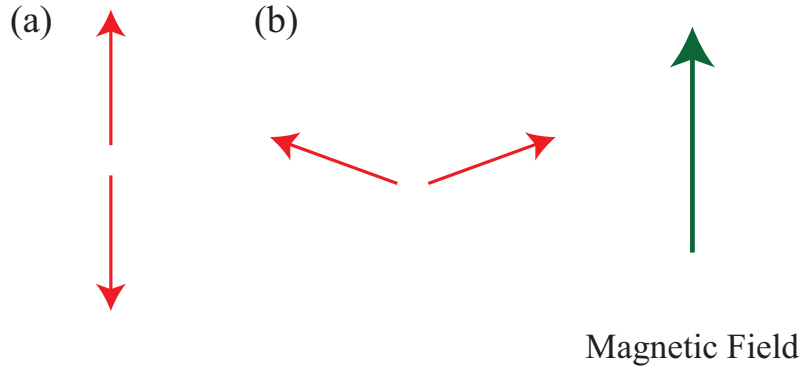

Figure 3.1: (a) An antiferromagnet with Ising anisotropy in a small magnetic field. The spins align parallel to the field direction. (b) A Heisenberg antiferromagnet in a magnetic field. The spins align not parallel to the field direction. This figure is taken from Ref. [14].

Figure 3.1 [14] shows the image of the collinear and noncollinear magnets. Figure 3.1 (a) shows an Ising antiferromagnets in fields, and we see that spins and fields are collinear to each other. Figure 3.1 (b) shows Heisenberg antiferromagnets in fields, and we see that spins and a field are noncollinear.

There are several works studied on the Ising antiferromagnets [87–90] while there are only a few for the noncollinear case [92], which contains ambiguity for the definition. This thesis propose a reliable definitions of spin current operators.

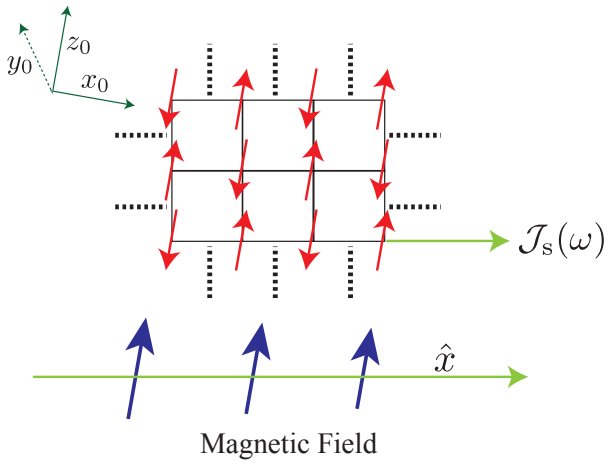

Figure 3.2: Induced spin current $\mathcal{J}_s(\omega)$ flows along a direction of field gradient $\hat{x}$. The spins align parallel to the field direction z for antiferromagnets with the Ising anisotropy. This figure is taken from Ref. [14].

3.2 Definition of Spin and Energy Current in Magnetic Insulators

One of the main goals of this section is to define a spin and energy current density operator, which is valid for any magnetic insulators whose magnetization is conserved. The operators are defined using conservations of energy and spins. The reliability of definitions are checked by applying the definition to qSLHAFs and showing the satisfactions of sum rule for each conductivity. The author notes that this section is based on Refs. [14, 45, 94, 95]. The author believes that this definition contributes not only to reveal the spin and thermal conductivity but also to a realization of spintronics.

Figure 3.2 [14] shows how an induced spin current $\mathcal{J}_s(\omega)$ flows in square lattice Ising antiferromagnets, where a direction for quantization axis of spins z and a magnetic field are parallel to z direction, and $\hat{x}$ denotes a field gradient direction. We expect that spins align parallel or antiparallel to the field direction and $\mathcal{J}_s(\omega)$ flows along the $\hat{x}$ direction.

Figure 3.3 [14] shows how the induced spin current $\mathcal{J}_s(\omega)$ flows in qSLHAFs, where $\hat{x}$ denotes the direction of magnetic field gradient and z_0 denotes the direction of magnetic field.

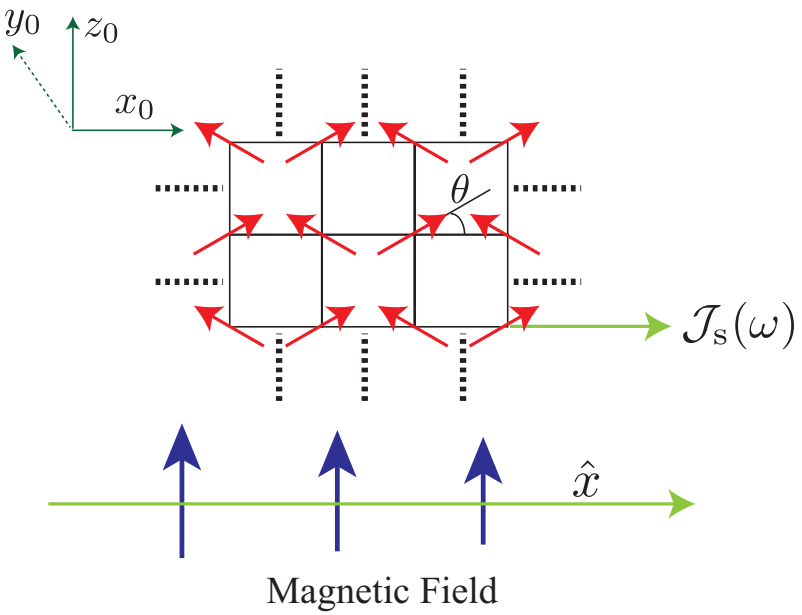

Figure 3.3: Induced spin current $\mathcal{J}_s(\omega)$ flows along a direction of field gradient $\hat{x}$. The spins align not parallel to the field direction z_0 for the Heisenberg antiferromagnets. This figure is recited from Ref. [14].

The Hamiltonian of XXZ model of qSLHAFs with anisotropy Δ is

$$\begin{aligned} \mathcal{H} =& \mathcal{H}_0 - HM, \\ \mathcal{H}_0 =& \sum_{<i,j>} J_{i,j} \left[S_i^{x_0} S_j^{x_0} + S_i^{y_0} S_j^{y_0} + \Delta S_i^{z_0} S_j^{z_0} \right], \\ M =& \sum_i S_i^{z_0}, \end{aligned} \tag{3.1}$$

where we set z_0 direction as a field direction.

It is shown in Appendix A that the magnetization $M = \sum_i S_i^{z_0}/N$ and energy $\mathcal{H}_0$ is conserved

$$\begin{aligned} [\mathcal{H}, M] =& 0, \\ [\mathcal{H}, \mathcal{H}_0] =& 0, \end{aligned} \tag{3.2}$$

in XXZ magnets.

Definitions of spin current and energy current density operators for XXZ magnets, whose magnetization is conserved are reviewed. It is possible to define

spin current by the continuity equation by using the conservation law [59–62, 68]

$$\frac{\partial \rho_i}{\partial t} = -\nabla J_i, \tag{3.3}$$

where ρ_i denotes a local density of conserved quantity and J_i denotes the current of conserved quantity, to define the current density operator.

Here, equation of motion for ρ_i is written as

$$\frac{\partial \rho_i}{\partial t} = \mathrm{i}[\mathcal{H}, \rho_i] = -\nabla J_i. \tag{3.4}$$

by using the equation of motion.

Now, spin and energy current operator is defined by inserting ρ_i to a local magnetization density $S_i^{z_0}$

$$\begin{aligned} \frac{\mathrm{d}}{\mathrm{d}t} S_i^{z_0} =& -\sum_{\hat{\mu}} \left(j_{\mathrm{s},i,i+\hat{\mu}} - j_{\mathrm{s},i-\hat{\mu},i} \right), \\ j_{\mathrm{s},i,i+\hat{\mu}} =& J_{i,i+\hat{\mu}} \left(S_i^{x_0} S_{i+\hat{\mu}}^{y_0} - S_i^{y_0} S_{i+\hat{\mu}}^{x_0} \right), \end{aligned} \tag{3.5}$$

where $j_{\mathrm{s},i,i+\hat{\mu}}$ $[\hat{\mu} = (\hat{x}, \hat{y}, \hat{z})]$ denotes a spin current density operator, and a local energy density $(J_{i,j}\mathbf{S}_i \cdot \mathbf{S}_j)$

$$\begin{aligned} \frac{\mathrm{d}}{\mathrm{d}t} \left(J_{i,j} \mathbf{S}_i \cdot \mathbf{S}_j \right) =& -\sum_{\hat{\mu}_1, \hat{\mu}_2} \left(j_{\mathrm{e},i,i+\hat{\mu}_1,i+\hat{\mu}_1+\hat{\mu}_2} - j_{\mathrm{e},i-\hat{\mu}_2,i,i+\hat{\mu}_1} \right), \\ j_{\mathrm{e},i-\hat{\mu}_1,i,i+\hat{\mu}_2} =& J_{i-\hat{\mu}_1,i} J_{i,i+\hat{\mu}_2} \, \mathbf{S}_{i-\hat{\mu}_1} \cdot \left(\mathbf{S}_i \times \mathbf{S}_{i+\hat{\mu}_2} \right), \end{aligned} \tag{3.6}$$

where $j_{\mathrm{e},i-\hat{\mu}_1,i,i+\hat{\mu}_2}$ is an energy current density operator. These are definitions of current operators, which is valid for any magnets including noncollinear as well as collinear magnets.

We obtain the same $j_{\mathrm{s},i,i+\hat{\mu}}$ by the gauge transformations in the next subsection.

3.2.1 Magnetization in Collinear Magnets

In this subsection, we show magnetization in collinear magnets by HP bosons.

As we have already discussed, we focus on the system whose z_0 components of magnetization $M = \sum_i S_i^{z_0}/N$ is conserved.

For collinear magnets, we expect a two sublattice (A-and B-sublattice) structure. For A-sublattice, spin operators in HP representation is

$$\begin{aligned} S_i^+ =& \sqrt{2S} f_{i,A}\, \mathcal{A}_i \\ S_i^- =& \sqrt{2S} \mathcal{A}_i^\dagger f_{i,A} \\ S_i^{z_0} =& S - \mathcal{A}_i^\dagger \mathcal{A}_i, \end{aligned} \tag{3.7}$$

with HP bosons $\mathcal{A}_i^\dagger$ and

$$f_{i,A} = \sqrt{1 - \frac{\mathcal{A}_i^\dagger \mathcal{A}_i}{2S}}. \tag{3.8}$$

For B-sublattice,

$$\begin{aligned} S_i^+ =& \sqrt{2S} \mathcal{B}_i^\dagger f_{i,B} \\ S_i^- =& \sqrt{2S} f_{i,B}\, \mathcal{B}_i \\ S_i^{z_0} =& \mathcal{B}_i^\dagger \mathcal{B}_i - S, \end{aligned} \tag{3.9}$$

with HP bosons $\mathcal{B}_i^\dagger$ and

$$f_{i,B} = \sqrt{1 - \frac{\mathcal{B}_i^\dagger \mathcal{B}_i}{2S}}. \tag{3.10}$$

We used two different bosons for each sublattice since fluctuations of A-and B-sublattice are not equal.

The magnetization for collinear magnet [7, 87, 88] is

$$M = \frac{2}{N} \sum_{iB} (\mathcal{B}_i^\dagger \mathcal{B}_i - \mathcal{A}_i^\dagger \mathcal{A}_i). \tag{3.11}$$

We see from Eq. (3.11) that the magnetization is a difference of magnon number operator for A- and B-sublattice. We also see that the spin operators defined from the continuity equations are written by even numbers of HP operators [87–90].

3.2.2 Magnetizations in Noncollinear Magnets

In this subsection, we show magnetization in noncollinear magnets by HP bosons.

We discuss qSLHAFs in fields as a representative of noncolliner magnets. As we have discussed in Chapter 2, the magnetization for the system is

$$M = \frac{1}{N}\sum_i \left(S_i^z \sin\theta - S_i^x \cos\theta \mathrm{e}^{\mathrm{i}\mathbf{Q}\cdot\mathbf{R}_i}\right), \tag{3.12}$$

using Eq. (2.5), where S_i^μ ($\mu = x, y, z$) are rotated spin operators. After HP transformations by using Eq. (2.6),

$$M = \frac{1}{N}\sum_i \left((S - n_i)\sin\theta - \sqrt{2S}\left(f_i a_i + a_i^\dagger f_i\right)\cos\theta \mathrm{e}^{\mathrm{i}\mathbf{Q}\cdot\mathbf{R}_i}\right). \tag{3.13}$$

We see from Eq. (3.13), the magnetization has terms that are written by odd number of HP boson operators. These terms are coming from transverse fluctuations, and appear when the directions of spin alignment and field are not collinear. The odd number of HP boson operators in magnetization cause terms of spin current operators written by odd number of bosons, which do not appear in previous works for collinear case in Refs. [87–90].

The appearance of transverse components in noncollinear systems is the main difference from collinear ones [14, 94]. Therefore, we need to check a reliability of our new definition in noncollinear magnets. The reliability is to be shown by satisfaction of sum rule in the later section 3.9.

3.3 Definition of Spin Current by the Gauge Transformation

We now derive spin current density operator in a different way. We show that the same spin current operators as section 3.2 is obtained in this section. This fact strongly indicates the reliability of definition. This subsection is along the lines of Refs. [61, 64, 124].

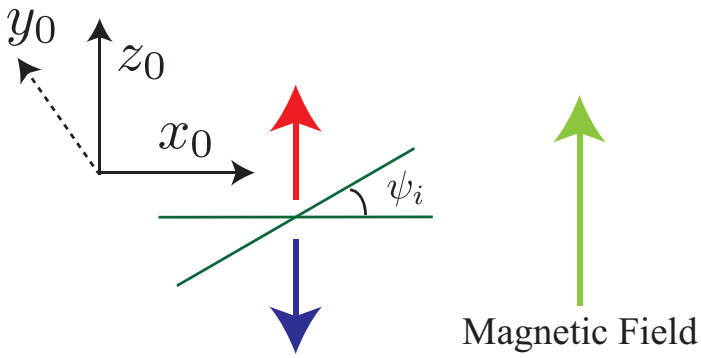

Figure 3.4: A uniform twist ψ_i perpendicular to the z_0 plane is applied at sites i in collinear magnets. The total magnetization does not change by the twist.

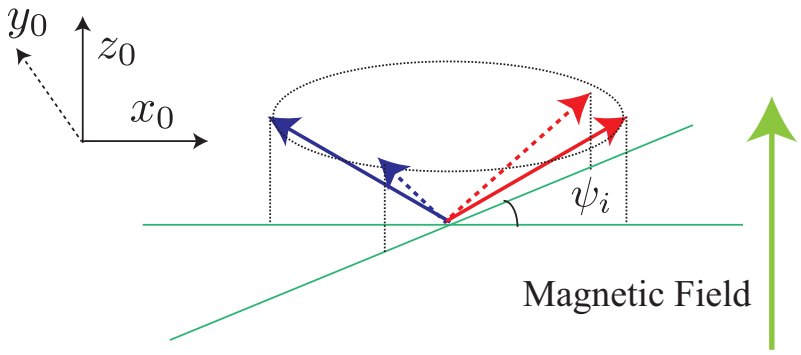

Figure 3.5: A uniform twist ψ_i perpendicular to the z_0 plane is applied at sites i in noncollinear magnets. We see that the total magnetization does not change by the twist. This figure is taken from Ref. [14].

Firstly, an uniform twist ψ_i at site i perpendicular to the z_0 plane is applied (see Fig. 3.4 for collinear magnets and Fig. 3.5 [14] for noncollinear magnets).

The spin operators on the laboratory frame are transformed into [99, 124, 125]

$$\begin{aligned} \tilde{S}_i^{+} &\rightarrow \tilde{S}_i^{+} \mathrm{e}^{\mathrm{i}\psi_i}, \\ \tilde{S}_i^{-} &\rightarrow \tilde{S}_i^{+} \mathrm{e}^{-\mathrm{i}\psi_i}, \\ S_i^{z_0} &\rightarrow S_i^{z_0}, \end{aligned} \tag{3.14}$$

where

$$\begin{aligned} \tilde{S}_i^{+} &= S_i^{x_0} + \mathrm{i} S_i^{y_0}, \\ \tilde{S}_i^{-} &= S_i^{x_0} - \mathrm{i} S_i^{y_0}. \end{aligned} \tag{3.15}$$

We obtain

$$\begin{aligned} \hat{\mathcal{H}}(\psi) =& \sum_{<i,j>} J_{i,j} \left[\frac{S_i^{+} S_j^{-} \mathrm{e}^{\mathrm{i}\psi} + S_i^{-} S_j^{+} \mathrm{e}^{-\mathrm{i}\psi}}{2} + S_i^{z_0} S_j^{z_0} \right] - H \sum_i S_i^{z_0} \\ =& \sum_{<i,j>} J_{i,j} \left[\frac{\tilde{S}_i^{+} \tilde{S}_j^{-} + \tilde{S}_i^{-} \tilde{S}_j^{+}}{2} + S_i^{z_0} S_j^{z_0} \right] - H \sum_i S_i^{z_0} \\ &+ \psi \sum_{<i,j>} \mathrm{i} J_{i,j} \left[\frac{\tilde{S}_i^{+} \tilde{S}_j^{-} - \tilde{S}_i^{-} \tilde{S}_j^{+}}{2} \right] \\ &- \frac{\psi^2}{2} \sum_{<i,j>} J_{i,j} \left[\frac{\tilde{S}_i^{+} \tilde{S}_j^{-} + \tilde{S}_i^{-} \tilde{S}_j^{+}}{2} \right] + O(\psi^3) \\ =& \hat{\mathcal{H}} + \psi \sum_i (j_{\mathrm{s}\, i,i+\hat{x}} + j_{\mathrm{s}\, i,i+\hat{y}} + j_{\mathrm{s}\, i,i+\hat{z}}) \\ &- \frac{\psi^2}{2} \left(\hat{T}_{i,i+\hat{x}} + \hat{T}_{i,i+\hat{y}} + \hat{T}_{i,i+\hat{z}} \right) + O(\psi^3), \end{aligned} \tag{3.16}$$

where

$$j_{\mathrm{s}\, i,i+\hat{\mu}} = \mathrm{i} J_{i,i+\hat{\mu}} \left[\frac{\tilde{S}_i^{+} \tilde{S}_{i+\hat{\mu}}^{-} - \tilde{S}_i^{-} \tilde{S}_{i+\hat{\mu}}^{+}}{2} \right], \tag{3.17}$$

and

$$\hat{T}_{i,i+\hat{\mu}} = \sum_i J_{i,i+\hat{\mu}} \left[\frac{\tilde{S}_i^{+} \tilde{S}_{i+\hat{\mu}}^{-} + \tilde{S}_i^{-} \tilde{S}_{i+\hat{\mu}}^{+}}{2} \right]. \tag{3.18}$$

By differentiations, we obtain $j_{\mathrm{s},i,i+\hat{x}}$

$$\begin{aligned} \frac{\mathrm{d}}{\mathrm{d}\Psi}\hat{\mathcal{H}}(\Psi)|_{\psi=0} =& \sum_{i,\mu} j_{\mathrm{s},i,i+\hat{\mu}}, \\ j_{\mathrm{s},i,i+\hat{\mu}} =& J_{i,i+\hat{\mu}} \left(S_i^{x_0} S_{i+\hat{\mu}}^{y_0} - S_i^{y_0} S_{i+\hat{\mu}}^{x_0} \right) \end{aligned} \tag{3.19}$$

and ρ_{s}

$$\begin{aligned} \rho_{\mathrm{s}} =& -\frac{\mathrm{d}^2}{\mathrm{d}\Psi^2}\hat{\mathcal{H}}(\Psi)|_{\Psi=0} = -\frac{1}{N}\frac{\partial^2 \hat{\mathcal{H}}(\Psi)}{\partial \Psi^2}|_{\psi=0}, \\ \rho_{\mathrm{s}} =& \frac{1}{N}\sum_{i,\hat{\mu}} \left(S_i^{x_0} S_{i+\hat{\mu}}^{x_0} + S_i^{y_0} S_{i+\hat{\mu}}^{y_0} \right). \end{aligned} \tag{3.20}$$

In addition, the spin stiffness is related to an integrated intensity of the spin conductivity, which is to be discussed later.

The similar relations as Eq. (3.16) exists as well for electric conductivity and charge stiffness after the gauge transformation [88,125–128]. This correspondence indicates the reliability for definition of $j_{\mathrm{s},i,i+\hat{x}}$.

3.4 Spin and Energy Current Operators for qSLHAFs

In this section, spin and energy current density operators in qSLHAFs are shown. We show each current operator in HP representation using the formalism of Chapter 2.

3.4.1 Spin Current Operators in the Holstein-Primakoff Representations

The spin current operator of Eq. (3.5) for qSLHAFs is shown using spin wave formalism of Chapter 2.

Equation (3.5) after rotation of the quantization axis is

$$\begin{aligned} j_{\mathrm{s},\, i,i+\hat{\mu}} =& J_{i,i+\hat{\mu}} \sin\theta \left(S_i^x S_{i+\hat{\mu}}^y - S_i^y S_{i+\hat{\mu}}^x \right) \\ &+ \mathrm{e}^{\mathrm{i}\mathbf{Q}\cdot\mathbf{r}_i} J_{i,i+\hat{\mu}} \cos\theta \left(S_i^z S_{i+\hat{\mu}}^y + S_i^y S_{i+\hat{\mu}}^z \right), \end{aligned} \tag{3.21}$$

where $\hat{\mu}$ denotes a direction of exchange bonds.

Then, we perform HP transformation

$$\begin{aligned} j_{\mathrm{s},\, i,i+\hat{\mu}} =& -\mathrm{i} J_{i,i+\hat{\mu}} S \sin\theta \left(a_i^\dagger f_i f_{i+\hat{\mu}} a_{i+\hat{\mu}} - a_{i+\hat{\mu}}^\dagger f_i f_{i+\hat{\mu}} a_i \right) \\ &- \mathrm{i}\mathrm{e}^{\mathrm{i}\mathbf{Q}\cdot\mathbf{r}_i} J_{i,i+\hat{\mu}} \cos\theta S \sqrt{\frac{S}{2}} \left[(S - n_i)(f_{i+\hat{\mu}} a_{i+\hat{\mu}} - a_{i+\hat{\mu}}^\dagger f_{i+\hat{\mu}}) \right] \\ &- \mathrm{i}\mathrm{e}^{\mathrm{i}\mathbf{Q}\cdot\mathbf{r}_i} J_{i,i+\hat{\mu}} \cos\theta S \sqrt{\frac{S}{2}} \left[(f_i a_i - a_i^\dagger f_i)(S - n_{i+\hat{\mu}}) \right]. \end{aligned} \tag{3.22}$$

We now divide the operator into $j_{\mathrm{s},\, i,i+\hat{\mu}\ \mathrm{even}}$, that is written by even number of bosons after HP expansion

$$j_{\mathrm{s},\, i,i+\hat{\mu}\ \mathrm{odd}} = -\mathrm{i} J_{i,i+\hat{\mu}} S \sin\theta \left(a_i^\dagger f_i f_{i+\hat{\mu}} a_{i+\hat{\mu}} - a_{i+\hat{\mu}}^\dagger f_i f_{i+\hat{\mu}} a_i \right), \tag{3.23}$$

and $j_{\mathrm{s},\, i,i+\hat{\mu}\ \mathrm{odd}}$, that is written by odd number of HP bosons

$$\begin{aligned} j_{\mathrm{s},\, i,i+\hat{\mu}\ \mathrm{even}} =& -\mathrm{i}\mathrm{e}^{\mathrm{i}\mathbf{Q}\cdot\mathbf{r}_i} J_{i,i+\hat{\mu}} \cos\theta S \sqrt{\frac{S}{2}} \left[(S - n_i)(f_{i+\hat{\mu}} a_{i+\hat{\mu}} - a_{i+\hat{\mu}}^\dagger f_{i+\hat{\mu}}) \right] \\ &- \mathrm{i}\mathrm{e}^{\mathrm{i}\mathbf{Q}\cdot\mathbf{r}_i} J_{i,i+\hat{\mu}} \cos\theta S \sqrt{\frac{S}{2}} \left[(f_i a_i - a_i^\dagger f_i)(S - n_{i+\hat{\mu}}) \right]. \end{aligned} \tag{3.24}$$

The author note that spin operators written by odd number of bosons $j_{\mathrm{s},\ i,i+\hat{\mu}\ \mathrm{odd}}$ appear only when the spins have noncollinear structure and they do not appear in collinear magnets in Refs. [87–90].

The author also note that $j_{\mathrm{s},\ i,i+\hat{\mu}\ \mathrm{even}}$ vanishes in zero field since it satisfy the equation

$$j_{\mathrm{s},\ i,i+\hat{\mu}\ \mathrm{even}} \propto \sin\theta. \tag{3.25}$$

Then, we perform HP expansion and we name parts of spin current operators which is written in the n-th order of HP bosons as $j_{\mathrm{s},(4-\mathrm{n})/2}$. The leading term of the $j_{\mathrm{s},\ \mathrm{i},\mathrm{i}+\hat{\mu}}$ is

$$j_{\mathrm{s},\ ,i,i+\hat{\mu},3/2} = -\,\mathrm{i}J_{i,i+\hat{\mu}}\cos\theta S\sqrt{\frac{S}{2}}\mathrm{e}^{\mathrm{i}\mathbf{Q}\cdot\mathbf{r}_i}(a_i - a_i^\dagger + a_{i+\hat{\mu}} - a_{i+\hat{\mu}}^\dagger), \tag{3.26}$$

which appears from $j_{\mathrm{s},\ i,i+\hat{\mu}\ \mathrm{odd}}$, and $j_{\mathrm{s},\ ,i,i+\hat{\mu},1}$ is

$$j_{\mathrm{s},\ ,i,i+\hat{\mu},1} = -\,J_{i,i+\hat{\mu}}\mathrm{i}S\sin\theta(a_i^\dagger a_{i+\hat{\mu}} - a_i a_{i+\hat{\mu}}^\dagger), \tag{3.27}$$

which appears from $j_{\mathrm{s},\ i,i+\hat{\mu}\ \mathrm{even}}$. Then, $j_{\mathrm{s},\ ,i,i+\hat{\mu},1/2}$ is

$$\begin{aligned} j_{\mathrm{s},\ ,i,i+\hat{\mu},1/2} =& \mathrm{i}J_{\hat{\mu}}\cos\theta\sqrt{\frac{S}{2}}\mathrm{e}^{\mathrm{i}\mathbf{Q}\cdot\mathbf{r}_i}[n_{i+\hat{\mu}}(a_i - a_i^\dagger) + n_i(a_{i+\hat{\mu}} - a_{i+\hat{\mu}}^\dagger)] \\ &+ \frac{\mathrm{i}J_{\hat{\mu}}\cos\theta}{4}\mathrm{e}^{\mathrm{i}\mathbf{Q}\cdot\mathbf{r}_i}[(n_i a_i - a_i^\dagger n_i) + n_i(n_{i+\hat{\mu}}a_{i+\hat{\mu}} - a_{i+\hat{\mu}}^\dagger n_{i+\hat{\mu}})]. \end{aligned} \tag{3.28}$$

Then, we do HF decoupling to $j_{\mathrm{s},\ ,\mathrm{i},\mathrm{i}+\hat{\mu},1/2}$ and we obtain

$$\begin{aligned} J^{\mathrm{HF}}_{\mathrm{s},\ ,\mathrm{i},\mathrm{i}+\hat{\mu},1/2} =& \mathrm{i}J_{\hat{\mu}}\cos\theta\sqrt{\frac{S}{2}}\mathrm{e}^{\mathrm{i}\mathbf{Q}\cdot\mathbf{r}_i}[a_i - a_i^\dagger + a_{i+\hat{\mu}} - a_{i+\hat{\mu}}^\dagger] \\ &\left[n + m_{\hat{\mu}} - \Delta_{\hat{\mu}} + \frac{2n-\delta}{4}\right]. \end{aligned} \tag{3.29}$$

3.4.2 Energy Current Operators in the Holstein-Primakoff Representations

The energy current operator (see Eq. (3.6)) after rotation of the quantization axis is:

$$\begin{aligned}\frac{j_{\mathrm{e},i-\hat{\mu}_1,i,i+\hat{\mu}_2}}{J_{i-\hat{\mu}_1,i}J_{i,i+\hat{\mu}_2}} =& S^y_{i-\hat{\mu}_1}\left[-\mathrm{e}^{\mathrm{i}\mathbf{Q}\cdot\mathrm{r}_i}\sin 2\theta(S^z_i S^z_{i+\hat{\mu}_2}+S^x_i S^x_{i+\hat{\mu}_2})\right.\\ &\left.-\cos 2\theta(S^z_i S^x_{i+\hat{\mu}_2}-S^x_i S^z_{i+\hat{\mu}_2})\right]\\ &-S^y_i\left[(S^z_{i-\hat{\mu}_1}S^x_{i+\hat{\mu}_2}-S^x_{i-\hat{\mu}_1}S^z_{i+\hat{\mu}_2})\right]\\ &+S^y_{i+\hat{\mu}_2}\left[\mathrm{e}^{\mathrm{i}\mathbf{Q}\cdot\mathrm{r}_i}\sin 2\theta(S^z_{i-\hat{\mu}_1}S^z_i+S^x_{i-\hat{\mu}_1}S^x_i)\right.\\ &\left.-\cos 2\theta(S^z_{i-\hat{\mu}_1}S^x_i-S^x_{i-\hat{\mu}_1}S^z_i)\right]\\ =& j_{\mathrm{e},i-\hat{\mu}_1,i,i+\hat{\mu}_2,\mathrm{odd}}+j_{\mathrm{e},i-\hat{\mu}_1,i,i+\hat{\mu}_2,\mathrm{even}},\end{aligned} \tag{3.30}$$

where

$$\begin{aligned}\frac{j_{\mathrm{e},i-\hat{\mu}_1,i,i+\hat{\mu}_2,\mathrm{odd}}}{J_{i-\hat{\mu}_1,i}J_{i,i+\hat{\mu}_2}} =& \mathrm{e}^{\mathrm{i}\mathbf{Q}\cdot\mathrm{r}_i}\sin 2\theta\left[S^y_{i+\hat{\mu}_2}(S^z_{i-\hat{\mu}_1}S^z_i+S^x_{i-\hat{\mu}_1}S^x_i)\right.\\ &\left.-S^y_{i-\hat{\mu}_1}(S^z_i S^z_{i+\hat{\mu}_2}+S^x_i S^x_{i+\hat{\mu}_2})\right],\end{aligned} \tag{3.31}$$

which produce odd number of the boson term after HP expansions, and

$$\begin{aligned}\frac{j_{\mathrm{e},i-\hat{\mu}_1,i,i+\hat{\mu}_2,\mathrm{even}}}{J_{i-\hat{\mu}_1,i}J_{i,i+\hat{\mu}_2}} =& \cos 2\theta S^z_i(S^x_{i-\hat{\mu}_1}S^y_{i+\hat{\mu}_2}-S^y_{i-\hat{\mu}_1}S^x_{i+\hat{\mu}_2})\\ &-S^z_{i-\hat{\mu}_1}(S^x_{i+\hat{\mu}_2}S^y_i+\cos 2\theta S^x_i S^y_{i+\hat{\mu}_2})\\ &+S^z_{i+x}(S^x_{i-\hat{\mu}_1}S^y_i+\cos 2\theta S^x_i S^y_{i-\hat{\mu}_1}),\end{aligned} \tag{3.32}$$

which produce even number of the boson term after HP expansions.

We perform HP transformation and we obtain

$$\begin{aligned}j_{\mathrm{e},i-\hat{\mu}_1,i,i+\hat{\mu}_2,\mathrm{odd}} =& \mathrm{e}^{\mathrm{i}\mathbf{Q}\cdot\mathbf{R}_i}\sin 2\theta\frac{1}{\mathrm{i}}\sqrt{\frac{S}{2}}(f_{i+\hat{\mu}_2}a_{i+\hat{\mu}_2}-a^\dagger_{i+\hat{\mu}_2}f_{i+\hat{\mu}_2})\\ &\left[\frac{S}{2}(f_{i-\hat{\mu}_1}a_{i-\hat{\mu}_1}+a^\dagger_{i-\hat{\mu}_1}f_{i-\hat{\mu}_1})(f_i a_i+a^\dagger_i f_i)+(S-n_i)(S-n_{i-\hat{\mu}_1})\right]\\ &-\mathrm{e}^{\mathrm{i}\mathbf{Q}\cdot\mathbf{R}_i}\sin 2\theta\frac{1}{\mathrm{i}}\sqrt{\frac{S}{2}}(f_{i-\hat{\mu}_1}a_{i-\hat{\mu}_1}-a^\dagger_{i-\hat{\mu}_1}f_{i-\hat{\mu}_1})\\ &\left[\frac{S}{2}(f_{i+\hat{\mu}_2}a_{i+\hat{\mu}_2}+a^\dagger_{i+\hat{\mu}_2}f_{i+\hat{\mu}_2})(f_i a_i+a^\dagger_i f_i)+(S-n_i)(S-n_{i+\hat{\mu}_2})\right],\end{aligned} \tag{3.33}$$

and

$$
\begin{aligned}
j_{\mathrm{e},i-\hat{\mu}_1,i,i+\hat{\mu}_2,\mathrm{even}} =& \frac{S}{2\mathrm{i}}(f_i a_i - a_i^\dagger f_i)\Big[(S-n_{i+\hat{\mu}_2})(f_{i-\hat{\mu}_1}a_{i-\hat{\mu}_1}+a_{i-\hat{\mu}_1}^\dagger f_{i-\hat{\mu}_1}) \\
&\qquad -(S-n_{i-\hat{\mu}_1})(f_{i+\hat{\mu}_2}a_{i+\hat{\mu}_2}+a_{i+\hat{\mu}_2}^\dagger f_{i+\hat{\mu}_2})\Big] \\
&+\frac{S\cos 2\theta}{2\mathrm{i}}(f_{i+\hat{\mu}_2}a_{i+\hat{\mu}_2}-a_{i+\hat{\mu}_2}^\dagger f_{i+\hat{\mu}_2})\Big[-(S-n_{i-\hat{\mu}_1})(f_i a_i + a_i^\dagger f_i) \\
&\qquad +(S-n_i)(f_{i-\hat{\mu}_1}a_{i-\hat{\mu}_1}+a_{i-\hat{\mu}_1}^\dagger f_{i-\hat{\mu}_1})\Big] \\
&-\frac{S\cos 2\theta}{2\mathrm{i}}(f_{i-\hat{\mu}_1}a_{i-\hat{\mu}_1}-a_{i-\hat{\mu}_1}^\dagger f_{i-\hat{\mu}_1})\Big[-(S-n_{i+\hat{\mu}_2})(f_i a_i + a_i^\dagger f_i) \\
&\qquad +(S-n_i)(f_{i+\hat{\mu}_2}a_{i+\hat{\mu}_2}+a_{i+\hat{\mu}_2}^\dagger f_{i+\hat{\mu}_2})\Big]\,.
\end{aligned}
\tag{3.34}
$$

We see that $j_{\mathrm{e},i-\hat{\mu}_1,i,i+\hat{\mu}_2,\mathrm{odd}}$ vanishes in zero field since it satisfies

$$
j_{\mathrm{e},i-\hat{\mu}_1,i,i+\hat{\mu}_2,\mathrm{odd}} \propto \sin\theta. \tag{3.35}
$$

Then, we perform HP expansion to $j_{\mathrm{e},i-\hat{\mu}_1,i,i+\hat{\mu}_2,\mathrm{odd}}$ and $j_{\mathrm{e},i-\hat{\mu}_1,i,i+\hat{\mu}_2,\mathrm{even}}$ and we name the part of current operators which is written by n-th order of HP bosons for $j_{\mathrm{e},i-\hat{\mu}_1,i,i+\hat{\mu}_2,(6-n)/2}$. The leading therm of $j_{\mathrm{e},i-\hat{\mu}_1,i,i+\hat{\mu}_2}$ is

$$
\begin{aligned}
j_{\mathrm{e},i-\hat{\mu}_1,i,i+\hat{\mu}_2,5/2} =& \sum_{\hat{\mu}_1,\,\hat{\mu}_2}\frac{J_{i-\hat{\mu}_1,i}J_{i,i+\hat{\mu}_2}\mathrm{e}^{\mathrm{i}\mathbf{Q}\cdot\mathrm{r}_i}\sin 2\theta S^2}{\mathrm{i}}\sqrt{\frac{S}{2}} \\
&\qquad \Big[\Big(a_{i+\hat{\mu}_2}-a_{i+\hat{\mu}_2}^\dagger\Big)-\Big(a_{i-\hat{\mu}_1}-a_{i-\hat{\mu}_1}^\dagger\Big)\Big] \\
=& \sum_{\hat{\mu}_1,\,\hat{\mu}_2}\frac{J_{i-\hat{\mu}_1,i}J_{i,i+\hat{\mu}}\sin 2\theta S^2}{\mathrm{i}}\sqrt{\frac{S}{2N}} \\
&\qquad \sum_{\mathbf{k}}(u_k-v_k)(b_{\mathbf{k}}-b_{-\mathbf{k}}^\dagger)\mathrm{e}^{\mathrm{i}(\mathbf{k}+\mathbf{Q})\cdot\mathrm{r}_i}(\mathrm{e}^{\mathrm{i}k\tau}-\mathrm{e}^{-\mathrm{i}k\tau}) \\
=& \sum_{\hat{\mu}_1}\frac{J_{i-\hat{\mu}_1,i}J_{i,i+\hat{\mu}}\sin 2\theta S^2}{\mathrm{i}}\sqrt{\frac{S}{2N}} \\
&\qquad \sum_{\mathbf{k}}(u_k-v_k)(b_{\mathbf{k}}-b_{-\mathbf{k}}^\dagger)\mathrm{e}^{\mathrm{i}(\mathbf{k}+\mathbf{Q})\cdot\mathrm{r}_i}(2\sin k_{\hat{\mu}_1}),
\end{aligned}
\tag{3.36}
$$

and $j_{\mathrm{e},i-\hat{\mu}_1,i,i+\hat{\mu}_2,2}$ is

$$\begin{aligned} j_{\mathrm{e},i-\hat{\mu}_1,i,i+\hat{\mu}_2,2} =& \sum_{\tau,\,\tau_1} \frac{S^2 J_{i-\hat{\mu}_1,i} J_{i,i+\hat{\mu}_2} \cos 2\theta}{\mathrm{i}} (a^\dagger_{i-\hat{\mu}_1} a_{i+\hat{\mu}} - a^\dagger_{i+\hat{\mu}} a_{i-\hat{\mu}_1}) \\ &+ \sum_{\tau,\,\tau_1} \frac{S^2 J_{i-\hat{\mu}_1,i} J_{i,i+\hat{\mu}} \cos^2\theta}{\mathrm{i}} \\ &\qquad \left[\left(a_i a_{i+\hat{\mu}} - a^\dagger_i a^\dagger_{i+\hat{\mu}} \right) - \left(a_i a_{i-\hat{\mu}_1} - a^\dagger_i a^\dagger_{i-\hat{\mu}_1} \right) \right] \\ &+ \sum_{\tau,\,\tau_1} \frac{S^2 J_{i-\hat{\mu}_1,i} J_{i,i+\hat{\mu}} \sin^2\theta}{\mathrm{i}} \\ &\qquad \left[\left(a^\dagger_i a_{i+\hat{\mu}} - a_i a^\dagger_{i+\hat{\mu}} \right) + \left(a_i a^\dagger_{i-\hat{\mu}_1} - a_i a^\dagger_{i-\hat{\mu}_1} \right) \right], \end{aligned} \tag{3.37}$$

and $j_{\mathrm{e},i-\hat{\mu}_1,i,i+\hat{\mu}_2,3/2}$ is

$$\begin{aligned} j_{\mathrm{e},i-\hat{\mu}_1,i,i+\hat{\mu}_2,3/2} =& -\mathrm{i} \sum_{\tau,\,\tau_1} J_{i-\hat{\mu}_1,i} J_{i,i+\hat{\mu}_2} \mathrm{e}^{\mathrm{i}\mathbf{Q}\cdot\mathrm{r}_i} \sin 2\theta S \sqrt{\frac{S}{2}} \\ &\left[\left(a_{i+\hat{\mu}_2} - a^\dagger_{i+\hat{\mu}_2} \right) \left\{ \frac{(a_i + a^\dagger_i)(a_{i-\hat{\mu}_1} + a^\dagger_{i-\hat{\mu}_1})}{2} - n_i - n_{i-\hat{\mu}_1} \} \right\} \right. \\ &\left. - \left(a_{i-\hat{\mu}_1} - a^\dagger_{i-\hat{\mu}_1} \right) \left\{ \frac{(a_i + a^\dagger_i)(a_{i+\hat{\mu}_2} + a^\dagger_{i+\hat{\mu}_2})}{2} - n_i - n_{i+\hat{\mu}_2} \right\} \right]. \end{aligned} \tag{3.38}$$

Then, we perform HF decoupling to $j_{\mathrm{e},i-\hat{\mu}_1,i,i+\hat{\mu}_2,3/2}$ and we obtain

$$\begin{aligned} j^{\mathrm{HF}}_{\mathrm{e},i-\hat{\mu}_1,i,i+\hat{\mu}_2,3/2} =& \frac{\sin 2\theta S \mathrm{e}^{\mathrm{i}\mathbf{Q}\cdot\mathrm{r}_i}}{\mathrm{i}} \sqrt{\frac{S}{2}} \sum_{\hat{\mu}_2,\,\hat{\mu}_1} J_{i-\hat{\mu}_1,i} J_{i,i+\hat{\mu}_2} \\ &\left[\left(a_i - a^\dagger_i \right) + \left(a_{i-\hat{\mu}_1} - a^\dagger_{i-\hat{\mu}_1} \right) \right] \\ &\left[\Delta_{\hat{\mu}} + m_{\hat{\mu}} + m_{\hat{\mu}+\hat{\mu}_1} - \Delta_{\hat{\mu}+\hat{\mu}_1} - m_{\hat{\mu}_1} + \Delta_{\hat{\mu}_1} - 2n - \frac{2n-\delta}{4} \right]. \end{aligned} \tag{3.39}$$

3.5 Thermal Currents

The thermal current is derived in this section on the basis of Refs. [3,69,129–131].

We consider the entropy density s generation, which is written as

$$T\mathrm{d}s = \mathrm{d}\rho_{\mathrm{e}} - H\mathrm{d}\rho_{\mathrm{m}}, \tag{3.40}$$

where ρ_{e} is an energy density and ρ_{m} is a magnetization density.

We consider the time derivative of Eq. (3.40)

$$T\frac{\partial s}{\partial t} = \frac{\partial \rho_{\mathrm{e}}}{\partial t} - H\frac{\partial \rho_{\mathrm{s}}}{\partial t}, \tag{3.41}$$

and we obtain

$$\begin{aligned} T\frac{\partial s}{\partial t} =& -\nabla\mathcal{J}_{\mathrm{e}} + H\nabla\mathcal{J}_{\mathrm{s}} \\ =& -\nabla(\mathcal{J}_{\mathrm{e}} - H\mathcal{J}_{\mathrm{s}}) - \mathcal{J}_{\mathrm{s}}\nabla H, \end{aligned} \tag{3.42}$$

by using the continuity equation (see Eq. (3.3)) where $\mathcal{J}_{\mathrm{e}}$ is an energy current and $\mathcal{J}_{\mathrm{s}}$ is a spin current. Then, we obtain

$$T\left[\frac{\partial s}{\partial t} + \nabla\left(\frac{\mathcal{J}_{\mathrm{th}}}{T}\right)\right] = -\mathcal{J}_{\mathrm{th}}\left(\frac{\nabla T}{T}\right) - \mathcal{J}_{\mathrm{s}}\nabla H. \tag{3.43}$$

where $\mathcal{J}_{\mathrm{th}}$ is thermal currents

$$\mathcal{J}_{\mathrm{th}} = \mathcal{J}_{\mathrm{e}} - H\mathcal{J}_{\mathrm{s}} \tag{3.44}$$

and we used an identity [129]

$$\nabla\mathcal{J}_{\mathrm{th}} = T\left[\nabla\left(\frac{\mathcal{J}_{\mathrm{th}}}{T}\right) + \mathcal{J}_{\mathrm{th}}\left(\frac{\nabla T}{T^2}\right)\right]. \tag{3.45}$$

It is noted that Eq. (3.44) correspond to the thermodynamic relation for magnetic insulators in Eq. (3.40) [69].

Then, we integrate Eq. (3.43) over a sufficiently large volume to satisfy

$$\int \mathrm{d}\mathbf{r}\nabla\left(\frac{\mathcal{J}_{\mathrm{th}}}{T}\right) = 0, \tag{3.46}$$

which means that the thermal current is zero at the outer surface, and we now obtain

$$T\frac{\partial S}{\partial t} = \int \mathrm{d}\mathbf{r} \left[-\mathcal{J}_{\mathrm{th}} \left(\frac{\nabla T}{T} \right) - \mathcal{J}_{\mathrm{s}} \nabla H \right], \tag{3.47}$$

where S is the entropy [3, 129–131].

In reversible non-dissipative case, the entropy generation vanishes

$$\frac{\partial S}{\partial t} = 0. \tag{3.48}$$

Therefore, the spin currents and thermal currents also vanish [129]

$$\mathcal{J}_{\mathrm{th}} = 0, \text{ and } \mathcal{J}_{\mathrm{s}} = 0. \tag{3.49}$$

On the other hand, the entropy generation should be positive

$$\frac{\partial S}{\partial t} > 0, \tag{3.50}$$

in dissipative systems.

The spin current and the thermal current vanish when ∇T and ∇H is zero. We assume the linear response, that induced currents $\mathcal{J}_i$, where $\mathcal{J}_i$ is substituted by $\mathcal{J}_{\mathrm{s}}$ or $\mathcal{J}_{\mathrm{th}}$, are proportional to X_j, where X_j is substituted by ∇H or $(\nabla T)/T$. We now obtain

$$\mathcal{J}_i = \sum_j L_{i,j} X_j, \tag{3.51}$$

where $L_{i,j}$ is a coefficient.

By inserting Eq. (3.51) to Eq. (3.47) we obtain

$$\begin{aligned} \frac{\partial S}{\partial t} &= \int \mathrm{d}\mathbf{r} \sum_i X_i \mathcal{J}_i \\ &= \int \mathrm{d}\mathbf{r} \sum_i \sum_j L_{i,j} X_j X_i. \end{aligned} \tag{3.52}$$

We now obtain the Onsager relation

$$L_{i,j} = L_{j,i} \tag{3.53}$$

from Eq. (3.52).

We now obtain the linear response equations for Eq. (3.51)

$$\begin{pmatrix} \mathcal{J}_{\rm s} \\ \mathcal{J}_{\rm th} \end{pmatrix} = \begin{pmatrix} L_{\rm s,s}, & L_{\rm s,th} \\ L_{\rm th,s}, & L_{\rm th,th} \end{pmatrix} \begin{pmatrix} \nabla H \\ -\left(\frac{\nabla T}{T}\right) \end{pmatrix}. \tag{3.54}$$

We see from Eq. (3.54) that $L_{\rm s,th}$ and $L_{\rm th,s}$ play role for the magneto-thermal effects, where ∇h is induced by ∇T and vice versa due to the couplings of spin currents and energy currents. The magneto-thermal effects is discussed in the next section.

It is noted that there are equivalent equations of Eq. (3.54) for $\mathcal{J}_{\rm s}$, and $\mathcal{J}_{\rm e}$

$$\begin{pmatrix} \mathcal{J}_{\rm s} \\ \mathcal{J}_{\rm e} \end{pmatrix} = \begin{pmatrix} L_{\rm s,s}, & L_{\rm s,e} \\ L_{\rm e,s}, & L_{\rm th,e} \end{pmatrix} \begin{pmatrix} \nabla H \\ -\left(\frac{\nabla T}{T}\right) \end{pmatrix}. \tag{3.55}$$

The followings equations are satisfied

$$\begin{aligned} L_{\rm th,s} =& L_{\rm s,th} = L_{\rm s,e} - HL_{\rm s,s}, \\ L_{\rm th,th} =& L_{\rm e,e} - 2HL_{\rm e,s} + H^2 L_{\rm s,s}, \end{aligned} \tag{3.56}$$

by using $\mathcal{J}_{\rm th} = \mathcal{J}_{\rm e} - H\mathcal{J}_{\rm s}$ [3, 61, 69].

We also see from Eq. (3.56) that equations

$$\begin{aligned} L_{\rm s,th} =& L_{\rm s,e}, \\ L_{\rm th,th} =& L_{\rm e,e}, \end{aligned} \tag{3.57}$$

are true at $H = 0$.

The conductivity $\sigma_{m,n}(\omega)$ is defined by

$$\mathrm{Re}\left[L_{m,n}(\omega)\right] = \sigma_{m,n}(\omega), \tag{3.58}$$

where m and n are substituted by s, th or e. The conductivity $\sigma_{m,n}(\omega)$ can be divided into Drude wights $D_{m,n}$ for $\omega = 0$ and the regular parts $\sigma_{\mathrm{regular},\, m,n}(\mathbf{q}, \omega)$

$$\sigma_{m,n}(\omega) = D_{m,n}\delta(\omega) + \sigma_{\mathrm{regular},\, m,n}(\omega). \tag{3.59}$$

The Onsager relation is satisfied in this system

$$L_{\rm s,th} = L_{\rm th,s}, \tag{3.60}$$

even in a magnetic field [65, 132, 133]. The Onsager relation is satisfied when the Hamiltonian has the symmetry, which is invariant under two operations: the time reversal and field reversal [133]. For the qSLHAFs in fields, Hamiltonian has the symmetry, and that is why the Onsager relation is satisfied. The author notes that the satisfaction of the Onsager relation is shown previously in one dimensional magnets in Refs. [60, 61, 67, 69].

3.6 Magneto-Thermal Effects

In this section, we discuss the magneto-thermal effects in magnetic insulators. This section is along the lines of Refs. [3, 5, 69, 133].

3.6.1 Magneto-Thermal Effects in Nonzero Magnetic Fields

In this subsection, we consider an magnetic insulator in nonzero magnetic fields $H \neq 0$ on the basis of Refs. [3, 5, 65, 69].

We suppose that no spin current is flowing in the system

$$\mathcal{J}_{\rm s} = 0. \tag{3.61}$$

We substitute Eq. (3.54) by Eq. (3.61) and we obtain

$$\nabla H = \frac{L_{\rm s,th}}{L_{\rm s,s}} \frac{\nabla T}{T}. \tag{3.62}$$

This correspond to the thermoelectric power in metals, and we call it a thermo-magnetic power.

We deform Eq. (3.62) and obtain

$$\mathcal{S} = \frac{\nabla H}{\nabla T} = \frac{L_{\rm s,th}}{T L_{\rm s,s}}, \tag{3.63}$$

where $\mathcal{S}$ is a magnetic Seebeck coefficient, which correspond to the Seebeck coefficient in metals [67, 69]. Equation (3.63) means that temperature gradients ∇T in magnetic insulators induce magnetic field gradients ∇H when $\mathcal{S} \neq 0$.

The thermal conductivity $\kappa_{\rm th}(\omega)$ is defined under the condition, when there is only a thermal current flowing, therefore $\kappa_{\rm th}(\omega)$ is obtained substituting Eq. (3.62) in Eq. (3.54) [60, 69]

$$\kappa_{\rm th}(\omega) = \frac{1}{T}\left(\sigma_{\rm th,th}(\omega) - \frac{\sigma_{\rm s,th}(\omega)\sigma_{\rm th,s}(\omega)}{\sigma_{\rm s,s}(\omega)}\right). \tag{3.64}$$

We also obtain

$$\kappa_{\rm th}(\omega) = \frac{1}{T}\left(\sigma_{\rm e,e}(\omega) - \frac{\sigma_{\rm s,e}(\omega)\sigma_{\rm e,s}(\omega)}{\sigma_{\rm s,s}(\omega)}\right), \tag{3.65}$$

by inserting Eq. (3.56).

Then, we suppose that there is no temperature gradient in a system. We insert $\nabla T = 0$ to Eq. (3.54), and we obtain

$$\mathcal{J}_{\rm th} = \frac{L_{\rm th,s}}{L_{\rm s,s}} \mathcal{J}_{\rm s} = \Pi \mathcal{J}_{\rm s}, \tag{3.66}$$

where Π is a magneto-Peltier coefficient, which corresponds to the Peltier coefficient in metals.

Recently, these magneto-thermal coefficients (the magneto-Seebeck and magneto-Peltier coefficients) are experimentally observed in some magnets [134–136].

3.6.2 Magneto-Thermal Effects in Zero Magnetic Field

In this subsection, we consider magnetic insulators in zero field. This subsection refers to Refs. [65, 67, 69].

The spin reversal operation is defined by [137]

$$\begin{aligned} S_i^{z_0} &\to - S_i^{z_0}, \\ \tilde{S}_i^{+} &\to \tilde{S}_i^{-}, \\ \tilde{S}_i^{-} &\to \tilde{S}_i^{+}. \end{aligned} \tag{3.67}$$

The spin current operator is odd, and the energy current operator is even for the operation. The couplings of spin currents and energy currents vanish in the systems, whose Hamiltonian is invariant under the spin reversal operation [65,67,69]. Therefore, magneto-thermal effects vanish for the Heisenberg antiferromagnets in zero field.

It is shown in this thesis that off-diagonal terms $L_{\rm s,e}$ for qSLHAFs in Eq. (3.54) vanishes, which means there are no magneto-thermal effects, for qSLHAFs in zero field because of the symmetry, which is discussed in Subsection 3.7.2.

3.7 Linear Response Theory

In this subsection, we focus on phenomenological theory of spin conductivity and energy conductivity in magnetic insulators by using the linear response theory [138, 139]. We derive the correlation function, that describes linear response, called the Kubo formula [3]. The subsection is based on the theory of charge conductivity in metals [3, 5, 129, 133], spin conductivity in one- [58–69] and two-dimensional magnets [87, 88], and also our papers [14, 45, 94, 95].

3.7.1 Kubo Formula of Spin and Energy Conductivity at $T = 0$

Firstly, we focus on the spin conductivity, energy conductivity and off-diagonal conductivity in the low temperature limit [3, 87, 88].

We study an induced spin current $\mathcal{J}_{\rm s}(l,t)$ and an energy current $\mathcal{J}_{\rm e}(l,t)$ in response to a magnetic field $H(i,t)$ and temperature $T(i,t)$.

We start a derivation from the Hamiltonian

$$\mathcal{H} = \mathcal{H}_0 + \mathcal{H}', \tag{3.68}$$

$$\mathcal{H}' = \mathcal{H}'_{\rm s} + \mathcal{H}'_{\rm e}, \tag{3.69}$$

where $\mathcal{H}_0$ is the Heisenberg Hamiltonian in uniform magnetic field H,

$$\mathcal{H} = \sum_{<i,j>} J_{i,j} \left(S_i^{x_0} S_j^{x_0} + S_i^{y_0} S_j^{y_0} + \Delta S_i^{z_0} S_j^{z_0} \right) - H \sum_i S_i^{z_0}, \tag{3.70}$$

and $\mathcal{H}'_{\rm s}(t)$ and $\mathcal{H}'_{\rm e}(t)$ are the perturbation Hamiltonian:

$$\mathcal{H}'_{\rm s} = -\sum_i S_i^{z_0} \Psi_{\rm s}(i), \tag{3.71}$$

where $\Psi_{\rm s}(i)$ is the magnetic field at site i, and

$$\mathcal{H}'_{\rm e} = \sum_i h_{\rm e}(i) \Psi_{\rm e}(i), \tag{3.72}$$

where

$$\begin{aligned} h_{\rm e}(i) =& \sum_\tau J_{i,i+\tau} \left(S_i^{x_0} S_{i+\tau}^{x_0} + S_i^{y_0} S_{i+\tau}^{y_0} + \Delta S_i^{z_0} S_{i+\tau}^{z_0} \right) \\ \Psi_{\rm e}(i) =& \frac{T(i)}{T}, \end{aligned} \tag{3.73}$$

with $T(i)$ being the temperature at site i.

We put $\Psi_{\rm e}(i)$ to derive energy conductivity. We see that $\Psi_{\rm e}(i)$ goes to 1 when the temperature of system is uniform. One of the biggest difficulties in deriving a formula for the energy conductivity is that we need a temperature gradient while we calculate the conductivity through correlation functions using the thermal average, which assumes a uniform temperature [3].

However, the energy conductivity can still be defined in the limit of $\Psi_{\rm e}(i) \to 1$, as well as in the low temperature limit. In this thesis, we consider systems only in the limit of $\Psi_{\rm e}(i) \to 1$ to justify the evaluation of the conductivity under a single temperature.

Induced spin current $\mathcal{J}_{\rm s}(l,t)$ and energy current $\mathcal{J}_{\rm e}(l,t)$ (which we call $\mathcal{J}_n(l,t)$ in the following formulas) are written as

$$\mathcal{J}_n(l,t) = \langle\psi_{\rm s}|\, {\rm e}^{{\rm i}(\mathcal{H}_0+\hat{\mathcal{H}}')t} J_n(l) {\rm e}^{-{\rm i}(\mathcal{H}_0+\hat{\mathcal{H}}')t}\, |\psi_{\rm s}\rangle\,, \tag{3.74}$$

where $|\psi_{\rm s}\rangle$ is the ground state in the Schödinger representation.

We insert the time evolution operator,

$$\begin{aligned} \hat{U}(t) =& {\rm e}^{{\rm i}\mathcal{H}_0 t}{\rm e}^{-{\rm i}(\mathcal{H}_0+\mathcal{H}')t}, \\ {\rm e}^{-{\rm i}\mathcal{H}_0 t}\hat{U}(t) =& {\rm e}^{-{\rm i}(\mathcal{H}_0+\mathcal{H}')t}, \end{aligned} \tag{3.75}$$

to Eq. (3.74) and we obtain

$$\begin{aligned} \mathcal{J}_n(l,t) &= \langle\psi_{\rm s}|\, \hat{U}^\dagger(t){\rm e}^{{\rm i}\mathcal{H}_0 t} J_n(l) {\rm e}^{-{\rm i}\mathcal{H}_0 t}\hat{U}(t)\, |\psi_{\rm s}\rangle \\ &= \langle\psi_{\rm s}|\, \hat{U}^\dagger(t) J_n(l,t) \hat{U}(t)\, |\psi_{\rm s}\rangle\,, \end{aligned} \tag{3.76}$$

where

$$\mathcal{A}(l,t) = {\rm e}^{{\rm i}\mathcal{H}_0 t}\mathcal{A}(l){\rm e}^{-{\rm i}\mathcal{H}_0 t}, \tag{3.77}$$

with $\mathcal{A}$ being an arbitrary operator.

Then, we move to an interaction picture and take the asymptotic limit to get a scattering state,

$$|\psi_{\rm s}\rangle = \mathcal{T}{\rm exp}\left[-{\rm i}\int_{-\infty}^{0} {\rm d}t'\mathcal{H}'(t')\right] |\psi_{\rm Hei}\rangle\,, \tag{3.78}$$

where $\mathcal{T}$ denotes the time ordering operator. We consider the time derivative of $U(t)$

$$\begin{aligned} \frac{\partial}{\partial t} U(t) =& -{\rm i}{\rm e}^{{\rm i}\mathcal{H}_0 t}\mathcal{H}'{\rm e}^{-{\rm i}(\mathcal{H}_0+\mathcal{H}')t} \\ =& -{\rm i}\mathcal{H}'(t)U(t). \end{aligned} \tag{3.79}$$

Then, we integrate both sides of the equation with respect to time and we obtain

$$U(t) = 1 - \mathrm{i}\int_0^t \mathrm{d}t' \mathcal{H}'(t') U(t'), \tag{3.80}$$

where we used

$$U(0) = 1. \tag{3.81}$$

We see that Eq. (3.80) has $U(t)$ in both sides of the equation. We obtain

$$U(t) = \sum_{n=0}^{\infty} (-\mathrm{i})^n \int_0^t \mathrm{d}t_1 \int_0^{t_1} \mathrm{d}t_2 \cdots \int_0^{t_{n-1}} \mathrm{d}t_n \mathcal{H}'(t_1)\mathcal{H}'(t_2)\cdots\mathcal{H}'(t_n), \tag{3.82}$$

by deforming Eq. (3.80). Using the time ordering operator $\mathcal{T}$, we now obtain

$$\begin{aligned} U(t) =& 1 + \sum_{n=1}^{\infty} \frac{(-\mathrm{i})^n}{n!} \int_0^t \mathrm{d}t_1 \int_0^{t_1} \mathrm{d}t_2 \cdots \int_0^{t_{n-1}} \mathrm{d}t_n \mathcal{T}\left[\mathcal{H}'(t_1)\mathcal{H}'(t_2)\cdots\mathcal{H}'(t_n)\right] \\ =& \mathcal{T}\exp\left[-\mathrm{i}\int_0^t \mathrm{d}t' \mathcal{H}'(t')\right]. \end{aligned} \tag{3.83}$$

We deform $\hat{U}(t)\left|\psi_{\mathrm{s}}\right\rangle$ by using Eq. (3.83) and Eq. (3.78), and we obtain

$$\begin{aligned} \hat{U}(t)\left|\psi_{\mathrm{s}}\right\rangle =& \mathcal{T}\exp\left[-\mathrm{i}\left(\int_0^t + \int_{-\infty}^0\right)\mathrm{d}t' \mathcal{H}'(t')\right]\left|\psi_{\mathrm{Hei}}\right\rangle, \\ =& \mathcal{T}\exp\left[-\mathrm{i}\int_{-\infty}^t \mathrm{d}t' \mathcal{H}'(t')\right]\left|\psi_{\mathrm{Hei}}\right\rangle \\ =& \mathcal{S}(-\infty, t)\left|\psi_{\mathrm{Hei}}\right\rangle, \end{aligned} \tag{3.84}$$

where we set $\mathcal{S}(-\infty, t)$ as

$$\begin{aligned} \mathcal{S}(-\infty, t) =& \mathcal{T}\exp\left[-\mathrm{i}\int_{-\infty}^t \mathrm{d}t' \hat{\mathcal{H}}'(t')\right] \\ =& 1 - \mathrm{i}\int_{-\infty}^t \mathrm{d}t' \mathcal{H}'(t') + O(\mathcal{H}'^2). \end{aligned} \tag{3.85}$$

We obtain $\mathcal{J}_n(l,t)$ by inserting Eq. (3.84) to Eq. (3.76)

$$\mathcal{J}_n(l,t) = \left\langle\psi_{\mathrm{Hei}}\right| \mathcal{S}^{\dagger}(-\infty, t) J_n(l,t) \mathcal{S}(-\infty, t)\left|\psi_{\mathrm{Hei}}\right\rangle. \tag{3.86}$$

We now approximate

$$\mathcal{S}(-\infty,t) \approx 1 - \mathrm{i}\int_{-\infty}^{t} \mathrm{d}t' \mathcal{H}'(t'), \tag{3.87}$$

for the linear response. We insert Eq. (3.87) to Eq. (3.86) and we obtain

$$\begin{aligned}
\mathcal{J}_n(l,t) \approx & \langle\psi_{\mathrm{Hei}}| \left[1 + \mathrm{i}\int_{-\infty}^{t} \mathrm{d}t' \mathcal{H}'(t')\right] J_n(l,t) \left[1 - \mathrm{i}\int_{-\infty}^{t} \mathrm{d}t' \mathcal{H}'(t')\right] |\psi_{\mathrm{Hei}}\rangle \\
= & \langle\psi_{\mathrm{Hei}}| J_n(l,t) |\psi_{\mathrm{Hei}}\rangle \\
& + \mathrm{i}\int_{-\infty}^{t} \mathrm{d}t' \langle\psi_{\mathrm{Hei}}| \left(\mathcal{H}'(t') J_n(l,t) - J_n(l,t)\mathcal{H}'(t')\right) |\psi_{\mathrm{Hei}}\rangle \\
= & \langle\psi_{\mathrm{Hei}}| J_{\mathrm{n}}(l,t) |\psi_{\mathrm{Hei}}\rangle \\
& + \mathrm{i}\int_{-\infty}^{t} \mathrm{d}t' \langle\psi_{\mathrm{Hei}}| \left[\mathcal{H}'(t'), J_n(l,t)\right] |\psi_{\mathrm{Hei}}\rangle .
\end{aligned} \tag{3.88}$$

We assume

$$\langle\psi_{\mathrm{Hei}}| J_n(l,t) |\psi_{\mathrm{Hei}}\rangle = 0, \tag{3.89}$$

since no spin current is expected to flow when there are no field gradients, and now we obtain

$$\begin{aligned}
\mathcal{J}_n(l,t) = & \mathrm{i}\int_{-\infty}^{t} \mathrm{d}t' \langle\psi_{\mathrm{Hei}}| \left[\mathcal{H}'(t'), J_n(l,t)\right] |\psi_{\mathrm{Hei}}\rangle \\
= & \mathrm{i}\int_{-\infty}^{\infty} \mathrm{d}t' \Theta(t-t') \langle\psi_{\mathrm{Hei}}| \left[\mathcal{H}'(t'), J_n(l,t)\right] |\psi_{\mathrm{Hei}}\rangle ,
\end{aligned} \tag{3.90}$$

where $\Theta(t-t')$ is the Heaviside step function.

Now, we insert Eqs. (3.69), (3.71) and (3.72) to Eq. (3.90), and we obtain

$$\begin{aligned}
\mathcal{J}_n(l,t) = & \mathrm{i}\sum_j \int_{-\infty}^{\infty} \mathrm{d}t' \Theta(t-t') \langle\psi_{\mathrm{Hei}}| \left[J_n(l,t), h_{\mathrm{s},j}(j,t')\right] |\psi_{\mathrm{Hei}}\rangle \Psi_{\mathrm{s}}(j,t') \\
& + \mathrm{i}\sum_j \int_{-\infty}^{\infty} \mathrm{d}t' \Theta(t-t') \langle\psi_{\mathrm{Hei}}| \left[J_n(l,t), h_{\mathrm{e},j}(t')\right] |\psi_{\mathrm{Hei}}\rangle \Psi_{\mathrm{e}}(j,t').
\end{aligned} \tag{3.91}$$

We can simplify Eq. (3.91)

$$\begin{aligned}
\mathcal{J}_n(l,t) = & \sum_{m=\mathrm{s,e}} \sum_j \int_{-\infty}^{\infty} \mathrm{d}t' \xi_{n,m}(l,j,t-t') \Psi_m(j,t'), \\
\xi_{n,m}(l,j,t-t') = & \mathrm{i}\Theta(t-t') \langle\psi_{\mathrm{Hei}}| \left[J_n(l,t), h_{m,j}(t')\right] |\psi_{\mathrm{Hei}}\rangle .
\end{aligned} \tag{3.92}$$

Then, we perform the Fourier transformation

$$\begin{aligned}\tilde{F}(l,\omega) &= \int_{-\infty}^{\infty} \mathrm{d}t F(l,t)\mathrm{e}^{\mathrm{i}\omega t},\\ F(l,t) &= \int_{-\infty}^{\infty} \frac{\mathrm{d}\omega}{2\pi}\tilde{F}(l,\omega)\mathrm{e}^{-\mathrm{i}\omega t},\end{aligned} \tag{3.93}$$

to Eq. (3.92), and we obtain

$$\begin{aligned}\mathcal{J}_n(l,\omega) &= \sum_{m=\mathrm{s,e}}\sum_j \int_{-\infty}^{\infty}\mathrm{d}t\int_{-\infty}^{\infty}\mathrm{d}t'\xi_{n,m}(l,j,t-t')\mathrm{e}^{\mathrm{i}\omega(t-t')}\Psi_m(j,t')\mathrm{e}^{\mathrm{i}\omega t'}\\ &= \sum_{m=\mathrm{s,e}}\sum_j \int_{-\infty}^{\infty}\mathrm{d}t_1\xi_{n,m}(l,j,t_1)\mathrm{e}^{\mathrm{i}\omega t_1}\int_{-\infty}^{\infty}\mathrm{d}t'\Psi_m(j,t')\mathrm{e}^{\mathrm{i}\omega t'}\\ &= \sum_{m=\mathrm{s,e}}\sum_j \xi_{n,m}(l,j,\omega)\Psi_m(j,\omega),\end{aligned} \tag{3.94}$$

where $t_1 = t - t'$.

For simplicity, $\xi_{n,m}(l,j,\omega)$ is transformed into

$$\begin{aligned}\xi_{n,m}(l,j,\omega) &= \mathrm{i}\int_{-\infty}^{\infty}\mathrm{d}t_1\Theta(t_1)\left\langle\psi_{\mathrm{Hei}}\right|\left[J_n(l,t),h_m(j,t-t_1)\right]\left|\psi_{\mathrm{Hei}}\right\rangle\mathrm{e}^{\mathrm{i}\omega t_1}\\ &= \mathrm{i}\int_0^{\infty}\mathrm{d}t_1\left\langle\psi_{\mathrm{Hei}}\right|\left[J_n(l,t_1),h_m(j,0)\right]\left|\psi_{\mathrm{Hei}}\right\rangle\mathrm{e}^{\mathrm{i}\omega t_1}.\end{aligned} \tag{3.95}$$

Then, we apply the Fourier transformation

$$\begin{aligned}\tilde{G}(\mathbf{q},\omega) &= \sum_l G(l,\omega)\mathrm{e}^{\mathrm{i}\mathbf{q}\cdot\mathbf{r}_l},\\ G(l,\omega) &= \frac{1}{N}\sum_{\mathbf{q}}\tilde{G}(\mathbf{q},\omega)\mathrm{e}^{-\mathrm{i}\mathbf{q}\cdot\mathbf{r}_l},\end{aligned} \tag{3.96}$$

and we obtain

$$\begin{aligned}\mathcal{J}_n(\mathbf{q},\omega) &= \sum_{m=\mathrm{s,e}}\sum_{l,j}\xi_{n,m}(l,j,\omega)\mathrm{e}^{\mathrm{i}\mathbf{q}\cdot\mathbf{r}_l}\Psi_m(j,\omega)\\ &= \sum_{m=\mathrm{s,e}}\sum_{l,j}\xi_{n,m}(l,j,\omega)\mathrm{e}^{\mathrm{i}\mathbf{q}\cdot\mathbf{r}_l}\left(\frac{1}{N}\sum_{\mathbf{p}}\Psi_m(\mathbf{p},\omega)\mathrm{e}^{-\mathrm{i}\mathbf{p}\cdot\mathbf{r}_j}\right)\\ &= \frac{1}{N}\left(\sum_{m=\mathrm{s,e}}\sum_{l,j}\sum_{\mathbf{p}}\xi_{n,m}(l,j,\omega)\mathrm{e}^{\mathrm{i}\mathbf{q}\cdot\mathbf{r}_l}\mathrm{e}^{-\mathrm{i}\mathbf{p}\cdot\mathbf{r}_j}\right)\Psi_m(\mathbf{p},\omega).\end{aligned} \tag{3.97}$$

Using the following equation

$$\begin{aligned}\sum_{\mathbf{p},l,j}\xi_{n,m}(l,j,\omega)\mathrm{e}^{\mathrm{i}(\mathbf{q}\cdot\mathbf{r}_l-\mathbf{p}\cdot\mathbf{r}_j)} &= \sum_{l,j}\sum_{\mathbf{p}}\langle\psi_{\mathrm{Hei}}|\left[J_n(l,t_1),h_m(j,0)\right]|\psi_{\mathrm{Hei}}\rangle\,\mathrm{e}^{\mathrm{i}(\mathbf{q}\cdot\mathbf{r}_l-\mathbf{p}\cdot\mathbf{r}_j)}\\ &= \sum_{\mathbf{p}}\langle\psi_{\mathrm{Hei}}|\left[J_n(\mathbf{q},t_1),h_m(0,-\mathbf{p})\right]|\psi_{\mathrm{Hei}}\rangle\\ &= \langle\psi_{\mathrm{Hei}}|\left[J_n(\mathbf{q},t_1),h_m(0,-\mathbf{q})\right]|\psi_{\mathrm{Hei}}\rangle\,,\end{aligned} \tag{3.98}$$

Eq. (3.97) is deformed into

$$\begin{aligned}\mathcal{J}_n(\mathbf{q},\omega) &= \sum_{m=\mathrm{s,e}}\xi_{n,m}(\mathbf{q},\omega)\Psi_m(\mathbf{q},\omega)\\ \xi_{n,m}(\mathbf{q},\omega) &= \frac{\mathrm{i}}{N}\int_0^\infty \mathrm{d}t_1\,\langle\psi_{\mathrm{I}}|\left[J_n(\mathbf{q},t_1),h_m(-\mathbf{q},0)\right]|\psi_{\mathrm{I}}\rangle\,\mathrm{e}^{\mathrm{i}\omega t_1}.\end{aligned} \tag{3.99}$$

We now perform an integration over $\xi_{n,m}(\mathbf{q},\omega)$

$$\begin{aligned}\xi_{n,m}(\mathbf{q},\omega) =& \frac{\mathrm{i}}{N}\int_0^\infty \mathrm{d}t_1\,\langle\psi_{\mathrm{Hei}}|\left[J_n(\mathbf{q},t_1),h_m(-\mathbf{q},0)\right]|\psi_{\mathrm{Hei}}\rangle\,\mathrm{e}^{\mathrm{i}(\omega+\mathrm{i}\delta)t_1}\\ =& -\frac{1}{N(\omega+\mathrm{i}\delta)}\langle\psi_{\mathrm{Hei}}|\left[J_n(\mathbf{q},0),h_m(-\mathbf{q},0)\right]|\psi_{\mathrm{Hei}}\rangle\\ & -\frac{1}{N(\omega+\mathrm{i}\delta)}\int_0^\infty \mathrm{d}t_1\,\langle\psi_{\mathrm{Hei}}|\left[J_n(\mathbf{q},t_1),\partial_t h_m(-\mathbf{q},0)\right]|\psi_{\mathrm{Hei}}\rangle\,\mathrm{e}^{\mathrm{i}(\omega+\mathrm{i}\delta)t_1},\end{aligned} \tag{3.100}$$

with convergence factor δ.

From here, we suppose that there is a current which satisfy the continuity equation in the Fourier representation

$$\partial_t h_m(-\mathbf{q},t) = \sum_{\mu=\hat{x},\hat{y},\hat{z}}\mathrm{i}q_\mu\cdot j_{m,\mu}(-\mathbf{q},t), \tag{3.101}$$

and we obtain

$$\begin{aligned}\xi_{n,m}(\mathbf{q},\omega) =& \sum_\mu\left[-\frac{\mathrm{i}}{N(\omega+\mathrm{i}\delta)}\left\langle\hat{T}_{n,m,\mu}\right\rangle\right.\\ & \left.-\frac{\mathrm{i}q_\mu}{N(\omega+\mathrm{i}\delta)}\int_0^\infty \mathrm{d}t_1\,\langle[J_n(\mathbf{q},t_1),j_{\mu,m}(-\mathbf{q},0)]\rangle\,\mathrm{e}^{\mathrm{i}(\omega+\mathrm{i}\delta)t_1}\right],\end{aligned} \tag{3.102}$$

where $\langle\mathcal{B}\rangle = \langle\psi|\,\mathcal{B}\,|\psi\rangle$ ($\mathcal{B}$ is an arbitrary operator), and

$$\left\langle \hat{T}_{n,m,\mu} \right\rangle = \langle [J_n(\mathbf{q},0), h_m(-\mathbf{q},0)] \rangle \,. \tag{3.103}$$

We now calculate the conductivity. The conductivity is obtained by calculating the real part of Eq. (3.100), therefore we focus on $\mathrm{Re}\,[\xi(\mathbf{q},\omega)]$. Using the Kramers-Kronig relations:

$$\frac{1}{\omega + \mathrm{i}\delta} = \mathrm{P}\left(\frac{1}{\omega}\right) - \mathrm{i}\pi\delta(\omega), \tag{3.104}$$

where P means the principal value, and we obtain

$$\begin{aligned}
\mathrm{Re}[\xi_{n,m}(\mathbf{q},\omega)] = \sum_{\mu} \Bigg[& \frac{\pi \left\langle \hat{T}_{n,m,\mu} \right\rangle}{N} \delta(\omega) \\
& - \frac{\mathrm{i}q_\mu \pi \delta(\omega)}{N} \mathrm{Im} \left[\int_0^\infty \mathrm{d}t_1 \, \langle [J_n(\mathbf{q},t_1), j_{m,\,\mu}(-\mathbf{q},0)] \rangle \, \mathrm{e}^{\mathrm{i}(\omega+\mathrm{i}\delta)t_1} \right] \\
& + \mathrm{P}\left(\frac{\mathrm{i}q_\mu}{N\,\omega}\right) \mathrm{Re} \left[\int_0^\infty \mathrm{d}t_1 \, \langle [J_n(\mathbf{q},t_1), j_{m,\,\mu}(-\mathbf{q},0)] \rangle \, \mathrm{e}^{\mathrm{i}(\omega+\mathrm{i}\delta)t_1} \right] \Bigg] .
\end{aligned} \tag{3.105}$$

For simplicity, we use $\zeta_{n,m,\mu}(\mathbf{q},\omega)$

$$\begin{aligned}
\zeta_{n,m}(\mathbf{q},\omega) &= \zeta'_{n,m}(\mathbf{q},\omega) + \mathrm{i}\zeta''_{n,m}(\mathbf{q},\omega), \\
\zeta'_{n,m}(\mathbf{q},\omega) &= \mathrm{Re} \left[\int_0^\infty \mathrm{d}t_1 \, \langle [J_n(\mathbf{q},t_1), j_{m,\,\mu}(-\mathbf{q},0)] \rangle \, \mathrm{e}^{\mathrm{i}(\omega+\mathrm{i}\delta)t_1} \right], \\
\zeta''_{n,m}(\mathbf{q},\omega) &= \mathrm{Im} \left[\int_0^\infty \mathrm{d}t_1 \, \langle [J_n(\mathbf{q},t_1), j_{m,\,\mu}(-\mathbf{q},0)] \rangle \, \mathrm{e}^{\mathrm{i}(\omega+\mathrm{i}\delta)t_1} \right],
\end{aligned} \tag{3.106}$$

where $\zeta'_{n,m}(\mathbf{q},\omega)$ and $\zeta''_{n,m}(\mathbf{q},\omega)$ satisfy the Kramers-Kronig relations

$$\begin{aligned}
\zeta'_{n,m}(\mathbf{q},\omega) &= \mathrm{P} \int_{-\infty}^{\infty} \frac{\mathrm{d}\omega'}{\pi} \frac{\zeta''_{n,m}(\mathbf{q},\omega)}{\omega' - \omega}, \\
\zeta''_{n,m}(\mathbf{q},\omega') &= \mathrm{P} \int_{-\infty}^{\infty} \frac{\mathrm{d}\omega}{\pi} \frac{\zeta'_{n,m}(\mathbf{q},\omega)}{\omega - \omega'}.
\end{aligned} \tag{3.107}$$

Eq. (3.105) is now deformed into

$$\mathrm{Re}[\xi_{n,m}(\mathbf{q},\omega)] = \sum_{\hat{\mu}} \frac{\mathrm{i}q_\mu}{N} \left[\left(\pi \left\langle \hat{T}_{m,n\,\hat{\mu}} \right\rangle - \zeta'_{m,n}(\mathbf{q},\omega) \right) \delta(\omega) + \zeta''_{m,n}(\mathbf{q},\omega) \right] . \tag{3.108}$$

Now, we calculate $\langle [J_n(\mathbf{q},t_1), j_{m,\mu}(-\mathbf{q},0)]\rangle$ to show $\zeta(\mathbf{q},\omega)$

$$\langle [J_n(\mathbf{q},t_1), j_{m,\mu}(-\mathbf{q},0)]\rangle = \langle [J_n(\mathbf{q},t_1) j_{m,\mu}(-\mathbf{q},0) - j_{m,\mu}(-\mathbf{q},0) J_n(\mathbf{q},t_1)]\rangle\,, \tag{3.109}$$

using the unit operator

$$\sum_n |n\rangle \langle n| = 1, \tag{3.110}$$

and we obtain (for $T = 0$)

$$\begin{aligned}\langle [J_n(\mathbf{q},t_1), j_{m,\mu}(-\mathbf{q},0)]\rangle = \sum_n \big(&\langle 0| J_n(\mathbf{q},t_1) |n\rangle \langle n| j_{m,\mu}(-\mathbf{q},0) |0\rangle \\ &- \langle 0| j_{m,\mu}(-\mathbf{q},0) |n\rangle \langle n| J_n(\mathbf{q},t_1) |0\rangle\big)\,,\end{aligned} \tag{3.111}$$

where $|0\rangle$ is the vacuum state. Then, we obtain

$$\begin{aligned}\zeta_{n,m}(\mathbf{q},\omega) &= \sum_{\hat{\mu}} \sum_n \left[\int_0^\infty \mathrm{d}t_1 \left(\langle 0| J_n(\mathbf{q},t_1) |k\rangle \langle k| j_{m,\mu}(-\mathbf{q},0) |0\rangle \right.\right. \\ &\qquad \left.\left. - \langle 0| j_{m,\mu}(-\mathbf{q},0) |k\rangle \langle k| J_n(\mathbf{q},t_1) |0\rangle\right) \mathrm{e}^{\mathrm{i}(\omega+\mathrm{i}\delta)t_1}\right] \\ &= -\sum_{\hat{\mu}} \sum_n \left[\frac{1}{\omega+\mathrm{i}\delta} \left(\langle 0| J_n(\mathbf{q},t_1) |k\rangle \langle k| j_{m,\mu}(-\mathbf{q},0) |0\rangle \right.\right. \\ &\qquad \left.\left. - \frac{1}{\omega+\mathrm{i}\delta} \langle 0| j_{m,\mu}(-\mathbf{q},0) |n\rangle \langle n| J_n(\mathbf{q},t_1) |0\rangle\right)\right],\end{aligned} \tag{3.112}$$

and

$$\begin{aligned}\langle 0| J_n(\mathbf{q},t_1) |k\rangle &= \langle 0| \mathrm{e}^{\mathrm{i}\hat{\mathcal{H}}t} J_n(\mathbf{q}) \mathrm{e}^{-\mathrm{i}\hat{\mathcal{H}}t} |k\rangle \\ &= \mathrm{e}^{-\mathrm{i}(E_k - E_0)t_1} \langle 0| J_n(\mathbf{q}) |k\rangle\,,\end{aligned} \tag{3.113}$$

where

$$\hat{\mathcal{H}} |k\rangle = E_k |k\rangle\,. \tag{3.114}$$

Then, we obtain $\zeta_{n,m}(\mathbf{q},\omega)$ as

$$\begin{aligned}\zeta_{n,m}(\mathbf{q},\omega) =& \int_0^\infty \mathrm{d}t_1 \left[\mathrm{e}^{\mathrm{i}(\omega-(E_m-E_0)+\mathrm{i}\delta)t_1} \sum_m \langle 0| J_n(\mathbf{q}) |m\rangle \langle m| j_{m,\mu}(-\mathbf{q}) |0\rangle \right. \\ & \left. - \sum_m \mathrm{e}^{\mathrm{i}(\omega+(E_m-E_0)+\mathrm{i}\delta)t_1} \langle 0| j_{m,\mu}(-\mathbf{q}) |m\rangle \langle m| J_n(\mathbf{q}) |0\rangle \right], \\ =& -\left[\mathrm{i} \sum_m \frac{\langle 0| J_n(\mathbf{q}) |m\rangle \langle m| j_{m,\mu}(-\mathbf{q}) |0\rangle}{\omega-(E_m-E_0)+\mathrm{i}\delta} \right] \\ & + \left[\mathrm{i} \sum_m \frac{\langle 0| j_{m,\mu}(-\mathbf{q}) |m\rangle \langle m| J_n(\mathbf{q}) |0\rangle}{\omega+(E_m-E_0)+\mathrm{i}\delta} \right],\end{aligned} \tag{3.115}$$

and $\zeta'_{n,m}(\mathbf{q},\omega)$ as

$$\begin{aligned}\frac{\zeta'_{n,m}(\mathbf{q},\omega)}{\omega} =& \pi \sum_m \frac{\langle 0| J_n(\mathbf{q}) |m\rangle \langle m| j_{m,\mu}(-\mathbf{q}) |0\rangle}{\omega} \delta(\omega-(E_m-E_0)) \\ & - \pi \sum_m \frac{\langle 0| j_{m,\mu}(-\mathbf{q}) |m\rangle \langle m| J_n(\mathbf{q}) |0\rangle}{\omega} \delta(\omega+(E_m-E_0)),\end{aligned} \tag{3.116}$$

and using Eq. (3.107), we obtain

$$\zeta''(\mathbf{q},\omega'\to 0) = \mathrm{P}\int_{-\infty}^{\infty} \frac{\mathrm{d}\omega}{\pi} \frac{\zeta'(\mathbf{q},\omega)}{\omega}. \tag{3.117}$$

We now define the conductivity when a field gradient is along μ-direction $\sigma_{m,n,\mu}(\mathbf{q},\omega)$

$$\mathcal{J}_n(\mathbf{q},\omega) = \sum_m \sum_\mu L_{n,m,\mu}(\mathbf{q},\omega) \Psi_m(\mathbf{q},\omega) \mathrm{i} q_\mu, \tag{3.118}$$

where

$$\mathrm{Re}[L_{n,m,\mu}(\mathbf{q},\omega)] = \sigma_{n,m,\mu}(\mathbf{q},\omega), \tag{3.119}$$

$$\sigma_{n,m,\mu}(\mathbf{q},\omega) = D_{n,m,\mu}\delta(\omega) + \sigma_{n,m,\mu,\mathrm{reg}}(\mathbf{q},\omega) \tag{3.120}$$

These equations correspond to Eqs. (3.58), (3.54) and (3.59).

We now obtain the regular parts of conductivity $\sigma_{n,m,\mu,\mathrm{reg}}(\mathbf{q},\omega)$ in the Lehman representation

$$\begin{aligned}\sigma_{n,m,\mu,\mathrm{reg}}(\mathbf{q},\omega) =& \frac{\pi}{N}\sum_{k}\frac{\langle 0|\, J_n(\mathbf{q})\,|k\rangle\,\langle k|\, j_{m,\mu}(-\mathbf{q})\,|0\rangle}{\omega}\delta(\omega-(E_k-E_0))\\ &-\frac{\pi}{N}\sum_{m}\frac{\langle 0|\, j_{m,\mu}(-\mathbf{q})\,|k\rangle\,\langle k|\, J_n(\mathbf{q})\,|0\rangle}{\omega}\delta(\omega+(E_k-E_0)).\end{aligned} \tag{3.121}$$

and Drude weights $D_{n,m,\,\mu}$:

$$\begin{aligned}D_{n,m,\mu} =& \left\langle \hat{T}_{n,m\hat{\mu}}\right\rangle - I_{n,m,\mu,\mathrm{reg}}\\ I_{n,m,\mu,\mathrm{reg}} =& 2\int_0^\infty \mathrm{d}\omega\,\sigma_{n,m,\mu,\mathrm{reg}}(\mathbf{q},\omega),\end{aligned} \tag{3.122}$$

To obtain Eq. (3.121), we suppose only a conservation of magnetization, whose current operator is defined by the continuity equation of Eq. (3.101), in arbitrary magnetic insulators. In other words, this formalism is valid for the systems with conserved magnetization, regardless of lattice shapes or structure of spins. Thus, the formalism is applicable for systems with noncollinear spin structures as well as the one with collinear structures.

The author notes that we obtain dominant terms of the conductivity for qSLHAFs in the spin wave expansion by inserting $j_{n,\mu}$ to $j_{\mathrm{s},3/2,\mu}$ and $j_{\mathrm{e},5/2,\mu}$.

We are now able to calculate spin and thermal conductivity via current operators: $j_{\mathrm{s},i,i+\mu}$ and $j_{\mathrm{e},i-\hat{\mu}_1,i,i+\hat{\mu}_2}$. Leading terms of conductivity $\sigma_{m,n}(\mathbf{q},\omega)$ $[m,n=\mathrm{s},\mathrm{e}]$ is obtained by inserting $j_{\mathrm{s},\,3/2}(\mathbf{q})$ ($j_{\mathrm{s},i,i+\mu,\,3/2}$ in the Fourier representation) and $j_{\mathrm{e},5/2}(\mathbf{q})$ ($j_{\mathrm{e},i-\hat{\mu}_1,i,i+\hat{\mu}_2,5/2}$ in the Fourier representation) to $j_m(\mathbf{q})$, $j_n(\mathbf{q})$ of Eq. (3.121).

3.7.2 Off-Diagonal Conductivity in Zero Field

In this subsection, we show that the off-diagonal conductivity in qSLHAFs vanishes in zero field due to the symmetry.

As we have already discussed, we obtain the off-diagonal conductivity in qSL-

HAFs by inserting $j_{\mathrm{s},i,i+\mu}$ and $j_{\mathrm{e},i-\hat{\mu}_1,i,i+\hat{\mu}_2}$ to Eq. (3.121). We obtain

$$\begin{aligned}\sigma_{\mathrm{e,s},\mu,\mathrm{reg}}(\omega) =& \frac{\pi}{N}\sum_k \frac{\langle 0|\, J_{\mathrm{s}}(\mathbf{q})\,|k\rangle\,\langle k|\, j_{\mathrm{e},\mu}(-\mathbf{q})\,|0\rangle}{\omega}\delta(\omega-(E_k-E_0)) \\ &- \frac{\pi}{N}\sum_m \frac{\langle 0|\, j_{\mathrm{e},\mu}(-\mathbf{q})\,|k\rangle\,\langle k|\, J_{\mathrm{s}}(\mathbf{q})\,|0\rangle}{\omega}\delta(\omega+(E_k-E_0)).\end{aligned} \tag{3.123}$$

We name

$$\begin{aligned}J_{\mathrm{s},i,\ \mathrm{even}} &= \sum_{\mu=\hat{x},\hat{y},\hat{z}} j_{\mathrm{s},i,i+\mu\ \mathrm{even}}, \\ J_{\mathrm{s},i,\ \mathrm{odd}} &= \sum_{\mu=\hat{x},\hat{y},\hat{z}} j_{\mathrm{s},i,i+\mu\ \mathrm{odd}},\end{aligned} \tag{3.124}$$

and Eq. (3.123) is deformed into

$$\begin{aligned}\sigma_{\mathrm{e,s},\mu,\mathrm{reg}}(\omega) =& \frac{\pi}{N}\sum_k \frac{\langle 0|\, J_{\mathrm{s\,even}}(\mathbf{q})\,|k\rangle\,\langle k|\, j_{\mathrm{e\,even},\mu}(-\mathbf{q})\,|0\rangle}{\omega}\delta(\omega-(E_k-E_0)) \\ &- \frac{\pi}{N}\sum_m \frac{\langle 0|\, j_{\mathrm{e},\mu\,\mathrm{even}}(-\mathbf{q})\,|k\rangle\,\langle k|\, J_{\mathrm{s\,even}}(\mathbf{q})\,|0\rangle}{\omega}\delta(\omega+(E_k-E_0)) \\ &+ \frac{\pi}{N}\sum_k \frac{\langle 0|\, J_{\mathrm{s\,odd}}(\mathbf{q})\,|k\rangle\,\langle k|\, j_{\mathrm{e},\mu\,\mathrm{odd}}(-\mathbf{q})\,|0\rangle}{\omega}\delta(\omega-(E_k-E_0)) \\ &- \frac{\pi}{N}\sum_m \frac{\langle 0|\, j_{\mathrm{e},\mu\,\mathrm{odd}}(-\mathbf{q})\,|k\rangle\,\langle k|\, J_{\mathrm{s\,odd}}(\mathbf{q})\,|0\rangle}{\omega}\delta(\omega+(E_k-E_0)),\end{aligned} \tag{3.125}$$

since all other terms vanish. Then, we insert Eq. (3.25) and Eq. (3.35), we see that the left hand side of Eq. (3.125) vanishes.

We now see that the off-diagonal conductivity vanishes

$$\sigma_{\mathrm{e,s},\mu,\mathrm{reg}}(\omega) = \sigma_{\mathrm{s,e},\mu,\mathrm{reg}}(\omega) = 0, \tag{3.126}$$

at $H = 0$. This is consistent to our discussions in Subsection 3.6.2.

3.8 Magneto-Thermal Conductivity at Finite Temperature

We have discussed the linear response theory in the low temperature limit ($T = 0$). Now, we discuss the spin conductivity in the case of finite temperatures by using the Matsubara method [3].

The current-current correlation function becomes

$$\begin{aligned} \xi_{n,m,\mu}(\mathbf{q},\tau) =& -\frac{1}{N}\left\langle T_\tau J_n^\dagger(\mathbf{q},\tau) j_{m,\mu}(\mathbf{q},\tau)\right\rangle, \\ \xi_{n,m,\mu}(\mathbf{q},\mathrm{i}\omega_n) =& \int_0^\beta \mathrm{d}\tau\ \xi_{n,m}(\mathbf{q},\tau)\mathrm{e}^{\mathrm{i}\omega_n\tau}, \end{aligned} \tag{3.127}$$

where β denotes the inverse temperature, $\tau = \mathrm{i}t$ and ω_n is the Matsubara frequency. We then perform

$$\mathrm{i}\omega_n \to \omega + \mathrm{i}\delta, \tag{3.128}$$

and we obtain

$$\xi_{n,m}(\mathbf{q},\mathrm{i}\omega_n) \to \xi_{n,m}(\mathbf{q},\omega). \tag{3.129}$$

Then, we obtain the regular part of conductivity

$$\begin{aligned} \sigma_{\mathrm{reg},n,m,\mu}(\omega) =& \frac{1}{N}\sum_{k,l}\frac{\langle k\left|J_n\right|l\rangle\langle l\left|j_{m,\mu}\right|k\rangle}{\omega}P_k\left(1-\mathrm{e}^{-\frac{E_l-E_k}{T}}\right)\delta(\omega-(E_l-E_k)), \\ P_k =& \frac{\mathrm{e}^{-\beta E_k/T}}{\sum_l \mathrm{e}^{-\beta E_l/T}}, \end{aligned} \tag{3.130}$$

and the Drude weights

$$\begin{aligned} D_{n,m,\mu} =& \left\langle \hat{T}_{n,m\hat{\mu}}\right\rangle - I_{\mathrm{reg}} \\ I_{n,m,\mathrm{reg},\mu} =& 2\int_0^\infty \mathrm{d}\omega\,\sigma_{\mathrm{reg},\,n,m}(\mathbf{q},\omega), \end{aligned} \tag{3.131}$$

and in other expressions,

$$D_{n,m,\mu} = \frac{1}{T^{n+1}}\sum_{k,l}\langle k\left|J_n\right|l\rangle\langle l\left|j_{m,\mu}\right|k\rangle P_k\left(1-\mathrm{e}^{-\frac{E_l-E_k}{T}}\right)\delta(\omega-(E_l-E_k)). \tag{3.132}$$

3.9 Sum Rules

In this section, we derive the integrated intensities of each conductivity. The linear response theory predicts that the integrated intensity becomes a constant of $\mathbf{q}$, ω

$$\left\langle \hat{T}_{n,m,\mu} \right\rangle = \int_{-\infty}^{\infty} \mathrm{d}\mathbf{q} \int_{-\infty}^{\infty} \mathrm{d}\omega \ \sigma_{n,m}(\mathbf{q},\omega), \tag{3.133}$$

for general systems. However, $\left\langle \hat{T}_{n,m,\mu} \right\rangle$ varies depending on m and n, and lattice shape, and we show $\left\langle \hat{T}_{n,m,\mu} \right\rangle$ in each conductivity.

The integrated intensity for each conductivity in one dimensional spin chain is shown in Refs. [62,65,126,140] and the intensity for spin conductivity in collinear magnets is shown in Ref. [87]. However, $\left\langle \hat{T}_{n,m,\mu} \right\rangle$ for spin and thermal conductivity in two-to three-dimensional system are unknown. In this thesis, we show $\left\langle \hat{T}_{n,m,\mu} \right\rangle$ which is applicable for any magnetic insulators as far as magnetization of the system is conserved. As far as the author's knowledge, this is first time to be shown the general forms of $\left\langle \hat{T}_{n,m,\mu} \right\rangle$. The author note that our general form is consistent with previously shown integrated intensity in one dimensional magnets [62, 65, 126, 140] and two dimensional collinear magnets [87]. Then, the intensity for each conductivity in qSLHAFs is shown.

3.9.1 Derivation of Sum Rule for Each Conductivity 1

We show the integrated intensity of each conductivity in the low temperature limit $I_{n,m}$. This is refereed to Refs. [14, 88, 94, 128].

The integrated intensity becomes

$$\begin{aligned} I_{n,m} =& \sum_{\mu} \frac{2N}{\pi} \int \mathrm{d}\mathbf{q} \int_0^{\infty} \mathrm{i}q_{\mu}\sigma_{n,m,\mu}(\mathbf{q},\omega)\mathrm{d}\omega \\ =& \sum_{l,\mu} \frac{\langle 0|J_n(\mathbf{q})|l\rangle \langle l\left|\mathrm{i}q_{\mu}\cdot j_{m,\mu}(-\mathbf{q})\right|0\rangle}{E_l - E_0} \\ & - \sum_{l,\mu} \frac{\langle 0\left|\mathrm{i}q_{\mu}\cdot J_{n,\mu}(-\mathbf{q})\right|l\rangle \langle l|J_m(\mathbf{q})|0\rangle}{-(E_l - E_0)}. \end{aligned} \tag{3.134}$$

Then, we insert the continuity equation Eq. (3.101) to Eq. (3.134) and we obtain

$$\begin{aligned} I_{n,m} =& \sum_{l} \frac{\langle 0|J_n(\mathbf{q})|l\rangle \langle l\left|\partial_t h_m(-\mathbf{q})\right|0\rangle}{E_l - E_0} \\ & + \sum_{l} \frac{\langle 0\left|\partial_t h_m(-\mathbf{q})\right|l\rangle \langle l|J_n(\mathbf{q})|0\rangle}{(E_l - E_0)}. \end{aligned} \tag{3.135}$$

We deform the equation into

$$\begin{aligned} I_{n,m} =& \sum_{l} \frac{(E_l - E_0)\langle 0|j_n(\mathbf{q})|l\rangle \langle l\left|h_m(-\mathbf{q})\right|0\rangle}{E_l - E_0} \\ & - \sum_{k,l} \frac{(E_l - E_0)\langle 0\left|h_m(-\mathbf{q})\right|l\rangle \langle l|J_n(\mathbf{q})|0\rangle}{(E_l - E_k)} \\ =& \mathrm{i}\sum_{l} \langle 0|J_n(\mathbf{q})|l\rangle \langle l\left|h_m(-\mathbf{q})\right|0\rangle \\ & - \mathrm{i}\sum_{l} \langle 0\left|h_m(-\mathbf{q})\right|l\rangle \langle l|J_n(\mathbf{q})|0\rangle \\ =& \mathrm{i}\left\langle J_n(\mathbf{q})h_m(-\mathbf{q}) - h_m(-\mathbf{q})J_n(\mathbf{q})\right\rangle, \\ =& \left\langle \mathrm{i}\left[J_n(\mathbf{q}), h_m(-\mathbf{q})\right]\right\rangle, \end{aligned} \tag{3.136}$$

where we use

$$\begin{aligned} \langle 0\left|\partial_t h_m(\mathbf{q})\right|l\rangle &= \left\langle 0\left|\mathrm{i}\left[\hat{H}, h_m(\mathbf{q})\right]\right|l\right\rangle \\ &= \mathrm{i}\left\langle 0\left|\hat{H}h_m(\mathbf{q}) - h_m(\mathbf{q})\hat{H}\right|l\right\rangle \\ &= \mathrm{i}(E_0 - E_l)\langle 0\left|h_m(\mathbf{q})\right|l\rangle. \end{aligned} \tag{3.137}$$

It is shown in the same way for $I_{m,n}$:

$$\begin{aligned} I_{m,n} =& -\mathrm{i}\sum_{l}\langle 0|h_n(-\mathbf{q})|l\rangle\,\langle l\,|J_m(\mathbf{q})|\,0\rangle \\ &+\mathrm{i}\sum_{l}\langle 0\,|J_m(\mathbf{q})|\,l\rangle\,\langle l|h_n(-\mathbf{q})|0\rangle \\ =& \langle \mathrm{i}\,[J_m(\mathbf{q}),h_n(-\mathbf{q})]\rangle\,. \end{aligned} \tag{3.138}$$

In this way, we obtain the integrated intensity for each conductivity

$$I_{\mathrm{s,s}} = \sum_{\mu}\mathrm{i}q_{\hat{\mu}}\left\langle \hat{T}_{\mathrm{s,s},\,\mu}\right\rangle = \langle \mathrm{i}[J_{\mathrm{s}}(\mathbf{q}),S^{z_0}(-\mathbf{q})]\rangle\,, \tag{3.139}$$

$$I_{\mathrm{e,e}} = \sum_{\mu}\mathrm{i}q_{\hat{\mu}}\left\langle \hat{T}_{\mathrm{e,e},\,\mu}\right\rangle = \left\langle \mathrm{i}[J_{\mathrm{e}}(\mathbf{q}),\hat{H}(-\mathbf{q})]\right\rangle, \tag{3.140}$$

$$I_{\mathrm{s,e}} = \sum_{\mu}\mathrm{i}q_{\hat{\mu}}\left\langle \hat{T}_{\mathrm{s,e},\,\mu}\right\rangle = \langle \mathrm{i}[J_{\mathrm{e}}(\mathbf{q}),S^{z_0}(-\mathbf{q})]\rangle\,, \tag{3.141}$$

$$I_{\mathrm{e,s}} = \sum_{\mu}\mathrm{i}q_{\hat{\mu}}\left\langle \hat{T}_{\mathrm{s,e},\,\mu}\right\rangle = \left\langle \mathrm{i}[J_{\mathrm{s}}(\mathbf{q}),\hat{H}(-\mathbf{q})]\right\rangle. \tag{3.142}$$

Eqs. (3.139), (3.140, (3.141, and (3.142) are valid for any noncollinear magnets as far as magnetization is conserved. We apply the formalism to SLHAFs in fields, which are to be discussed in the following subsections.

3.9.2 Derivation of Sum Rule for Each Conductivity 2

The satisfactions of sum rules for all conductivity are shown in this subsection. This subsection is along the lines of a proof in Ref. [88].

We simply integrate the conductivity and we obtain

$$\begin{aligned}\int_{-\infty}^{\infty} \mathrm{d}\omega \sigma_{n,m}(\mathbf{q},\omega) = &\left(\frac{\pi \left\langle \hat{T}_{n,m} \right\rangle}{N} - \frac{\pi\Omega}{N} \zeta''_{n,m}(\mathbf{q},\omega \to 0) \right) \\ &+ \mathrm{P} \int_{-\infty}^{\infty} \mathrm{d}\omega \frac{\pi}{N} \frac{\zeta'_{n,m}(\mathbf{q},\omega)}{\omega},\end{aligned} \tag{3.143}$$

and using the Kramers-Kronig relations, we obtain

$$\begin{aligned}\int_{-\infty}^{\infty} \mathrm{d}\omega \sigma_{\mathrm{s}}(\mathbf{q},\omega) &= \frac{\pi \left\langle \hat{T}_{n,m} \right\rangle}{N} - \frac{\pi}{N} \zeta''(\mathbf{q},\omega \to 0) + \frac{\pi}{N} \zeta''_{n,m}(\mathbf{q},\omega \to 0) \\ &= \frac{\pi \left\langle \hat{T}_{n,m} \right\rangle}{N}.\end{aligned} \tag{3.144}$$

3.9.3 Derivation of Sum Rule for Each Conductivity 3

In this subsection, we derive sum rules in other way. We set

$$\mathcal{O}(\mathbf{q},t) = \mathrm{e}^{\mathrm{i}\mathcal{H}t}\mathcal{O}_{\mathbf{q}}\mathrm{e}^{-\mathrm{i}\mathcal{H}t}, \tag{3.145}$$

as conserved quantity and we obtain

$$\mathcal{O}(\mathbf{q},t) = \mathcal{O}(\mathbf{q}) + \mathrm{i}t[\mathcal{H},\mathcal{O}(\mathbf{q})] - \frac{t^2}{2}[\mathcal{H},[\mathcal{H},\mathcal{O}(\mathbf{q})]] + \cdots. \tag{3.146}$$

Performing the differentiation by time, we obtain

$$\frac{\mathrm{d}}{\mathrm{d}t}\mathcal{O}(t) = \mathrm{i}[\mathcal{H},\mathcal{O}(\mathbf{q})], \tag{3.147}$$

$$\frac{\mathrm{d}^2}{\mathrm{d}t^2}\mathcal{O}(t) = \mathrm{i}[\mathcal{H},\mathrm{i}[\mathcal{H},\mathcal{O}(\mathbf{q})]]. \tag{3.148}$$

We see that this is the same shape as the continuity equations and the integrated intensity of Eqs. (3.139), (3.140), (3.141) and (3.142).

We insert $\mathcal{O}(\mathbf{q}) = h_2(\mathbf{q})$ and

$$\mathcal{H} = \sum_{<i,j>} \mathbf{S}_i \cdot \mathbf{S}_j - H\sum_i S_i^{z_0}, \tag{3.149}$$

to Eq. (3.147 and Eq. (3.148)). Then, we obtain

$$\begin{aligned}\frac{\mathrm{d}}{\mathrm{d}t}h_2(\mathbf{q},t) =& \mathrm{i}[\mathcal{H},h_2(\mathbf{q})] \\ =& -\sum_{\mu=\hat{x},\hat{y},\hat{z}} \mathrm{i}q_\mu(j_{\mathrm{e},\hat{\mu}}(\mathbf{q}) - Hj_{\mathrm{s},\hat{\mu}}(\mathbf{q})),\end{aligned} \tag{3.150}$$

where $(j_{\mathrm{e},\hat{\mu}}(\mathbf{q}) - Hj_{\mathrm{s},\hat{\mu}}(\mathbf{q}))$ is thermal current (Eq. (3.44)). We obtain the sum rule by

$$\begin{aligned}\frac{\mathrm{d}^2}{\mathrm{d}t^2}h_2(\mathbf{q},t) =& \mathrm{i}[\mathcal{H},\mathrm{i}[\mathcal{H},h_2(\mathbf{q})]] \\ =& \sum_{\mu=\hat{x},\hat{y},\hat{z}} \mathrm{i}q_\mu\left(\Theta_{\mathrm{e,e},\hat{\mu}} - 2H\Theta_{\mathrm{e,s},\hat{\mu}} + H^2\Theta_{\mathrm{s,s},\hat{\mu}}\right).\end{aligned} \tag{3.151}$$

We now obtained the spin current operatorsand energy current operators and the integrated intensities of each conductivity. The author has been shown several ways to define it and obtained the same results. This supports the reliability of methods.

3.10 Sum Rule for Each Conductivity in qSL-HAFs

In the previous section, we have shown the sum rule in general forms, which is robust for any magnetic insulators with conserved magnetization.

In this section, we calculate integrated intensities of each conductivity in SL-HAFs and CLHAFs. We deform the first term of Eq. (3.102)

$$\begin{aligned}
\mathrm{i}[J_{\mathrm{s}}(\mathbf{q}), S^{z_0}(-\mathbf{q})] =& \mathrm{i}\sum_{<i,j>}\sum_{l} J_{i,j}\left[S_i^{x_0}S_j^{y_0} - S_i^{y_0}S_j^{x_0}, S_l^{z_0}\right]\mathrm{e}^{\mathrm{i}\mathbf{q}\cdot(\mathbf{r_i}-\mathbf{r_l})} \\
=& \sum_{l,\hat{\mu}} J_{l,l+\hat{\mu}}(S_l^{x_0}S_{l+\hat{\mu}}^{x_0} + S_l^{y_0}S_{l+\hat{\mu}}^{y_0}) \\
& - \sum_{l,\hat{\mu}} J_{l,l+\hat{\mu}}(S_{l-\hat{\mu}}^{x_0}S_l^{x_0} + S_{l-\hat{\mu}}^{y_0}S_l^{y_0})\mathrm{e}^{-\mathrm{i}\mathbf{q}_{\hat{\mu}}} \\
=& \sum_{l,\hat{\mu}} J_{l,l+\hat{\mu}}(S_l^{x_0}S_{l+\hat{\mu}}^{x_0} + S_l^{y_0}S_{l+\hat{\mu}}^{y_0})(1-\mathrm{e}^{-\mathrm{i}\mathbf{q}_{\hat{\mu}}}) \\
=& (T_{\mathrm{s,s}\hat{x}}\,\mathrm{i}q_{\hat{x}} + T_{\mathrm{s,s}\hat{y}}\,\mathrm{i}q_{\hat{y}} + T_{\mathrm{s,s}\hat{z}}\,\mathrm{i}q_{\hat{z}})\,.
\end{aligned} \tag{3.152}$$

and we see that $T_{\mathrm{s,s},\,\hat{\mu}}$ in Eq. (3.152) is the same as that of Eq. (3.18). It means that the spin stiffness is proportional to the integrated intensities of spin conductivity [14, 94]. This is consistent to the previous works on integrated intensity for the spin conductivity in collinear magnets and conductivity in metals [88, 125–128].

The integrated intensity $\left\langle \hat{T}_{\mathrm{s,s}} \right\rangle$ is obtained by

$$\mathrm{i}\left[J_{\mathrm{s}}(\mathbf{q}), S^{z_0}(-\mathbf{q})\right] = \sum_{\mu} \hat{T}_{\mathrm{s,s},\mu}\,\mathrm{i}q_{\mu}, \tag{3.153}$$

and

$$\begin{aligned}
\hat{T}_{\mathrm{s,s},\mu} =& \sum_{i,\mu} J_{i,i+\mu}(S_i^{x_0}S_{i+\mu}^{x_0} + S_l^{y_0}S_{i+\mu}^{y_0}) \\
=& \sum_{i,\mu} J_{i,i+\mu}[\sin^2\theta S_i^x S_{i+\mu}^x - \cos^2\theta S_i^z S_{i+\mu}^z + S_i^y S_{i+\mu}^y] \\
& + \sum_{i,\mu} J_{i,i+\mu}\mathrm{e}^{\mathrm{i}\mathbf{Q}\cdot\mathbf{r}_i}\sin 2\theta(S_i^z S_{i+\mu}^x - S_i^x S_{i+\mu}^z).
\end{aligned} \tag{3.154}$$

Then, we perform HP expansion and the thermal average, we obtain

$$\begin{aligned}\frac{\left\langle \hat{T}_{\mathrm{s,s},\mu} \right\rangle}{JNS} =& -S\cos^2\theta + \left(\sin^2\theta + 1\right) m_\mu + \left(\sin^2\theta - 1\right)\Delta_\mu \\ &+ 2n\cos^2\theta + S\cos^2\theta + \sin^2\theta(n - m_\mu - \Delta_\mu),\end{aligned} \tag{3.155}$$

where we use

$$\begin{aligned}\Delta_{\hat{\mu}} &= \langle a_i a_{i+\hat{\mu}} \rangle\,, \\ m_{\hat{\mu}} &= \left\langle a_i^\dagger a_{i+\hat{\mu}} \right\rangle,\end{aligned} \tag{3.156}$$

Then, $[J_{\mathrm{e}}(\mathbf{q}), \hat{H}(-\mathbf{q})]$ is

$$\begin{aligned}\mathrm{i}[J_{\mathrm{e}}(\mathbf{q}), \hat{H}(-\mathbf{q})] =& \mathrm{i}\sum_{i,l} J_{\tau_1} J_{\tau_2} J_{\tau_3} \epsilon_{\mu_0,\xi_0,\lambda_0} \left[S^{\mu_0}_{i-\tau_1} S^{\xi_0}_i S^{\lambda_0}_{i+\tau_2}, \mathbf{S}_l \cdot \mathbf{S}_{l+\tau_3} \right] \mathrm{e}^{\mathrm{i}\mathbf{q}\cdot(\mathbf{r}_l - \mathbf{r}_i)} \\ =& -\sum_i \epsilon_{\mu,\xi,\lambda} J_{\tau_1} J_{\tau_2} J_{\tau_3} \\ & \{ S^{\mu_0}_{i-\tau_1} S^{\xi_0}_i [\mathrm{e}^{\mathrm{i}\mathbf{q}\cdot(\tau_2-\tau_3)} (S^{\mu_0}_{i+\tau_2-\tau_3} S^{\xi_0}_{i+\tau_2} - S^{\mu_0}_{i+\tau_2} S^{\xi_0}_{i+\tau_2-\tau_3}) \\ & \quad - \mathrm{e}^{\mathrm{i}\mathbf{q}\cdot\tau_2} (S^{\mu_0}_{i+\tau_2} S^{\xi_0}_{i+\tau_2+\tau_3} - S^{\mu_0}_{i+\tau_2+\tau_3} S^{\xi_0}_{i+\tau_2})] \\ & + S^{\mu_0}_{i-\tau_1} S^{\lambda_0}_{i+\tau_2} [(S^{\mu_0}_i S^{\lambda_0}_{i+\tau_3} - S^{\mu_0}_{i+\tau_3} S^{\lambda_0}_i) \\ & \quad - \mathrm{e}^{-\mathrm{i}\mathbf{q}\cdot\tau_3} (S^{\mu_0}_{i-\tau_3} S^{\lambda_0}_i - S^{\lambda_0}_{i-\tau_3} S^{\xi_0}_i)] \\ & + S^{\xi_0}_i S^{\lambda_0}_{i+\tau_2} [-\mathrm{e}^{-\mathrm{i}\mathbf{q}\cdot\tau_1} (S^{\xi_0}_{i-\tau_1} S^{\lambda_0}_{i-\tau_1+\tau_3} - S^{\xi_0}_{i-\tau_1+\tau_3} S^{\lambda_0}_{i-\tau_1}) \\ & \quad + \mathrm{e}^{-\mathrm{i}\mathbf{q}\cdot(\tau_3+\tau_1)} (S^{\xi_0}_{i-\tau_1-\tau_3} S^{\lambda_0}_{i-\tau_1} - S^{\lambda_0}_{i-\tau_1-\tau_3} S^{\xi_0}_{i-\tau_1})]\} \\ =& (T_{\mathrm{e,e}\,\hat{x}}\,\mathrm{i}q_{\hat{x}} + T_{\mathrm{e,e}\,\hat{y}}\,\mathrm{i}q_{\hat{y}} + T_{\mathrm{e,e}\,\hat{z}}\,\mathrm{i}q_{\hat{z}})\,.\end{aligned} \tag{3.157}$$

We deform $T_{\mathrm{e,e},\,\mu}$ into

$$\begin{aligned}T_{\mathrm{e,e},\,\mu} =& J\sum_i J_{\tau_1} J_{\tau_2} J_\mu \,[2(\mathbf{S}_{i-\tau_1} \times \mathbf{S}_i) \cdot (\mathbf{S}_{i+\mu} \times \mathbf{S}_{i+\mu+\tau_2}) \\ & + (\mathbf{S}_{i-\mu-\tau_2} \times \mathbf{S}_{i-\tau_2}) \cdot (\mathbf{S}_i \times \mathbf{S}_{i+\tau_1}) \\ & - 2(\mathbf{S}_{i-\mu} \times \mathbf{S}_{i-\mu+\tau_2}) \cdot (\mathbf{S}_i \times \mathbf{S}_{i+\tau_1}) \\ & + (\mathbf{S}_{i-\tau_1} \times \mathbf{S}_i) \cdot (\mathbf{S}_{i+\tau_2-\mu} \times \mathbf{S}_{i+\tau_2}) \\ & - (\mathbf{S}_{i-\mu} \times \mathbf{S}_i) \cdot (\mathbf{S}_{i-\tau_1} \times \mathbf{S}_{i+\tau_2})]\,.\end{aligned} \tag{3.158}$$

We now take the thermal average, and we obtain

$$\begin{aligned}\langle T_{\mathrm{e,e,}\,\mu}\rangle =& \cos^2 2\theta[7(m_{x+\tau}+\Delta_{x+\tau})-4(m_x+\Delta_x)\\ &-2(m_{x-\tau_1+\tau_2}+\Delta_{x-\tau_1+\tau_2})\\ &+(m_{x-\tau_1-\tau_2}+\Delta_{x-\tau_1-\tau_2})\\ &-3(m_{x+\tau_1+\tau_2}+\Delta_{x+\tau_1+\tau_2})+m_{x-\tau}+\Delta_{x-\tau}]\\ &+4\sin^2 2\theta[S-4n+2m_\tau+2\Delta_\tau]\\ &+32\sin^2\theta\cos 2\theta(n-m-\Delta)\\ &+\cos 2\theta[4(m_x-\Delta_x)+2(m_{x-\tau_1+\tau_2}-\Delta_{x-\tau_1+\tau_2})\\ &-(m_{x-\tau_1-\tau_2}-\Delta_{x-\tau_1-\tau_2})\\ &+3(m_{x+\tau_1+\tau_2}-\Delta_{x+\tau_1+\tau_2})+2m_{x-\tau}-2m_{x+\tau}]\\ &+7(m_{x+\tau}-\Delta_{x+\tau})+(m_{x-\tau}-\Delta_{x-\tau}),\end{aligned} \tag{3.159}$$

for qSLHAFs.

We use

$$\begin{aligned}\Delta_{\hat{\mu}\pm\tau} &= \langle a_i a_{i+\hat{\mu}\pm\tau}\rangle\,,\\ m_{\hat{\mu}\pm\tau} &= \left\langle a_i^\dagger a_{i+\hat{\mu}\pm\tau}\right\rangle,\end{aligned} \tag{3.160}$$

and

$$\begin{aligned}\Delta_{\hat{\mu}\pm\tau_1\pm\tau_2} &= \langle a_i a_{i+\hat{\mu}\pm\tau_1\pm\tau_2}\rangle\,,\\ m_{\hat{\mu}\pm\tau_1\pm\tau_2} &= \left\langle a_i^\dagger a_{i+\hat{\mu}\pm\tau_1\pm\tau_2}\right\rangle.\end{aligned} \tag{3.161}$$

We have used the following equations

$$\begin{aligned}&\left\langle S_i^{x_0}S_k^{x_0}S_j^{z_0}S_l^{z_0}+S_i^{z_0}S_k^{z_0}S_j^{x_0}S_l^{x_0}-S_i^{x_0}S_l^{x_0}S_j^{z_0}S_k^{z_0}-S_i^{z_0}S_l^{z_0}S_j^{x_0}S_k^{x_0}\right\rangle\\ =&(\sin^2\theta+\cos^2\theta\mathrm{e}^{\mathrm{i}\mathbf{Q}\cdot\mathbf{R}_{ij}})(\sin^2\theta+\cos^2\theta\mathrm{e}^{\mathrm{i}\mathbf{Q}\cdot\mathbf{R}_{kl}})\\ &(m_{ik}+\Delta_{ik}+m_{jl}+\Delta_{jl}-m_{jk}-\Delta_{jk}-m_{il}-\Delta_{il})\\ &+\sin^2\theta\cos^2\theta[(S-4n)+m_{ij}+\Delta_{ij}+m_{kl}+\Delta_{kl}],\end{aligned} \tag{3.162}$$

and

$$\begin{aligned}
&\big\langle (S_i^{x_0}S_k^{x_0}+S_i^{z_0}S_k^{z_0})S_j^{y_0}S_l^{y_0}+S_i^{y_0}S_k^{y_0}(S_j^{x_0}S_l^{x_0}+S_j^{z_0}S_l^{z_0})\\
&-(S_i^{x_0}S^{x_0}+S_i^{z_0}S^{z_0})_l S_j^{y_0}S_k^{y_0}-S_i^{y_0}S_l^{y_0}(S_j^{x_0}S_k^{x_0}+S_j^{z_0}S_k^{z_0})\big\rangle\\
&=S^3(\sin^2\theta+\cos^2\theta \mathrm{e}^{\mathrm{i}\mathbf{Q}\cdot\mathbf{r}_{ik}})(m_{jl}-\Delta_{jl})\\
&+S^3(\sin^2\theta+\cos^2\theta \mathrm{e}^{\mathrm{i}\mathbf{Q}\cdot\mathbf{r}_{jl}})(m_{ik}-\Delta_{ik})\\
&-S^3(\sin^2\theta+\cos^2\theta \mathrm{e}^{\mathrm{i}\mathbf{Q}\cdot\mathbf{r}_{il}})(m_{jk}-\Delta_{jk})\\
&-S^3(\sin^2\theta+\cos^2\theta \mathrm{e}^{\mathrm{i}\mathbf{Q}\cdot\mathbf{r}_{jk}})(m_{il}-\Delta_{il}).
\end{aligned} \tag{3.163}$$

The off- diagonal terms $\hat{T}_{\mathrm{e,s},\mu}$ are obtained by

$$\begin{aligned}
\mathrm{i}[J_{\mathrm{e}}(\mathbf{q}),S^{z_0}(-\mathbf{q})] &= \sum_{i,l,\tau,\tau_1,\tau_2} J_{i-\tau_2,i}J_{i,i+\tau_1}\epsilon_{\mu,\xi,\lambda}\mathrm{i}\left[S^{\mu_0}_{i-\tau_2}S^{\xi_0}_i S^{\lambda_0}_{i+\tau},S^{z_0}_l\right]\mathrm{e}^{\mathrm{i}\mathbf{q}\cdot(\mathbf{r}_l-\mathbf{r}_i)}\\
&=-\sum_{i,\tau_1,\tau_2}\big[-S_i^{x_0}(S^{z_0}_{i-\tau_2}S^{x_0}_{i+\boldsymbol{\tau_1}}-S^{x_0}_{i-\tau_2}S^{z_0}_{i+\boldsymbol{\tau_1}})\\
&\quad+S_i^{y_0}(S^{y_0}_{i-x}S^{z_0}_{i+\boldsymbol{\tau_1}}-S^{z_0}_{i-\tau_2}S^{y_0}_{i+\boldsymbol{\tau_1}})\\
&\quad+\mathrm{e}^{-\mathrm{i}\mathbf{q}\cdot\tau_2}S^{x_0}_{i-\boldsymbol{\tau_2}}(S_i^{z_0}S^{x_0}_{i+\boldsymbol{\tau_1}}-S_i^{x_0}S^{z_0}_{i+\boldsymbol{\tau_1}})\\
&\quad-\mathrm{e}^{-\mathrm{i}\mathbf{q}\cdot\tau_2}S^{y_0}_{i-\boldsymbol{\tau_2}}(S_i^{y_0}S^{z_0}_{i+\boldsymbol{\tau_1}}-S_i^{z_0}S^{y_0}_{i+\boldsymbol{\tau_1}})\\
&\quad+\mathrm{e}^{\mathrm{i}\mathbf{q}\cdot\tau_1}S^{x_0}_{i+\boldsymbol{\tau_1}}(S^{z_0}_{i-\tau_2}S_i^{x_0}-S^{x_0}_{i-\boldsymbol{\tau_2}}S_i^{z_0})\\
&\quad-\mathrm{e}^{\mathrm{i}\mathbf{q}\cdot\tau_1}S^{y_0}_{i+\boldsymbol{\tau_1}}(S^{y_0}_{i-\boldsymbol{\tau_2}}S_i^{z_0}-S^{z_0}_{i-\boldsymbol{\tau_2}}S_i^{y_0})\big]\\
&=-\sum_{i,\tau_1,\tau_2}\big[\mathbf{S}_i\times(\mathbf{S}_{i+\tau_1}\times\mathbf{S}_{i-\tau_2})+\mathrm{e}^{-\mathrm{i}\mathbf{q}\cdot\tau_2}\mathbf{S}_{i-\tau_2}\times(\mathbf{S}_i\times\mathbf{S}_{i+\tau_1})\\
&\qquad+\mathrm{e}^{\mathrm{i}\mathbf{q}\cdot\tau_1}\mathbf{S}_{i+\tau_1}\times(\mathbf{S}_{i-\tau_2}\times\mathbf{S}_i)\big],
\end{aligned} \tag{3.164}$$

We use the Jacobi identity

$$\mathbf{A}\times(\mathbf{B}\times\mathbf{C})+\mathbf{B}\times(\mathbf{C}\times\mathbf{A})+\mathbf{C}\times(\mathbf{B}\times\mathbf{A})=0, \tag{3.165}$$

we obtain

$$\begin{aligned}\left\langle \hat{T}_{\mathrm{e,s},\,\mu} \right\rangle &= \left\langle \sum_i \left[\mathbf{S}_{i-\mu} \times (\mathbf{S}_i \times \mathbf{S}_{i+\tau}) - \mathbf{S}_{i+\mu} \times (\mathbf{S}_{i-\tau} \times \mathbf{S}_i) \right]_{z_0} \right\rangle \\ &= \left\langle \sum_i [S^{z_0}_{i+\tau}(\mathbf{S}_{i-\mu} \cdot \mathbf{S}_i) + S^{z_0}_{i-\tau}(\mathbf{S}_{i+\mu} \cdot \mathbf{S}_i) - 2S^{z_0}_i(\mathbf{S}_{i-\tau} \cdot \mathbf{S}_{i+x})] \right\rangle \\ &= 4[(S-3n)\cos^2\theta + \sin^2\theta m_{\mu+\tau} - \cos^2\theta\Delta_{\mu+\tau} \\ &\quad + \cos^2\theta(m_\tau + \Delta_\tau) - \sin^2\theta m_\mu \\ &\quad + \cos^2\theta\Delta_\mu + (1 - 3\sin^2\theta)(n - m_\tau - \Delta_\tau)] \sin\theta S^2,\end{aligned} \tag{3.166}$$

where we use

$$\begin{aligned}\langle S^{z_0}_k \mathbf{S}_i \cdot \mathbf{S}_j \rangle &= \big\langle \sin\theta S^z_k [(\sin^2\theta + \cos^2\theta \mathrm{e}^{\mathrm{i}\mathbf{Q}\cdot\mathbf{R}_{i,j}})(S^x_i S^x_j + S^z_i S^z_j) + S^y_i S^y_j] \\ &\quad - \mathrm{e}^{\mathrm{i}\mathbf{Q}\cdot\mathbf{R}_k}(\mathrm{e}^{\mathrm{i}\mathbf{Q}\cdot\mathbf{R}_i} - \mathrm{e}^{\mathrm{i}\mathbf{Q}\cdot\mathbf{R}_j}) \sin\theta\cos^2\theta(S^z_i S^x_j S^x_k - S^x_i S^x_k S^z_j)\big\rangle \\ &= \sin\theta S^2[(\sin^2\theta + \cos^2\theta \mathrm{e}^{\mathrm{i}\mathbf{Q}\cdot\mathbf{R}_{i,j}})(S - 3n + m_{i,j} + \Delta_{i,j}) \\ &\quad + (m_{i,j} - \Delta_{i,j}) \\ &\quad + \mathrm{e}^{\mathrm{i}\mathbf{Q}\cdot\mathbf{R}_k}(\mathrm{e}^{\mathrm{i}\mathbf{Q}\cdot\mathbf{R}_i} - \mathrm{e}^{\mathrm{i}\mathbf{Q}\cdot\mathbf{R}_j})\cos^2\theta\{(m_{j,k} + \Delta_{j,k}) - (m_{i,k} + \Delta_{i,k})\}].\end{aligned} \tag{3.167}$$

The integrated intensity $\left\langle \hat{T}_{\mathrm{s,e}} \right\rangle$ is obtained by

$$\begin{aligned}\mathrm{i}\,[j_{\mathrm{s}}(\mathbf{q}), \mathcal{H}(-\mathbf{q})] &= \sum_{i,l,\hat{\mu}_1,\hat{\mu}_2} \mathrm{i}\left[S^{x_0}_i S^{y_0}_{i+\hat{\mu}_1}, \left(S^{x_0}_i S^{x_0}_{i+\hat{\mu}_2} + S^{y_0}_i S^{y_0}_{i+\hat{\mu}_2} + S^{z_0}_i S^{z_0}_{i+\hat{\mu}_2}\right)\right] \\ &\quad - \sum_{i,l,\hat{\mu}_1,\hat{\mu}_2} \mathrm{i}\left[S^{x_0}_i S^{x_0}_{i+\hat{\mu}}, \left(S^{x_0}_i S^{x_0}_{i+\hat{\mu}_2} + S^{y_0}_i S^{y_0}_{i+\hat{\mu}_2} + S^{z_0}_i S^{z_0}_{i+\hat{\mu}_2}\right)\right] \\ &= \sum_{i,\hat{\mu}_1,\hat{\mu}_2} \big[\mathbf{S}_i \times (\mathbf{S}_{i+\hat{\mu}_1} \times \mathbf{S}_{i+\hat{\mu}_1+\hat{\mu}_2})\,\mathrm{e}^{\mathrm{i}q_{\hat{\mu}_1}} - \mathbf{S}_{i+\hat{\mu}_1} \times (\mathbf{S}_i \times \mathbf{S}_{i+\hat{\mu}_2}) \\ &\qquad\qquad - \mathbf{S}_i \times (\mathbf{S}_{i+\hat{\mu}_1+\hat{\mu}_2} \times \mathbf{S}_{i+\hat{\mu}_1})\,\mathrm{e}^{\mathrm{i}(q_{\hat{\mu}_1}+q_{\hat{\mu}_2})}\big]_{z_0} \\ &= \sum_\mu T_{\mathrm{s,e},\,\mu}\mathrm{i}q_\mu.\end{aligned} \tag{3.168}$$

Then, we perform HP expansion, and the thermal average and we obtain

$$\begin{aligned}\frac{\mathrm{i}\left\langle[j_{\mathrm{s}}(\mathbf{q}),\mathcal{H}(-\mathbf{q})]\right\rangle}{(2+\beta)J^2NS^2\sin\theta} =&2\mathrm{i}\sum_{\mu_1,\mu_2}\Big[(q_{\mu_1}+q_{\mu_2})\Big[(S-3n)\cos^2\theta+m_{\mu_1+\mu_2}-\sin^2\theta m_{\tau_1}\\ &+\cos^2\theta(\Delta_{\mu_1}+\Delta_{\mu_2}+m_{\mu_2}-m_{\mu_1+\mu_2}-\Delta_{\mu_1+\mu_2})\Big]\\ &+(q_{\mu_1}-q_{\mu_2})\Big[(S-3n)\cos^2\theta+m_{\tau_1+\mu_2}-\sin^2\theta m_{\tau_1}\\ &+\cos^2\theta(\Delta_{\mu_1}+\Delta_{\mu_2}+m_{\mu_2}-m_{\mu_1-\mu_2}-\Delta_{\mu_1-\mu_2})\Big]\Big].\end{aligned} \tag{3.169}$$

We see from Eq. (3.169) the same result

$$\left\langle\hat{T}_{\mathrm{e,s},\,\mu}\right\rangle=\left\langle\hat{T}_{\mathrm{s,e},\,\mu}\right\rangle, \tag{3.170}$$

which indicates a satisfaction of the Onsager relation. Satisfactions of the Onsager relation of the integrated intensity are shown in one dimensional magnets [65], which is consistent to our results.

In the classical limit, integrated intensities of each conductivity are written by

$$\begin{aligned}\langle -T_{\mathrm{s,s},\,\mu}\rangle =&\pi JS^2\cos^2\theta,\\ \langle -T_{\mathrm{e,s},\,\mu}\rangle =&\langle -T_{\mathrm{s,e},\,\mu}\rangle=2\pi J^2(2+\beta)S^3\cos\theta\sin 2\theta,\\ \langle -T_{\mathrm{e,e},\,\mu}\rangle =&4\pi J^3(2+\beta)^2S^4\sin^2 2\theta.\end{aligned} \tag{3.171}$$

We see that the integrated intensity of the off-diagonal conductivity vanishes due to the symmetry.

3.11 Detecting Spin Conductivity

In this section, the relations between spin conductivity and dynamical spin susceptibility

$$S(\mathbf{q},\omega)=\frac{\mathrm{i}}{N}\int_0^\infty \mathrm{d}t_1\,\langle\psi_{\mathrm{Hei}}|\left[S^{z_0}_{\mathbf{q}}(t_1),S^{z_0}_{-\mathbf{q}}(0)\right]|\psi_{\mathrm{Hei}}\rangle\,\mathrm{e}^{\mathrm{i}\omega t_1}. \tag{3.172}$$

is shown. This section is on the basis of Ref. [45, 66, 141].

We integrate the right hand side of Eq. (3.172)

$$\begin{aligned}
S(\mathbf{q},\omega)=&-\frac{\mathrm{i}}{\mathrm{i}\omega N}\int_0^\infty \mathrm{d}t_1\left\langle\left[\partial_{t_1}S^{z_0}_{\mathbf{q}}(t_1),S^{z_0}_{-\mathbf{q}}(0)\right]\right\rangle\mathrm{e}^{\mathrm{i}\omega t_1}\\
=&-\frac{\mathrm{i}(1-\mathrm{e}^{\mathrm{i}\mathbf{q}\cdot\tau})}{\mathrm{i}\omega N}\int_0^\infty \mathrm{d}t_1\left\langle\left[J_{\mathrm{s}}(\mathbf{q},t_1),S^{z_0}_{-\mathbf{q}}(0)\right]\right\rangle\mathrm{e}^{\mathrm{i}\omega t_1}\\
=&\frac{\mathrm{i}(1-\mathrm{e}^{\mathrm{i}\mathbf{q}\cdot\tau})}{(\mathrm{i}\omega)^2 N}\left\langle\left[J_{\mathrm{s}}(\mathbf{q},0),S^{z_0}_{-\mathbf{q}}(0)\right]\right\rangle\\
&+\frac{-\mathrm{i}(1-\mathrm{e}^{\mathrm{i}\mathbf{q}\cdot\tau})(\mathrm{e}^{-\mathrm{i}\mathbf{q}\cdot\tau}-1)}{(\mathrm{i}\omega)^2 N}\int_0^\infty \mathrm{d}t_1\,\langle[J_{\mathrm{s}}(\mathbf{q},t_1),J_{\mathrm{s}}(-\mathbf{q},0)]\rangle\,\mathrm{e}^{\mathrm{i}\omega t_1},
\end{aligned} \tag{3.173}$$

and we now obtain

$$\mathrm{i}\omega S(\mathbf{q},\omega)=\xi_{\mathrm{s,s},\mu}(\mathbf{q},\omega). \tag{3.174}$$

We now see that the spin conductivity and dynamical spin susceptibility is related to each other by Eq. (3.174) [45, 66, 141]. Therefore, the spin conductivity is important to investigate the physical properties of magnets.

3.12 Results of Square and Cubic Lattice Heisenberg Antiferromagnets

In this section, we apply the formalism to SLHAFs and CLHAFs using the spin wave theory [25, 26], which is discussed in Chapter 2, and show results of the magneto-thermal conductivity [45, 94, 95]. Each conductivity is calculated at $T = 0$ limit in several h. Firstly, we show a satisfaction of sum rule and then, we show the integrated intensity versus h and each conductivity in h. This section is on the basis of Refs. [45, 94, 95].

3.12.1 Sum Rule for Each Conductivity

We apply the formalism of spin and energy transports to SLHAFs and CLHAFs in fields and calculate the conductivity by using the spin wave formalism [45,94,95]. Firstly, we show the satisfaction of sum rule to check the reliability of formalism.

The integrated intensity of the spin conductivity $I_{\rm s,s}$ (cyan line) and $\left\langle \hat{T}_{\rm s,s} \right\rangle$ (dashed red line) versus h is shown in Fig. 3.6 [14, 94]. These are results for SLHAFs in fields within the linear spin wave approximations and these results fit from zero to the saturation field. We see from Fig. 3.6 that $I_{\rm s,s}$ and $\left\langle \hat{T}_{\rm s,s} \right\rangle$ fit very well from zero field to the saturation field. This means that the sum rule is satisfied for SLHAFs in the linear spin wave approximations in $0 \leq h \leq 1$.

We have been checked that the sum rule is satisfied for allconductivity within the linear spin wave and the second order perturbation calculations. This satisfaction strongly indicates reliabilities of spin and energy current operatorand our formalism.

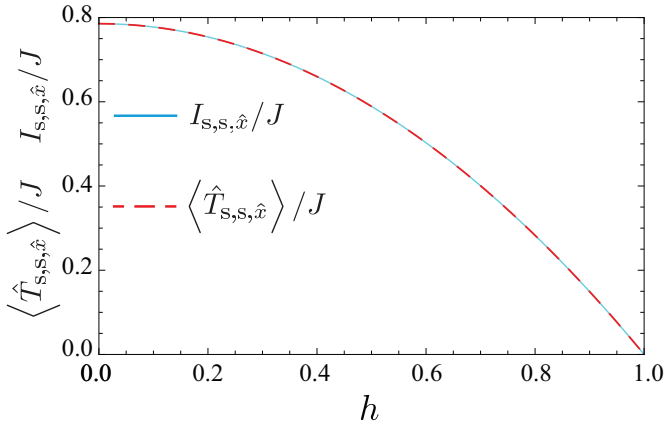

Figure 3.6: Calculated integrated intensity of $\sigma_{\mathrm{s,s},\hat{x}}(\mathbf{q},\omega)$: $I_{\mathrm{s,s},\hat{x}}$ and $\langle T_{\mathrm{s,s},\hat{\mathrm{x}}}\rangle$ of the leading therm of the spin wave calculations are shown. Cyan line indicates $I_{\mathrm{s,s},\hat{x}}$ and dashed red line indicates $\langle T_{\mathrm{s,s},\hat{\mathrm{x}}}\rangle$. The results are shifted for comparison but they fit completely. This figure is taken from Refs. [14, 94].

3.12.2 Integrated Intensity

The integrated intensities of each conductivity for SLHAFs and CLHAFs calculated by the spin wave theory are shown in this subsection.

The integrated intensity of $\langle T_{\mathrm{s,s},\,\hat{x}}\rangle$, $\langle T_{\mathrm{e,s},\hat{x}}\rangle$ and $\langle T_{\mathrm{e,e},\hat{x}}\rangle$ is shown in Figs. 3.7 (a) [14, 94, 95], (b) [95] and (c) [95]. The solid black line indicates results in the classical limit [the linear spin wave calculations] and dashed-blue (dotted-red) line is the conductivity with the $1/S$ corrections in SLHAFs (CLHAFs).

We see that $\langle T_{\mathrm{s,s},\mu}\rangle$ monotonically decrease to zero as the field increases to the saturation field because spins are locked toward the field direction. Non-monotonic response is observed when the $1/S$ corrections are taken into account. In low field, $\langle T_{\mathrm{s,s},\mu}\rangle$ is suppressed due to a shrinking of average lengths of spins (sublattice magnetization):

$$M_{\mathrm{sub}} = \frac{1}{N}\sum_i S_i^{z_0} \mathrm{e}^{\mathrm{i}\mathbf{Q}\cdot\mathbf{r}_i}. \tag{3.175}$$

Then, its length stretches as the field increases (see Fig. 3.8 [14]), this results in a recovery of spin conductivity. We see that $\langle T_{\mathrm{s,s}}\rangle$ in classical and with the $1/S$ corrections have the same value at $h \sim 0.25$, which is also observed for excitation spectrum in numerical [42] and the spin wave calculations [44].

In high magnetic fields, the effects from locking of spins play role. A competition between these two effects cause the non-monotonic behavior in two dimensional magnets. The same arguments are discussed on field dependence of spin stiffness in Ref. [42]. A shrinking of spin plays more important role in lower dimensional magnets. For $\beta = 1$ (CLHAFs), we no longer observe a non-monotonic behavior and the integrated intensity decreases monotonically since quantum corrections are much smaller than that of $\beta = 0$ (SLHAFs).

It is shown that $\langle T_{\mathrm{e,s},\,\hat{x}}\rangle$ vanishes in zero field. This is because the off-diagonal conductivity vanishes at zero field due to the symmetry [65, 67, 69]. It is observed that $\langle T_{\mathrm{e,s}\hat{x}}\rangle\,(=\langle T_{\mathrm{s,e},\,\hat{x}}\rangle) > 0$ in $h > 0$. Then, $\langle T_{\mathrm{e,s},\,\hat{x}}\rangle$ grows as the polarization grows and decrease in higher fields due to a rocking of spins toward field directions. We see that values of classical $\langle T_{\mathrm{e,s},\,\hat{x}}\rangle$ and the integrated intensity with the $1/S$ corrections have the same value at $h \sim 0.25$, which reason is the same as $\langle T_{\mathrm{s,s},\,\hat{x}}\rangle$.

The intensity $\langle T_{\mathrm{e,e},\,\hat{\mu}}\rangle$, where $\hat{\mu}$ denotes an arbitrary direction, vanishes in $h = 0$ and $T = 0$ but this result is not symmetry protected as for $\langle T_{\mathrm{e,s},\,\hat{\mu}}\rangle$. It is

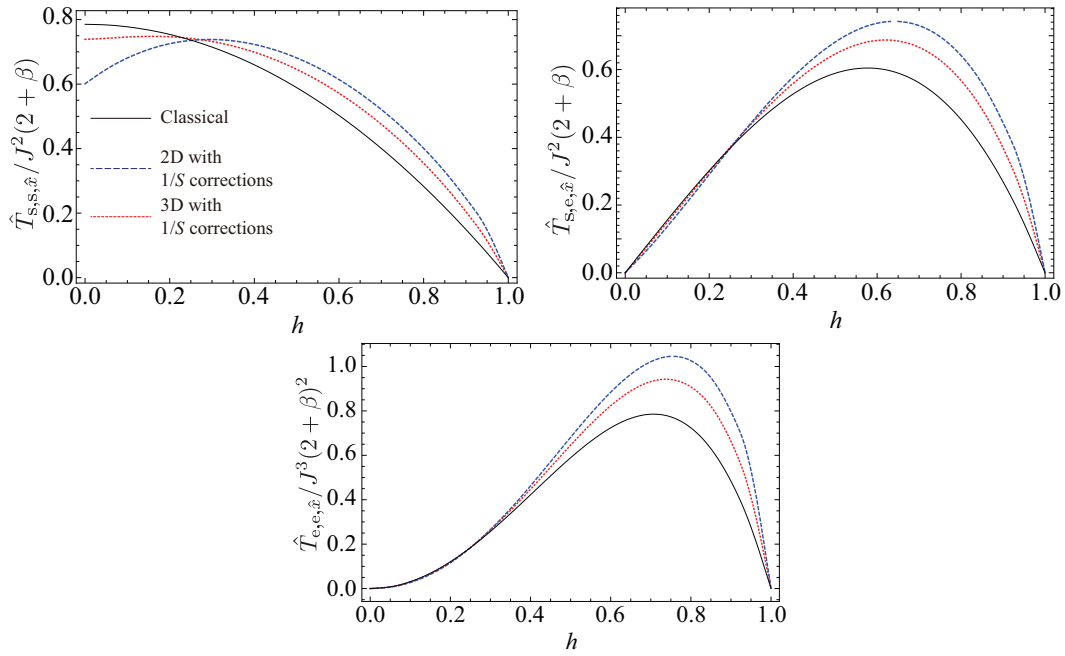

Figure 3.7: (a) Integrated intensity $\langle T_{\mathrm{s,s},\hat{x}} \rangle$ at $T = 0$ limit as a function of field is shown. Solid black line indicates results of the linear spin wave result (the classical limit), blue dashed (red-doted) line indicates results with the $1/S$ corrections of SLHAFs (CLHAFs). For the classical limit, $\langle T_{\mathrm{s,s},\hat{x}} \rangle$ decrease as a function of field due to the locking of spins toward the field direction while the integrated intensity with the $1/S$ correction is a non-monotonic function. The intensity is reduced by shrinking for the length of spins. The intensity grows in low fields due to the recovery of spin length. The intensity drops in high fields due to the locking of spins. (b) Integrated intensity $\langle T_{\mathrm{s,e},\hat{x}} \rangle$ at $T = 0$ limit as a function of field is shown. The intensity vanishes at $h = 0$ because of the symmetry. (c) Integrated intensity $\langle T_{\mathrm{e,e},\hat{x}} \rangle$ at $T = 0$ limit as a function of field is shown. The intensity also vanishes at $h = 0$ which is because the energy current cannot flow without flowing of a spin current at $T = 0$. The picture of (a) is taken from Refs. [14, 94, 95], the pictures of (b) and (c) are taken from Ref. [95].

shown that determinant:

$$\det \begin{vmatrix} \sigma_{\mathrm{s,s},\hat{\mu}}(\mathbf{q},\omega), & \sigma_{\mathrm{s,e},\hat{\mu}}(\mathbf{q},\omega) \\ \sigma_{\mathrm{e,s},\hat{\mu}}(\mathbf{q},\omega), & \sigma_{\mathrm{e,e},\hat{\mu}}(\mathbf{q},\omega) \end{vmatrix} = 0, \tag{3.176}$$

vanishes at $T = 0$ for all ω and h, which means that the energy current never

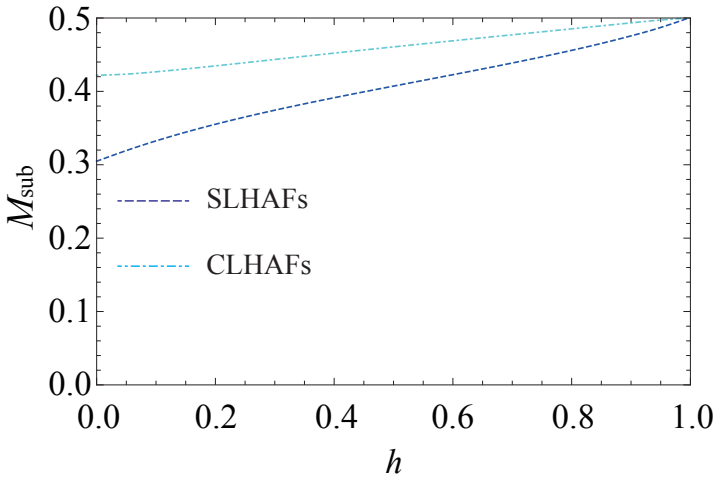

Figure 3.8: Sublattice magnetization in SLHAFs (CLHAFs) at $T = 0$ as a function of fields are shown in dashed blue (dash dotted cyan) line. In SLHAFs, the shrinking of sublattice magnetization is much larger than that of CLHAFs due to stronger quantum fluctuations. This figures is taken from Ref. [14].

flows independent to the spin current. In other words, thermal conductivity

$$\kappa_{\mathrm{th},\,\hat{\mu}}(\mathbf{q},\omega) = \frac{1}{T}\left(\sigma_{\mathrm{e,e},\,\hat{\mu}}(\mathbf{q},\omega) - \frac{\sigma_{\mathrm{s,e},\,\hat{\mu}}(\mathbf{q},\omega)^2}{\sigma_{\mathrm{s,s},\,\hat{\mu}}(\mathbf{q},\omega)}\right) \tag{3.177}$$

is always zero at $T = 0$. For $h = 0$ and at $T = 0$, $\sigma_{\mathrm{e,e}}(\mathbf{q},\omega)$ vanishes due to the vanishing of $\sigma_{\mathrm{e,s}}(\mathbf{q},\omega)$ for all ω. This is the reason of vanishing $\langle T_{\mathrm{e,e}}\rangle$ at $h = 0$.

We note that this is no longer true at $T \neq 0$. It is shown that the conductivity do not vanishes at $T > 0$ and $h = 0$ for one dimensional magnets in Refs. [62, 69]. Then, in the same reason as in $\langle T_{\mathrm{e,s}}\rangle$ that $\langle T_{\mathrm{e,e}}\rangle$ grows in low field and decrease to zero in high fields by a locking of spins.

3.12.3 Results of Frequency Dependent Conductivity

The conductivity of $\sigma_{\mathrm{s,s,}\hat{x}}(\mathbf{q},\omega)$, $\sigma_{\mathrm{e,s,}\hat{x}}(\mathbf{q},\omega)$ and $\sigma_{\mathrm{e,e,}\hat{x}}(\mathbf{q},\omega)$, where $\hat{x}$ is a bond direction gradients, in various fields for SLHAFs and CLHAFs are shown in this subsection.

Spin conductivity $\sigma_{\mathrm{s,s,}\hat{x}}(\mathbf{q},\omega)$ is shown in Fig. 3.9 (a) [95] and density of states (DOS) of the magnetic Brillouin zone by using the Lorentzian is shown in Fig. 3.9 (b) [95] for $h = 0.0$. Cyan-and blue-dot-dashed line indicates results of leading terms and the conductivity with the $1/S$ corrections in SLHAFs. Magenta and red-dashed line indicates the conductivity without and with the $1/S$ corrections in CLHAFs. Conductivities $\sigma_{\mathrm{s,e,}\hat{x}}(\mathbf{q},\omega)$, $\sigma_{\mathrm{e,e,}\hat{x}}(\mathbf{q},\omega)$ are not shown here since both vanish in $h = 0$. It is shown that the conductivity strongly reflects DOS and the Drude weight vanishes for the conductivity at $T = 0$. We see that a suppression of the conductivity by the $1/S$ corrections due to shrinking of a spin length [14, 45].

Conductivities $\sigma_{\mathrm{s,s,}\hat{x}}(\mathbf{q},\omega)$, $\sigma_{\mathrm{s,e,}\hat{x}}(\mathbf{q},\omega)$, $\sigma_{\mathrm{e,e,}\hat{x}}(\mathbf{q},\omega)$ and DOS is shown in Figs. 3.10 (a), (b), (c) and (d) for $h = 0.15$ [95]. Cyan and blue-dot-dashed line indicates results of the leading terms and with the $1/S$ corrections in SLHAFs. Magenta and red-dashed line indicates the conductivity without and with the $1/S$ corrections in CLHAFs. We see that these conductivity clearly reflect DOS. The area of conductivity varies by without and with the $1/S$ corrections and dimensionality to satisfy sum rules.

The calculations are done by inserting delta functions to Lorentzian:

$$\delta(\omega - \omega_0) \to \frac{\delta}{(\omega - \omega_0)^2 + \delta^2}, \tag{3.178}$$

and we put $\delta = 0.1$ for the calculations.

Conductivities $\sigma_{\mathrm{s,s,}\hat{x}}(\mathbf{q},\omega)$, $\sigma_{\mathrm{s,e,}\hat{x}}(\mathbf{q},\omega)$, $\sigma_{\mathrm{e,e,}\hat{x}}(\mathbf{q},\omega)$ and DOS of the magnetic Brillouin zone are shown in Figs. 3.11 (a), (b), (c) and (d) for $h = 0.3$ for SLHAFs an CLHAFs with and without the $1/S$ corrections [95]. The plot styles for each conductivity are the same as that of $h = 0.0$ and $h = 0.15$. Qualitatively the same results as $h = 0.3$ are observed. The small differences between dimensions and with and without the $1/S$ corrections are coming from change of DOS and integrated intensity of each conductivity by varying fields.

Conductivities $\sigma_{\mathrm{s,s,}\hat{x}}(\mathbf{q},\omega)$, $\sigma_{\mathrm{s,e,}\hat{x}}(\mathbf{q},\omega)$, $\sigma_{\mathrm{e,e,}\hat{x}}(\mathbf{q},\omega)$ and DOS of the magnetic Brillouin zone are shown in Figs. 3.12 (a), (b), (c) and (d) for $h = 0.6$ [95]. The plot styles are the same as that of $h = 0.0$, 0.15, 0.3. We see that the energy at Γ

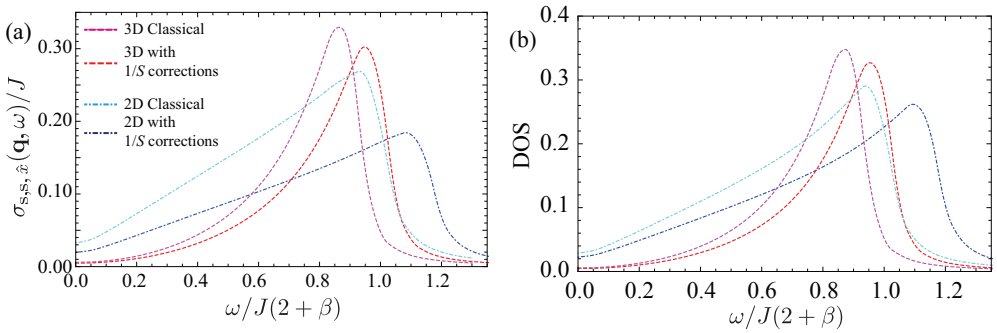

Figure 3.9: (a) $\sigma_{s,s,\hat{x}}(\mathbf{q},\omega)$ in $h=0$, where $\hat{x}$ is a direction of gradient along bonds, is shown. Cyan and blue dot-dashed line is a result of SLHAFs without and with the $1/S$ corrections. Magenta line and red dashed line are results of CLHAFs without and with the $1/S$ corrections. Threshold of the conductivity is determined by a band width. The van-Hove singularity for the magnetic Brillouin zone boundary is observed at high frequency region. The conductivity is suppressed by shrinking of spins in low fields. It is shown that each conductivity satisfy a sum rule. (b) Density of states (DOS) for the magnetic Brillouin zone is shown. We now see that the conductivity clearly reflects DOS. Figures (a) and (b) are taken from [95].

point determines a high frequency threshold at $\omega = 4(2+\beta)JSh$ and that of the magnetic Brillouin zone boundary is for a low frequency, $\omega = 2(2+\beta)JS$ in the classical limit. This is because $4(2+\beta)JSh > 2(2+\beta)JS$ a field region $h > 1/2$.

We see from Figs. 3.9 [95], 3.10 [95], 3.11 [95] and 3.12 [95] that each conductivity for various fields strongly reflects DOS [95]. In addition, these results are qualitatively the same though there are some differences by changing of DOS by fields. We see low frequency thresholds for $h = 0$, 0.15, 0.3 and high frequency threshold for $h = 0.6$ is at $\omega = 4(2+\beta)JSh$ which comes from the energy of Γ point, and high frequency thresholds for $h = 0$, 0.15, 0.3 comes from the magnetic Brillouin zone boundary. This is due to the band width of spin wave spectrum.

For the classical limit, an energy of the magnetic Brillouin zone boundary is $\omega = 2(2+\beta)JS$ [14, 94] but its energy shifts by taking the $1/S$ corrections into account [45]. The divergence around $\omega = 4(2+\beta)JS$ is caused by the van-Hove singularity at the magnetic Brillouin zone boundary. Frequency thresholds from the energy of Γ point: $\omega = 4(2+\beta)JSh(= H)$ do not move at all neither by the $1/S$ corrections nor the dimensionality. Shapes of conductivity vary depending on a dimensionality because of a changing for DOS.

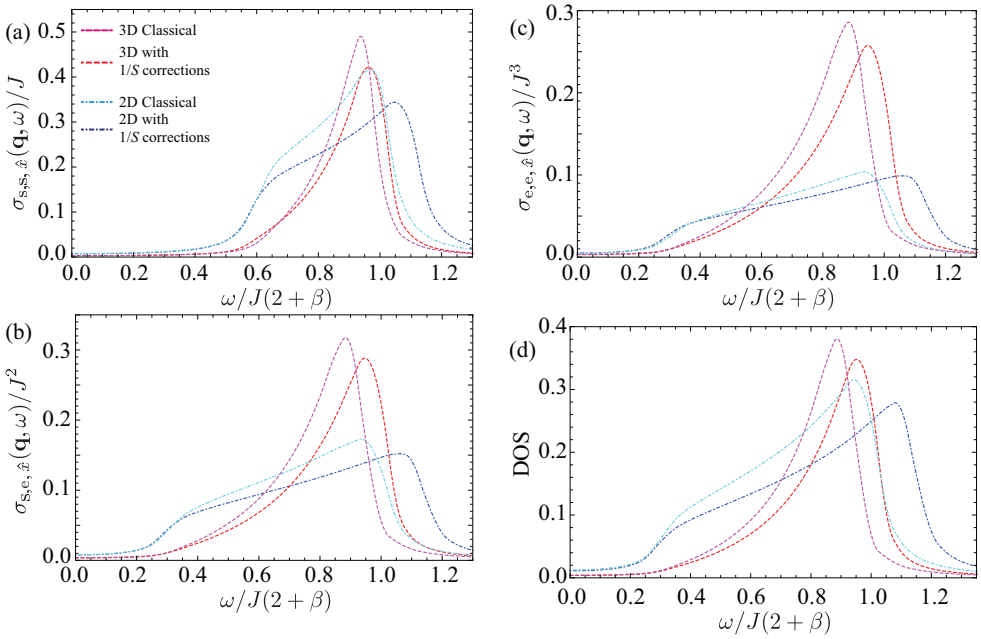

Figure 3.10: (a) The conductivity $\sigma_{\mathrm{s,s},\hat{x}}(\mathbf{q},\omega)$ in $h = 0.15$ is shown. Cyan and blue dot-dashed line is a result of SLHAFs without and with the $1/S$ corrections. Magenta line and red dashed line are results of CLHAFs without and with the $1/S$ corrections. Lower frequency thresholds of the conductivity is from the energy of Γ point. (b) The conductivity $\sigma_{\mathrm{s,e},\hat{x}}(\mathbf{q},\omega)$ in $h = 0.15$ is shown. (c) The conductivity $\sigma_{\mathrm{e,e},\hat{x}}(\mathbf{q},\omega)$ in $h = 0.15$ is shown. We see from (a), (b) and (c) that the dynamical conductivity has the same shape. (d) DOS in $h = 0.15$ is shown. We see that each conductivity reflects DOS. It has been checked that each conductivity satisfy sum rules. Figures (a), (b), (c) and (d) are taken from [95].

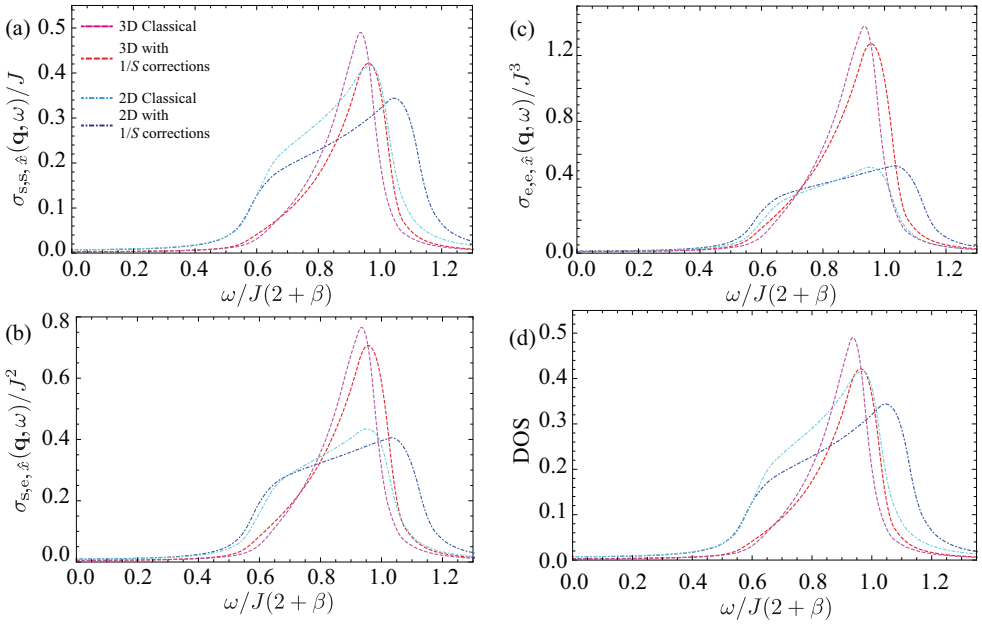

Figure 3.11: (a)The conductivity $\sigma_{\mathrm{s,s},\hat{x}}(\mathbf{q},\omega)$ in $h = 0.3$ is shown. The indexes of each line are the same as that of $h = 0$ and $h = 0.15$. (b) The conductivity $\sigma_{\mathrm{s,e},\hat{x}}(\mathbf{q},\omega)$ in $h = 0.3$ is shown. (c) The conductivity $\sigma_{\mathrm{e,e},\hat{x}}(\mathbf{q},\omega)$ in $h = 0.3$ is shown. (d) DOS in $h = 0.3$ is shown. Conductivities change as a result of the changes in DOS but qualitatively the same results are obtained. It is checked that the area of conductivity satisfies sum rule. Figures (a), (b), (c) and (d) are taken from [95].

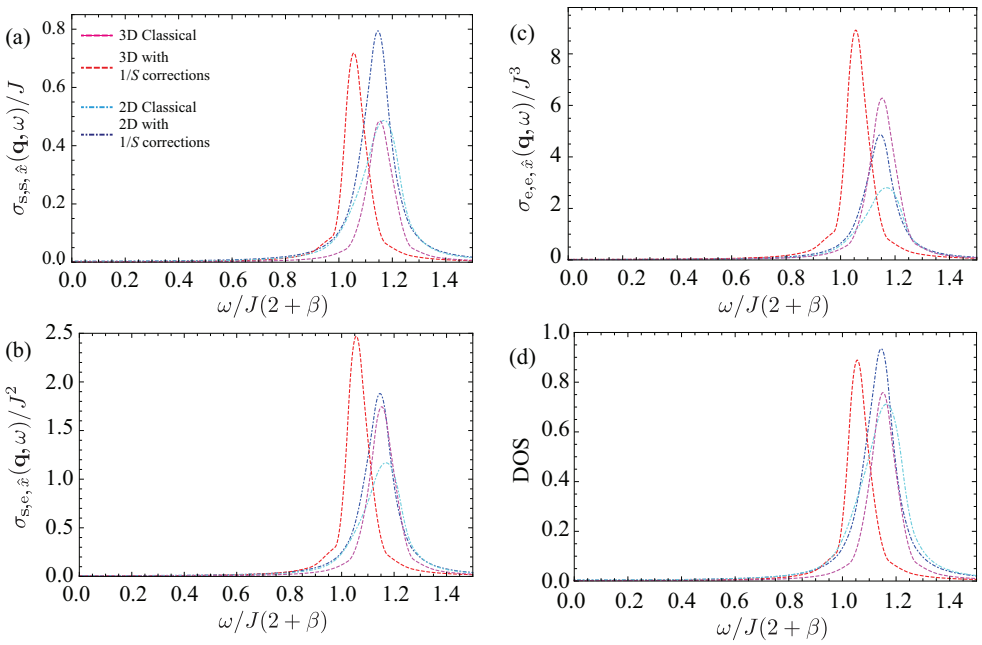

Figure 3.12: (a) The conductivity $\sigma_{\mathrm{s,s},\hat{x}}(\mathbf{q},\omega)$ in $h = 0.6$ is shown. The index of each line is the same as that of $h = 0$, $h = 0.15$ and $h = 0.3$. (b) The conductivity $\sigma_{\mathrm{s,e},\hat{x}}(\mathbf{q},\omega)$ in $h = 0.6$ is shown. (c) The conductivity $\sigma_{\mathrm{e,e},\hat{x}}(\mathbf{q},\omega)$in $h = 0.6$ is shown. (d) DOS in $h = 0.6$ is shown. The energy of *Gamma* point is now high frequency threshold of the conductivity and that of the magnetic Brillouin zone boundary is on the lower frequency threshold. Conductivities change reflecting changes of DOS but qualitatively the same results are obtained. It is checked that the conductivity satisfies sum rule. Figures (a), (b), (c) and (d) are taken from [95].

We also see that Drude weights vanish for all conductivity in various fields. The Drude weights are basically vanished for non-integrable models at $T = 0$, which reasons is discussed in detail using an example of the XXZ spin chain in Appendix B. Since SLHAFs and CLHAFs are non-integrable, vanishing Drude weights at $T = 0$ in this study is reasonable. In addition, the vanishing of Drude weights at $T = 0$ are observed also for spin conductivity in two- and three-dimensional magnets in Refs. [87–90], that are consistent to our results.

We have been checked that each conductivity satisfy sum rules in each fields with and without the $1/S$ corrections. This strongly indicates the reliability of our formalism. This formalism opens possibilities to study transports in various magnets including noncollinear magnets as far as the magnetization is conserved.

3.12.4 Comparison between Triangular- and Square-Lattice Heisenberg Antiferromagnets

In this subsection, $\sigma_{\mathrm{s,s},\hat{x}}(\mathbf{q},\omega)$ calculated in the classical limit at $T = 0$ in SLHAFs and Triangular lattice Heisenberg antiferromagnets (TLHAFs) (three-sublattice 120 degree structure) are compared. This is along the lines of Refs. [14, 94].

Spin conductivity $\sigma_{\mathrm{s,s},\hat{x}}(\mathbf{q},\omega)$ in the classical limit for SLHAFs and TLHAFs is shown in Fig. 3.13 [14, 94]. For the triangular lattice antiferromagnets, we use the spin wave formalism in Appendix C though there are some problems. We suppose the fluctuations of three-sublattice to be the same in this formalism. However, this assumption is not correct in the presence of magnetic fields and this method has some problems [14]. We set $\delta = 5 \times 10^{-3}$ of Eq. (3.178) for both SLHAFs and TLHAFs.

The author show $\sigma_{\mathrm{s,s},\hat{x}}(\mathbf{q},\omega)$ of SLHAFs at $h = 0$ (plotted in black line), $h = 0.375$ (plotted in blue line), and $h = 0.75$ (plotted in red line) in Fig. 3.13 (a) [14, 94]. We see that the conductivity clearly reflects DOS as being discussed in the previous subsection.

The author shows $\sigma_{\mathrm{s,s},\hat{x}}(\mathbf{q},\omega)$ of TLHAFs in Fig. 3.13 (b) [14, 94]. We set $h = H/9JS$ which is fields normalized by the saturation field $H_{\mathrm{s}} = 9JS$. The conductivity $\sigma_{\mathrm{s,s},\hat{x}}(\mathbf{q},\omega)$ at $h = 0$ is plotted in black line, $h = 1/9$ is plotted in blue line, and $h = 2/9$ is plotted in red line [14, 94].

The conductivity clearly reflects DOS and satisfies sum rules. We do not see any clear qualitative differences between SLHAFs and TLHAFs. Though there are problems for the spin wave calculations, we expect to get qualitatively the same results, reflecting DOS and satisfying sum rules, for the spin conductivity mediated by spins.

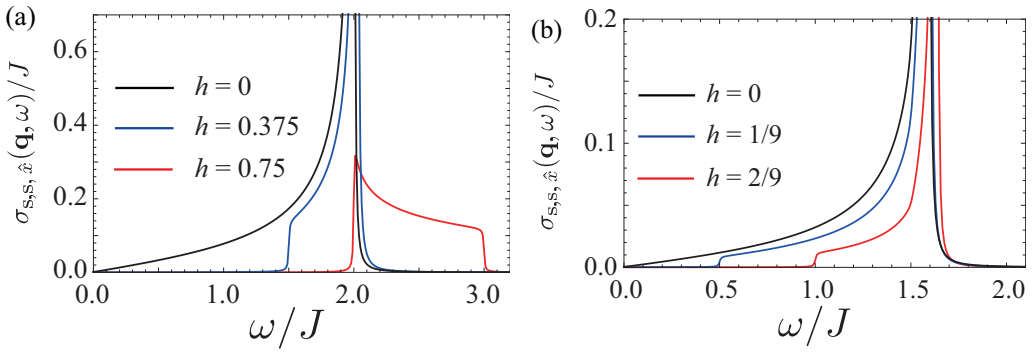

Figure 3.13: (a) Spin conductivity in various h for SLHAFs calculated in the classical limit. Black line is for $h = 0$ and Blue line is for $h = 0.375$ and red line is for $h = 0.75$. We see that thresholds for all conductivity are determined by its bandwidth. The energy of Γ point and that of the magnetic Brillouin zone boundary determines the threshold frequency. This figure is cited from Refs. [14, 94]. (b) Spin conductivity in various h for TLHAFs in the classical limit. In the same way as SLHAFs, we obtain the conductivity threshold determined by energy of the Γ point and the magnetic Brillouin zone boundary. This figure is cited from Refs. [14, 94].

3.13 Summary

Thanks to the previous theoretical and experimental investigation, it is now shown that spins in magnets carry spin and thermal conductivity. Nowadays, they are trying to manipulate the spin current. However, one of the biggest problems for developments of spin and thermal conductivity is how to define spin current operators. This is because spins are not always conserved quantity unlike charge. The previous studies on spin and thermal conductivity are restricted to the system, where spins and fields are collinear or one-dimensional magnets using a conservation of magnetization [60–62, 67, 87, 88].

We have defined a spin current operator which is applicable for noncollinear magnets as well as in collinear magnets [14, 94] using a conservation of magnetization. We have also defined energy current operators, which is applicable for noncollinear as well as collinear systems. The sum rules for each calculated conductivity are shown to be satisfied in qSLHAFs by using the spin wave theory and the linear response theory. This supports a reliability of our formalism. We believe that this definition is applicable as far as magnetization is conserved and it broadens possibilities for theoretically studying magneto-thermal conductivity.

We have applied the definitions to qSLHAFs at $T = 0$ limits at various fields. The integrated intensity $\left\langle \hat{T}_{\mathrm{s,s},\,\hat{x}} \right\rangle$ monotonically decrease as h increases for the classical limit. This is due to a rocking of spins toward the field direction, and the conductivity vanishes at the saturation field since spins cannot move at all. A reduction in spin conductivity $\sigma_{\mathrm{s,s}}(\mathbf{q}, \omega)$, which is due to the shrinking of spin length, has been observed by taking the $1/S$ corrections into account. The spin length recovers by field increases, which result in the conductivity increase at low field. A competition between effects for rocking of spins and length recoveries induce a non-monotonic response for the integrated intensity $\left\langle \hat{T}_{\mathrm{s,s},\,\hat{x}} \right\rangle$.

It is shown that the integrated intensity of off-diagonal conductivity $\left\langle \hat{T}_{\mathrm{s,e},\,\hat{x}} \right\rangle = \left\langle \hat{T}_{\mathrm{e,s},\,\hat{x}} \right\rangle$ vanishes at $h = 0$ due to the symmetry [65, 67, 69]. The integrated intensity $\left\langle \hat{T}_{\mathrm{s,e},\,\hat{x}} \right\rangle = \left\langle \hat{T}_{\mathrm{e,s},\,\hat{x}} \right\rangle$ grows as the field increases because a polarization of spins toward a field direction grows as we increase the field. Then, the magneto-thermal conductivity drops in high fields due to the rocking of spins. A competition between increasing polarization and locking of spins induces the non-monotonic behavior.

An integrated intensity of energy conductivity $\left\langle \hat{T}_{\mathrm{e,e},\hat{x}} \right\rangle$ vanishes at $T = 0$. This is true only for $T = 0$ and $\sigma_{\mathrm{e,e},\hat{x}}(\mathbf{q}, \omega)$ is expected to appear at $T \neq 0$. The vanishing of $\left\langle \hat{T}_{\mathrm{e,e},\hat{x}} \right\rangle$ is attributed to two reasons:

1. $\sigma_{\mathrm{s,e},\hat{x}}(\mathbf{q}, \omega)$ vanishes at $h = 0$ due to the symmetry [65, 67, 69],
2. Eq. (3.176), which means energy current cannot flow under the condition when there is no spin current flowing, is satisfied at $T = 0$.

The non-monotonic behavior of $\left\langle \hat{T}_{\mathrm{e,e},\hat{x}} \right\rangle$ has been explained in the same way as $\left\langle \hat{T}_{\mathrm{s,e},\hat{x}} \right\rangle = \left\langle \hat{T}_{\mathrm{e,s},\hat{x}} \right\rangle$.

The dynamical conductivity $\sigma_{n,m,\hat{x}}(\mathbf{q}, \omega)$ has upper and lower frequency thresholds. One is from an energy of the magnetic Brillouin zone boundary and the other is from the Γ point in the reciprocal space. The van-Hove singularity has been observed on the magnetic Brillouin zone threshold. The thresholds for each conductivity move by taking the $1/S$ corrections, which is due to the changes of spectrum shape. All conductivity varies by dimensions and fields due to the changes of DOS, but we obtain qualitatively the same results. We have checked that the sum rules are satisfied for each h and dimension in each conductivity. This indicates the reliability of our definitions for spin and thermal current operators, and formalism.

We believe that this formalism is valid in other systems as far as magnetization is conserved. Therefore, the method and definition opens possibilities to investigate the conductivity theoretically and it guides interpreting experimental results. We believe that theoretical investigations would make thermal conductivity easier be interpreted and more powerful tools to reveal an elementary excitations [83]. We expect that the formalism will help to reveal transport properties in magnets and will contribute to practical realization of spintronics.

Chapter 4

Summary and Conclusion

In this thesis, we have studied the spin wave spectrum on SLHAFs and discussed an existence of a high field phase, and then built formalism of magneto-thermal transports and applied the formalism to qSLHAFs by using the spin wave theory within the second order perturbation calculations [14,44,45,94]. We have focused on qSLHAFs in magnetic fields, which are one of the most basic and ideal models for studying the nature of noncollinear magnets.

The effects of three-magnon interactions, which play important roles in noncollinear antiferromagnets, have been investigated by the spin wave spectrum in qSLHAFs. The excitation spectrum of SLHAFs in zero field is well-known to be in good agreements with the linear spin wave results in zero field with quantitative corrections [11,108]. It was shown by Refs. [26,27,42,43,96,100] that dynamical physical properties qualitatively change and deviate from the linear spin wave results in SLHAFs at $h \gtrsim 0.75$. On the other hand, Refs. [25–27,41–43,96,97] show that static physical properties such as magnetization do not show any significant anomalies from zero to the saturation field.

We see from Mourigal *et al.* [27] that the strong $1/S$ corrections induce an unphysical 'negative excitation energy' at certain wave vectors at $h = 0.8$. Zhitomirsky and Chernyshev [26, 27], Mourigal *et al.* [27] and Fuhrman *et al.* [28] attribute 'negative excitation energy' to limitations of the second order perturbation calculations, and have tried to overcome the problem. However, they could not obtain reliable results which support their predictions.

In a response to these works [26–28], we have guessed that the unphysical result is attributed to an existence of a quantum phase, which is different from

a simple canted state, at $h \geq h_{\rm c}$ in a reminiscent of the Kohn anomaly [46]. We have investigated SLHAFs, and obtained clues of the quantum phase in $h \geq h_{\rm c}$ [14, 44, 45].

The excitation spectrum just below the critical field $h < h_{\rm c}$ has been studied in detail to obtain some clues for the new phase. A roton appears from $h \sim 0.75$ and its gap drops rapidly to zero by less than 1% increases of h. It is possible to detect the rotons and its softening by the specific heat and neutron scattering measurements on materials such as pyrazine family material [108, 113, 114]. The gap $\Delta_{\rm rot}$ drops to zero at $h = h_{\rm c} \sim 0.75$ and an unphysical 'negative excitation energy' appears at $h > h_{\rm c}$. This indicates a possibility for an existence of new phase.

We believe that the Bose-Einstein condensation occurs [110] and magnon freezes at $\mathbf{k} = \mathbf{k}_{\rm c}$ in $h = h_{\rm c}$. A new phase, which has incommensurate $\pi/k_{\rm rot}$ periodic structure, appears at $h > h_{\rm c}$.

However, this prediction based on the spin wave theory calculated within the second order perturbation calculation, which is a kind of approximation method. It means that our results include limitations of approximations. To clarify the existence of new phase, we should take the higher order perturbation terms into account or do non-biased numerical calculations such as Quantum Monte Carlo simulations. These are the future work of this thesis.

It has been shown that the three-magnon interactions are extremely strong on the intersection of the Γ-M line and the threshold of the magnon decay line. The roton appears at the intersection due to the strong interactions. It has been shown that roton gap $\Delta_{\rm rot}$ drops as a function of the roton wave vector $\mathbf{k}_{\rm rot}$. It means that a rapid and complete softening of roton is attributed to the strong three-magnon interactions induced by the positive curvature.

The cause of softening is a linear mode with positive curvature, which induces extremely strong three-magnon interactions. We believe that the appearance and softening of roton as a precursor for phase transition might also occur for other antiferromagnets in high fields. We expect that the recent experimental results of quantum phases in high fields [32, 35–40] might be related to the softening of rotons.

The nature for noncollinear antiferomagnets has also been studied via magntothermal transports. One of the biggest problems on studying the transports is how to define the spin current operators. As a way for avoiding problems, the

previous studies used the continuity equation of conserved quantities such as magnetization to define spin current operators. However, the method is applicable to the systems where spins and fields are collinear to each other [87–90].

We have defined a spin current operator, which is applicable for noncollinear magnets as well as collinear magnets when magnetization is conserved [14, 45, 94]. We have shown that the current operator has some terms written by even number of HP bosons, whose terms do not appear in collinear magnets [87, 88, 90]. We believe that it will make us possible to investigate the thermal conductivity in noncollinear magnets and help us understand experiments [76–86] by using our definition.

Here, we have applied the definition to qSLHAFs at $T = 0$ limit for various fields within the second order perturbation calculations and the linear response theory. We have derived an integrated intensity $\left\langle \hat{T}_{n,m} \right\rangle$ for each conductivity $\sigma_{n,m}(\mathbf{q}, \omega)$, which has been shown to satisfy sum rules. This fact supports a reliability of our definition.

For the classical limit, we have shown that the integrated intensity of spin conductivity $\left\langle \hat{T}_{\mathrm{s,s}} \right\rangle$ monotonically decreases as h grows. This is due to a locking of spins toward the field direction. Non-monotonic behaviors are observed when we take the $1/S$ corrections into account. A shrinking for spin length by quantum fluctuations reduces the spin conductivity. A spin length recovers by applying fields, and the conductivity $\left\langle \hat{T}_{\mathrm{s,s},\hat{x}} \right\rangle$ increases at low fields. A non-monotonic response of $\left\langle \hat{T}_{\mathrm{s,s},\hat{x}} \right\rangle$ is induced due to a rocking of spins and length recovery.

Integrated intensities for the off-diagonal part of the conductivity $\left\langle \hat{T}_{\mathrm{s,e},\hat{x}} \right\rangle = \left\langle \hat{T}_{\mathrm{e,s},\hat{x}} \right\rangle$ vanish at $h = 0$ because of the symmetry. A intensity $\left\langle \hat{T}_{\mathrm{s,e},\hat{x}} \right\rangle$ increases at low fields because of an increasing polarization for spins while the intensity $\left\langle \hat{T}_{\mathrm{s,e},\hat{x}} \right\rangle$ decrease at high fields due to the locking of spins toward the field direction.

The vanishing of intensity at $h = 0$ is also observed for $\left\langle \hat{T}_{\mathrm{e,e},\hat{x}} \right\rangle$, which is attributed to the vanishing of $\left\langle \hat{T}_{\mathrm{s,e},\hat{x}} \right\rangle$. A non-monotonic response of $\left\langle \hat{T}_{\mathrm{e,e},\hat{x}} \right\rangle$ for varying h is observed, whose cause is the same as that of $\left\langle \hat{T}_{\mathrm{s,e},\hat{x}} \right\rangle$.

Each dynamical conductivity $\sigma_{n,m}(\mathbf{q}, \omega)$ has been shown to reflect DOS in various fields, and qualitatively the same results are obtained except for the small differences of DOS. The conductivity $\sigma_{n,m}(\mathbf{q}, \omega)$ is suppressed by taking the $1/S$

corrections in low fields due to the shrinking of spin length. Energy at the Γ point in the reciprocal space and the magnetic Brillouin zone boundary determines thresholds of each conductivity. The van-Hove singularity which comes from the magnetic Brillouin zone boundary is observed.

We believe that our definition and formalism are robust for any other systems as far as the magnetization is conserved [14, 94]. We also believe that our formalism opens the possibilities to study the conductivity for any magnets with conserved magnetization. We are interested in applying this formalism to frustrated magnets which has strong quantum fluctuations. We believe that this formalism is a first step for interpreting the results of non-monotonic behaviors for thermal conductivity in frustrated magnets [76–86]. We expect that investigations through the magneto-thermal conductivity open the possibilities for practical developments and realizations of spintronics.

Appendix A

Conservation of Magnetization

A.1 Conservation of Magnetization for the XXZ Model

The conservation of magnetization in any XXZ antiferromagnets are shown in this section [14]. The Hamiltonian $\mathcal{H}$ and magnetization M is:

$$\begin{aligned}\mathcal{H} =& \frac{1}{N}\sum_{<i,j>} J_{i,j}\left[S_i^x S_j^x + S_i^y S_j^y + \Delta S_i^z S_j^z\right] - HM,\\ M =& \sum_i S_i^z.\end{aligned} \tag{A.1}$$

We see from Eq. (A.1) that this is generalized Hamiltonian which is robust for any lattice shape.

The commutation relations are

$$\begin{aligned}[\mathcal{H}, M] =& \sum_l \sum_{<i,j>} J_{i,j}\left([S_i^x S_j^x, S_l^z] + [S_i^y S_j^y, S_l^z]\right)\\ =& \sum_{<i,j>} \mathrm{i}J_{i,j}\left(-S_i^y S_j^x - S_i^x S_j^y + S_i^y S_j^x + S_i^x S_j^y\right) = 0.\end{aligned} \tag{A.2}$$

Now, we see that M is conserved in any XXZ magnets.

A.2 Conservation of Magnetization in qSLHAFs 1

The conservation of magnetization in qSLHAFs for Zhitomirsky, Nikuni and Chernyshev formalism [25–28, 96] is shown in this section [14].

A.2.1 Commutation Relations after Rotation of Quantization Axis

Here, we show that commutation relations are not changed by performing rotation of the quantization axis.

A commutation relation $[S_i^{x_0}, S_i^{y_0}]$ is:

$$\begin{aligned} \mathrm{i}[S_i^{x_0}, S_i^{y_0}] =& \mathrm{i}\left[S_i^x \sin\theta + S_i^z \mathrm{e}^{\mathrm{i}\mathbf{Q}\cdot\mathbf{R}_i}\cos\theta, S_i^y\right] \\ =& -\left(S_i^z \sin\theta - S_i^x \mathrm{e}^{\mathrm{i}\mathbf{Q}\cdot\mathbf{R}_i}\cos\theta\right) = -S_i^{z_0}, \end{aligned} \tag{A.3}$$

and a commutation relation $[S_i^{y_0}, S_i^{z_0}]$ is:

$$\begin{aligned} \mathrm{i}[S_i^{y_0}, S_i^{z_0}] =& \mathrm{i}\left[S_i^y, S_i^z \sin\theta - S_i^x \mathrm{e}^{\mathrm{i}\mathbf{Q}\cdot\mathbf{R}_i\cos\theta}\right] \\ =& -\left(S_i^x \sin\theta + S_i^z \mathrm{e}^{\mathrm{i}\mathbf{Q}\cdot\mathbf{R}_i}\cos\theta\right) = -S_i^{x_0}, \end{aligned} \tag{A.4}$$

and a commutation relation $[S_i^{z_0}, S_i^{x_0}]$ is:

$$\begin{aligned} \mathrm{i}[S_i^{z_0}, S_i^{x_0}] =& \mathrm{i}\left[S_i^z \sin\theta - S_i^x \mathrm{e}^{\mathrm{i}\mathbf{Q}\cdot\mathbf{R}_i}\cos\theta, S_i^x \sin\theta + S_i^z \mathrm{e}^{\mathrm{i}\mathbf{Q}\cdot\mathbf{R}_i}\cos\theta\right] \\ =& -S_i^y \left(\sin^2\theta + \cos^2\theta\right) = -S_i^{y_0}. \end{aligned} \tag{A.5}$$

We now see that commutation relations of the spin operators do not change after rotations of quantization axises.

A.2.2 Commutation Relations after the Holstein-Primakoff Transformations

In this subsection, we check that the spin operator obeys its commutation relation after the HP transformations.

Firstly, we check that commutation relations of spin operators. HP bosons satisfy:

$$\begin{aligned}[n_i, a_i] =& -[a_i, a_i^\dagger]a_i = -a_i, \\ [n_i, a_i^\dagger] =& a_i^\dagger [a_i, a_i^\dagger] = a_i^\dagger.\end{aligned} \tag{A.6}$$

We set

$$f(n_i) = \sqrt{1 - \frac{n_i}{2S}} = 1 - \frac{n_i}{4S} - \frac{n_i^2}{32S^2} + \cdots, \tag{A.7}$$

and we obtain:

$$\begin{aligned}a_i f(n_i) &= a_i \sqrt{1 - \frac{n_i}{2S}} = \sqrt{1 - \frac{n_i + 1}{2S}} a_i = f(n_i + 1) a_i, \\ a_i^\dagger f(n_i) &= a_i^\dagger \sqrt{1 - \frac{n_i}{2S}} = \sqrt{1 - \frac{n_i - 1}{2S}} a_i^\dagger = f(n_i - 1) a_i^\dagger.\end{aligned} \tag{A.8}$$

Using Eqs. (A.6, A.8), we obtain:

$$[S_i^-, S_i^z] = \sqrt{2S} \left[a_i^\dagger f(n_i), (S - n_i) \right] = \sqrt{2S}\, a_i^\dagger f(n_i) = S_i^-, \tag{A.9}$$

$$[S_i^+, S_i^z] = \sqrt{2S}\, [f(n_i) a_i, (S - n_i)] = -\sqrt{2S} f(n_i) a_i = -S_i^+, \tag{A.10}$$

and

$$\begin{aligned}[S_i^-, S_i^+] =& 2S [a_i^\dagger f(n_i), f(n_i) a_i] \\ =& 2S \left[a_i^\dagger \left(1 - \frac{n_i}{2S} \right) a_i - f(n_i) \left(1 + n_i \right) f(n_i) \right] \\ =& 2S \left[a_i^\dagger \left(1 - \frac{n_i}{2S} \right) a_i - \left(1 - \frac{n_i}{2S} \right) - a_i^\dagger \left(1 - \frac{n_i + 1}{2S} \right) a_i \right] \\ =& -2 \left(S - n_i \right) = -2 S_i^z.\end{aligned} \tag{A.11}$$

We see from Eqs. (A.10) and (A.11) that spin operators obey commutation relations of spins after the HF transformation.

A.3 Conservation of Magnetization in qSLHAFs 2

It has been shown in the previous subsection that the magnetization is conserved even after a rotation of the quantization axis and HF transformation since the commutation relation is satisfied even under the operations. However, we prove a conservation of magnetization in another way.

We divide magnetization M:

$$\begin{aligned} M &= \frac{1}{N}\sum_i S_i^{z_0} \\ &= \frac{1}{N}\sum_i (S-n_i)\sin\theta - \frac{1}{N}\sqrt{\frac{S}{2}}\sum_i \mathrm{e}^{\mathrm{i}\mathbf{Q}\cdot\mathbf{r}_i}[f(n_i)a_i + a_i^\dagger f(n_i)]\cos\theta, \end{aligned} \tag{A.12}$$

into two parts:

$$M = \frac{1}{N}\left(\mathcal{M}_z + \mathcal{M}_x\right), \tag{A.13}$$

where

$$\begin{aligned} \mathcal{M}_z &= \frac{1}{N}\sum_i (S-n_i)\sin\theta, \\ \mathcal{M}_x &= -\frac{1}{N}\sqrt{\frac{S}{2}}\sum_i \mathrm{e}^{\mathrm{i}\mathbf{Q}\cdot\mathbf{r}_i}[f(n_i)a_i + a_i^\dagger f(n_i)]\cos\theta. \end{aligned} \tag{A.14}$$

We divide Hamiltonian into four parts:

$$
\begin{aligned}
\mathcal{H} =&\hat{\mathcal{H}}_{\mathrm{a}}+\hat{\mathcal{H}}_{\mathrm{b}}+\hat{\mathcal{H}}_{\mathrm{c}}+\hat{\mathcal{H}}_{\mathrm{d}},\\
\mathcal{H}_{\mathrm{a}} =&S\sum_{<i,j>}J_{i,j}\left[\sin^2\theta a_i^\dagger f(n_i)f(n_j)a_j-\cos^2\theta a_i^\dagger a_j^\dagger f(n_i)f(n_j)\right]\\
&+S\sum_{<i,j>}J_{i,j}\left[\sin^2\theta a_j^\dagger f(n_i)f(n_j)a_i-\cos^2\theta f(n_i)f(n_j)a_ia_j\right],\\
\mathcal{H}_{\mathrm{b}} =&-\sum_{<i,j>}J_{i,j}\cos 2\theta(S-n_i)(S-n_j),\\
\mathcal{H}_{\mathrm{c}} =&\sqrt{\frac{S}{2}}\sin 2\theta\sum_{<i,j>}J_{i,j}\left[(S-n_i)a_j^\dagger f(n_j)-f(n_i)a_i(S-n_j)\right]\\
&-\sqrt{\frac{S}{2}}\sin 2\theta\sum_{<i,j>}J_{i,j}\left[(S-n_i)a_i^\dagger f(n_j)-f(n_i)a_j(S-n_j)\right],\\
\mathcal{H}_{\mathrm{d}} =&H\sum_i\left[\sqrt{\frac{S}{2}}\cos\theta \mathrm{e}^{\mathrm{i}\mathbf{Q}\cdot\mathbf{r}_i}(a_i^\dagger f(n_i)+f(n_i)a_i)\right]\\
&-H\sum_i\left[(S-n_i)\sin\theta\right]\\
=&-HM.
\end{aligned}
\tag{A.15}
$$

Then, we calculate the commutation relations of Hamiltonian and magnetization: $[H,M]$.

We calculate $[\mathcal{H}_{\mathrm{a}},\mathcal{M}]$. The commutation relation $[\mathcal{H}_{\mathrm{a}},\mathcal{M}_z]$ is:

$$
\begin{aligned}
\frac{N[\hat{\mathcal{H}}_{\mathrm{a}},\mathcal{M}_z]}{S} =&\sin^3\theta\sum_{l,<i,j>}J_{i,j}\left[a_i^\dagger f(n_i)f(n_j)a_j,(S-n_l)\right]\\
&+\sin^3\theta\sum_{l,<i,j>}J_{i,j}\left[a_j^\dagger f(n_i)f(n_j)a_i,(S-n_l)\right]\\
&-\cos^2\theta\sin\theta\sum_{l,<i,j>}J_{i,j}\left[a_i^\dagger a_j^\dagger f(n_i)f(n_j),(S-n_l)\right]\\
&-\cos^2\theta\sin\theta\sum_{l,<i,j>}J_{i,j}\left[f(n_i)f(n_j)a_ia_j,(S-n_l)\right]\\
=&S\cos\theta\sin 2\theta\sum_{<i,j>}J_{i,j}[f(n_i)f(n_j)a_ia_j-a_i^\dagger a_j^\dagger f(n_i)f(n_j)],
\end{aligned}
\tag{A.16}
$$

and $[\mathcal{H}_{\rm a}, \mathcal{M}_x]$ is:

$$\begin{aligned}\frac{N[\hat{\mathcal{H}}_{\rm a}, \mathcal{M}_x]}{S} =& \cos^3\theta\sqrt{\frac{S}{2}}\sum_{l,<i,j>} J_{i,j}\mathrm{e}^{\mathrm{i}\mathbf{Q}\cdot\mathbf{r}_l}\left[a_i^\dagger a_j^\dagger f(n_i)f(n_j), f(n_l)a_l + a_l^\dagger f(n_l)\right] \\ &+ \cos^3\theta\sqrt{\frac{S}{2}}\sum_{l,<i,j>} J_{i,j}\mathrm{e}^{\mathrm{i}\mathbf{Q}\cdot\mathbf{r}_l}\left[f(n_i)f(n_j)a_i a_j, f(n_l)a_l + a_l^\dagger f(n_l)\right] \\ &- \cos\theta\sin^2\theta\sqrt{\frac{S}{2}}\sum_{l,<i,j>} J_{i,j}\mathrm{e}^{\mathrm{i}\mathbf{Q}\cdot\mathbf{r}_l}\left[a_i^\dagger f(n_i)f(n_j)a_j, f(n_l)a_l + a_l^\dagger f(n_l)\right] \\ &- \cos\theta\sin^2\theta\sqrt{\frac{S}{2}}\sum_{l,<i,j>} J_{i,j}\mathrm{e}^{\mathrm{i}\mathbf{Q}\cdot\mathbf{r}_l}\left[a_j^\dagger f(n_i)f(n_j)a_i, f(n_l)a_l + a_l^\dagger f(n_l)\right] \\ =& \sqrt{\frac{S}{2}}\cos\theta\sum_{<i,j>} J_{i,j}\mathrm{e}^{\mathrm{i}\mathbf{Q}\cdot\mathbf{r}_i}\left[(S-n_j)a_i^\dagger f(n_i) - (S-n_i)a_j^\dagger f(n_j)\right] \\ &+ \sqrt{\frac{S}{2}}\cos\theta\sum_{<i,j>} J_{i,j}\mathrm{e}^{\mathrm{i}\mathbf{Q}\cdot\mathbf{r}_i}\left[(S-n_j)f(n_i)a_i - (S-n_i)f(n_j)a_j\right].\end{aligned} \tag{A.17}$$

Then, we calculate $[\mathcal{H}_{\rm b}, \mathcal{M}]$. The commutation relation $[\mathcal{H}_{\rm b}, \mathcal{M}_x]$ is:

$$\begin{aligned}\frac{N[\hat{\mathcal{H}}_{\rm b}, \mathcal{M}_x]}{S(\cos\theta - \sin\theta\sin 2\theta)} =& \sqrt{\frac{S}{2}}\sum_{l,<i,j>} J_{i,j}\mathrm{e}^{\mathrm{i}\mathbf{Q}\cdot\mathbf{r}_l}[(S-n_i)(S-n_j), a_l^\dagger f(n_l)] \\ &+ \sqrt{\frac{S}{2}}\sum_{l,<i,j>} J_{i,j}\mathrm{e}^{\mathrm{i}\mathbf{Q}\cdot\mathbf{r}_l}[(S-n_i)(S-n_j), f(n_l)a_l] \\ =& \sqrt{\frac{S}{2}}\sum_{<i,j>} J_{i,j}\mathrm{e}^{\mathrm{i}\mathbf{Q}\cdot\mathbf{r}_i}\left[(S-n_i)a_j^\dagger f(n_j) - (S-n_j)a_i^\dagger f(n_i)\right] \\ &- \sqrt{\frac{S}{2}}\sum_{<i,j>} J_{i,j}\mathrm{e}^{\mathrm{i}\mathbf{Q}\cdot\mathbf{r}_i}\left[(S-n_i)f(n_j)a_j - (S-n_j)f(n_i)a_i\right]\end{aligned} \tag{A.18}$$

where we have used

$$\cos\theta\cos 2\theta = \cos\theta - \sin\theta\sin 2\theta. \tag{A.19}$$

It is clear that

$$[\mathcal{H}_{\rm b}, \mathcal{M}_z] = 0. \tag{A.20}$$

We then calculate $[\mathcal{H}_{\rm c}, \mathcal{M}]$. The commutation relation $[\mathcal{H}_{\rm c}, \mathcal{M}_x]$ is:

$$\begin{aligned}\frac{N[\mathcal{H}_{\rm c}, \mathcal{M}_x]}{S\cos\theta\sin 2\theta} =& \frac{1}{2}\sum_{l,<i,j>} J_{i,j}\mathrm{e}^{\mathrm{i}\mathbf{Q}\cdot(\mathbf{r}_i+\mathbf{r}_l)}[(S-n_j)f(n_i)a_i, f(n_l)a_l + a_l^\dagger f(n_l)] \\ &- \frac{1}{2}\sum_{l,<i,j>} J_{i,j}\mathrm{e}^{\mathrm{i}\mathbf{Q}\cdot(\mathbf{r}_i+\mathbf{r}_l)}[(S-n_i)f(n_j)a_j, f(n_l)a_l + a_l^\dagger f(n_l)] \\ &+ \frac{1}{2}\sum_{l,<i,j>} J_{i,j}\mathrm{e}^{\mathrm{i}\mathbf{Q}\cdot(\mathbf{r}_i+\mathbf{r}_l)}[(S-n_j)a_i^\dagger f(n_i), f(n_l)a_l + a_l^\dagger f(n_l)] \\ &- \frac{1}{2}\sum_{l,<i,j>} J_{i,j}\mathrm{e}^{\mathrm{i}\mathbf{Q}\cdot(\mathbf{r}_i+\mathbf{r}_l)}[(S-n_i)a_j^\dagger f(n_j), f(n_l)a_l + a_l^\dagger f(n_l)] \\ =& -\sum_{<i,j>} J_{i,j}[f(n_i)f(n_j)a_i a_j - a_i^\dagger a_j^\dagger f(n_i)f(n_j)], \end{aligned} \tag{A.21}$$

and $[\mathcal{H}_{\rm c}, \mathcal{M}_z]$ is

$$\begin{aligned}\frac{N[\mathcal{H}_{\rm c}, \mathcal{M}_z]}{J\sin\theta\sin 2\theta} =& \sqrt{\frac{S}{2}}\sum_{l,<i,j>} \mathrm{e}^{\mathrm{i}\mathbf{Q}\cdot\mathbf{r}_i}(S-n_i)[a_j^\dagger f(n_j), (S-n_l)] \\ &- \sqrt{\frac{S}{2}}\sum_{l,<i,j>} \mathrm{e}^{\mathrm{i}\mathbf{Q}\cdot\mathbf{r}_i}(S-n_j)[a_i^\dagger f(n_i), (S-n_l)] \\ &+ \sqrt{\frac{S}{2}}\sum_{l,<i,j>} \mathrm{e}^{\mathrm{i}\mathbf{Q}\cdot\mathbf{r}_i}(S-n_i)[f(n_j)a_j, (S-n_l)] \\ &- \sqrt{\frac{S}{2}}\sum_{l,<i,j>} \mathrm{e}^{\mathrm{i}\mathbf{Q}\cdot\mathbf{r}_i}(S-n_j)[f(n_i)a_i, (S-n_l)] \\ =& \sqrt{\frac{S}{2}}\sum_{<i,j>} \mathrm{e}^{\mathrm{i}\mathbf{Q}\cdot\mathbf{r}_i}[(S-n_i)a_j^\dagger f(n_j) - (S-n_j)a_i^\dagger f(n_i)] \\ &- \sqrt{\frac{S}{2}}\sum_{<i,j>} \mathrm{e}^{\mathrm{i}\mathbf{Q}\cdot\mathbf{r}_i}[(S-n_i)f(n_j)a_j - (S-n_j)f(n_i)a_i]. \end{aligned} \tag{A.22}$$

It is clear from $\mathcal{H}_{\rm d}$ in Eq. (3.1) that

$$[\mathcal{H}_{\rm d}, M] = -H\,[M, M] = 0. \tag{A.23}$$

We now see that Eqs. (A.16) and (A.21) cancel each other, and Eqs. (A.17) Eqs. (A.18) and (A.22) also cancel each other, which means:

$$[\mathcal{H}, M] = 0, \tag{A.24}$$

and the magnetization is conserved in qSLHAFs even after the rotation of quantization axis and HF transformation. This conservation law still holds after the HF expansion.

Appendix B

Ballistic Conductivity in the Integrable XXZ Magnets

In this section, we discuss ballistic conductivity in the one-dimensional XXZ chain. In the same way as metals [125, 142, 143], ballistic conductivity is defined as:

$$D_{m,n} > 0. \tag{B.1}$$

On the other hand, diffusive conductivity is defined as:

$$D_{m,n} = 0. \tag{B.2}$$

Ballistic transport is expected in the system with conserved current J_n:

$$[J_n, \mathcal{H}] = 0, \tag{B.3}$$

and in other cases ballistic transports are basically not expected. In the XXZ one dimensional magnets, it is shown that

$$[J_{\mathrm{e}}, \mathcal{H}] = 0, \tag{B.4}$$

and

$$[J_{\mathrm{s}}, \mathcal{H}] = 0, \tag{B.5}$$

only for XY magnets. Therefore, $D_{2,2} > 0$ is expected for the XXZ magnets. For XY magnets, $D_{n,m} > 0$ is expected for $n, m = 1, 2$.

However, Zotos *et al.* [144] showed the possibility of ballistic transports with some help of conserved quantity by using Mazur inequality [145]. Here, we divide j_n into diagonal $j_{n,0}$ and off-diagonal part $j_{n,1}$ [69]. Suppose there are orthogonalized conserved quantities

$$[\mathcal{O}_n, \mathcal{H}] = 0, \tag{B.6}$$

and it satisfies

$$\langle \mathcal{O}_n \mathcal{O}_m \rangle = \left\langle \mathcal{O}_n^2 \right\rangle \delta_{m,n}, \tag{B.7}$$

and we obtain

$$j_{n,0} = \sum_m \mathcal{O}_m \frac{\langle j_{n,0} \mathcal{O}_m \rangle}{\langle \mathcal{O}_m^2 \rangle}, \tag{B.8}$$

where the summation is for all the conserved quantities.

Then we obtain

$$D_{i,j} = \frac{1}{T} \sum_m \frac{\langle j_{i,0} \mathcal{O}_m \rangle \langle j_{j,0} \mathcal{O}_m \rangle}{\langle \mathcal{O}_m^2 \rangle} \tag{B.9}$$

by inserting Eq. (B.8) to Eq. (3.132) [69, 146]. We now see from Eq. (B.9) that Drude weight and conserved quantity is related to each other.

The equation has a lower limit which called Mazur inequality [144, 145]:

$$D_{i,j} = \frac{1}{T} \sum_m \frac{\langle j_{i,0} \mathcal{O}_m \rangle \langle j_{j,0} \mathcal{O}_m \rangle}{\langle \mathcal{O}_m^2 \rangle} \geq \frac{1}{T} \frac{\langle j_{i,0} \mathcal{O}_n \rangle \langle j_{j,0} \mathcal{O}_n \rangle}{\langle \mathcal{O}_m^2 \rangle}. \tag{B.10}$$

Eq. (B.10) means that if one could find conserved quantity which satisfies $\langle j_{j,0} \mathcal{O}_m \rangle > 0$, ballistic conductivity is expected. It is known that there are many conserved quantity in integrable models such as in the one dimensional XXZ magnets. In other words, the ballistic conductivity is more likely to exist in integrable models than non-integrable models.

It is shown that at $h = 0$, conductivity is calculated by exact solution:

$$D_{2,2} = \frac{\pi v_s T}{3}, \tag{B.11}$$

$$D_{n,m} = \frac{\pi J \sin \gamma}{2\gamma(\pi - \gamma)}, \tag{B.12}$$

where v_{s} is the spinon velocity [68, 69]

$$\gamma = \arccos \Delta.$$

These are in good agreements with some other results of Meisner *et al*. [60, 61]. It is notable that ballistic spin conductivity is observed even under the condition when a spin current is not conserved quantity.

In SLHAFs and CLHAFs, it has been shown that Drude weights of spin conductivity, energy conductivity and off-diagonal conductivity vanish. In other words, ballistic conductivity is not observed at $T = 0$. One reason is that current operators are not conserved. The other is conserved quantities are not so many in non-integrable magnets and there are no conserved quantities which satisfies $\langle j_{j,0}\mathcal{O}_m\rangle > 0$.

Appendix C

Spin Wave Theory in Triangular Lattice Antiferromagnets

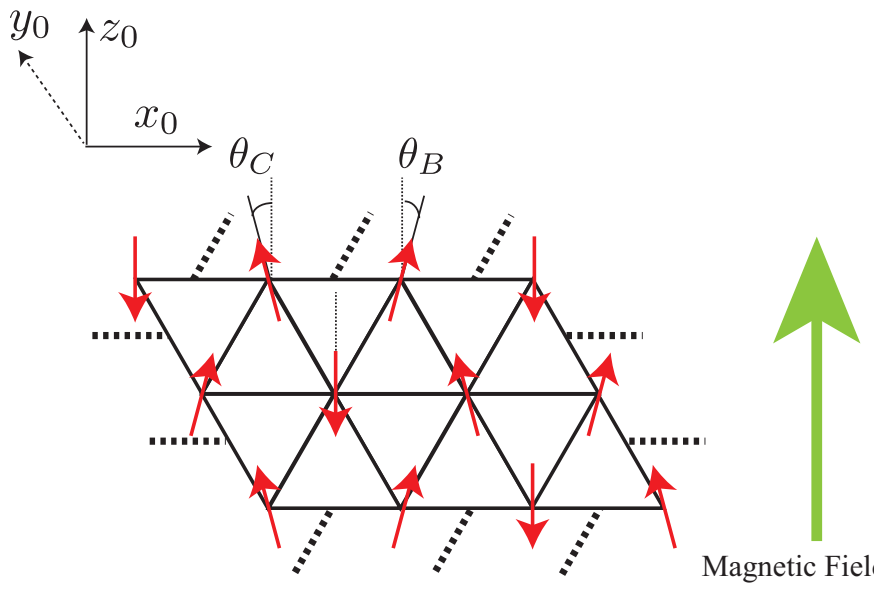

Figure C.1: Triangular lattice Heisenberg antiferromagnets (TLHAFs) in fields (along z_0 direction). TLHAFs have three sublattice 120 degree structure in zero field. In non-zero field, the spins of A-sublattice points opposite to the field directions while spins of B-and C-sublattice tilts toward the field direction. This figure is take from Ref. [14].

We show the spin wave calculations for triangular lattice Heisenberg antifer-

romagnets (TLHAFs) in fields:

$$\mathcal{H} = J \sum_{<i,j>} \left(S_i^{x_0} S_j^{x_0} + S_i^{y_0} S_j^{y_0} + S_i^{z_0} S_j^{z_0} \right) - H \sum_i S_i^{z_0}. \tag{C.1}$$

This section is along the lines of Ref. [14]. This formalism is refereed to TLHAFs in zero fields for Ref. [16], and the formalism of SLHAFs in fields for Refs. [25–27].

We suppose that spins form the structure in magnetic fields as Fig. C.1 [14]. We rotate the spin operators of laboratory frame $S_i^{\mu_0}$ $(\mu_0 = x_0, y_0, z_0)$ to that of rotated frame S_i^{μ} $(\mu = x, y, z)$:

$$\begin{pmatrix} S_i^{x_0} \\ S_i^{y_0} \\ S_i^{z_0} \end{pmatrix} = \begin{pmatrix} \cos\theta_i & 0 & \sin\theta_i \\ 0 & 1 & 0 \\ -\sin\theta_i & 0 & \cos\theta_i \end{pmatrix} \begin{pmatrix} S_i^{x} \\ S_i^{y} \\ S_i^{z} \end{pmatrix}. \tag{C.2}$$

Then, we differentiate the ground state energy and we obtain the canting angles for each sublattice $\theta_\mu (\mu = A, B, C)$:

$$\begin{aligned} \theta_A =& -\pi, \\ \theta_B =& \arccos\left[\frac{1}{2}\left(\frac{H}{3JS} + 1\right)\right], \\ \theta_C =& -\arccos\left[\frac{1}{2}\left(\frac{H}{3JS} + 1\right)\right], \end{aligned} \tag{C.3}$$

for $0 < H < 3JS$ [147]. We perform HP expansions, the Fourier transformation and the Bogoliubov transformation to diagonalize the Hamiltonian. Then, we obtain the linear spin wave spectrum:

$$\begin{aligned} \omega_{\mathbf{k}} =& \sqrt{(1 + 2\gamma_{\mathbf{k}})\left(1 + \gamma_{\mathbf{k}}\left(\frac{1}{3}\left(\frac{H}{3JS}\right)^2 - 1\right)\right)}, \\ \gamma_{\mathbf{k}} =& \frac{1}{3}\left(\cos k_x + 2\cos\frac{\sqrt{3}k_y}{2}\cos\frac{k_x}{2}\right). \end{aligned} \tag{C.4}$$

This formalism is reliable for the systems in zero field [16], because the fluctuations for all sublattices can be taken as the same. However, they are less reliable in magnetic fields since the fluctuations of A-sublattice and that of B and C are different. It means that our results of TLHAFs in fields include some wrong procedures. To overcome this problem, we need to calculate TLHAFs using three bosons like Ref. [148].

Bibliography

[1] *Spin Electronics*, ed. D. D. Awschalom, R. A. Buhrman, J. M. Daughton, S. von Molnr, and M. L. Roukes (Springer, 12 2003) 2004 ed.

[2] E. Saito and S. Murakami: *Spin Currents and Topological Insulators-Developments of Quantum Properties and Spintronics-(Frontier of Physics from Fundamental Law 1)* (Kyoritsu Shuppan Co., Ltd., 2 2014).

[3] G. D. Mahan: *Many-Particle Physics* (Plenum Press, New York, 2000) 3rd ed., p. 160.

[4] C. Kittel: *Introduction to Solid State Physics* (Wiley, 11 2004) 8 ed.

[5] N. David, C. University, and N. W. Ashcroft: *Solid State Physics* (Cengage, 12 2003) 1 ed.

[6] K. Kubo: BusseiKenkyu(Kyoto) **75** (2000) 175.

[7] K. Kubo and H. Tanaka: *Jisei I* (Asakura Publishing Co., Ltd., 2008) 2 ed., pp. 120–130.

[8] C. G. Shull and J. S. Smart: Phys. Rev. **76** (1949) 1256.

[9] J. Friedel: Phys. Today **54** (2001) 88.

[10] P. A. Lee: Science **321** (2008) 1306.

[11] N. S. Headings, S. M. Hayden, R. Coldea, and T. G. Perring: Phys. Rev. Lett. **105** (2010) 247001.

[12] A. V. Syromyatnikov: J Phys : Condens Matter **22** (2010) 216003.

[13] T. Oguchi: *Statistical Theory of Magnets (Physics book selection(12))* (Shokabo Co., Ltd., 11 1970).

[14] Y. Kubo: Bussei Kenkyu (Kyoto) **3** (2014) 033601.

[15] *Frustrated Spin Systems*, ed. H. T. Diep (World Scientific Pub Co Inc, 9 2013) 2 ed.

[16] A. L. Chernyshev and M. E. Zhitomirsky: Phys. Rev. B **79** (2009) 144416.

[17] S. J. Miyake: J. Phys. Soc. Jpn. **61** (1992) 983.

[18] A. V. Chubukov, S. Sachdev, and T. Senthil: J. Phys.: Condens. Matter **6** (1994) 8891.

[19] T. Jolicoeur and J. C. Le Guillou: Phys. Rev. B **40** (1989) 2727.

[20] J. Oh, M. D. Le, J. Jeong, J.-h. Lee, H. Woo, W.-Y. Song, T. G. Perring, W. J. L. Buyers, S.-W. Cheong, and J.-G. Park: Phys. Rev. Lett. **111** (2013) 257202.

[21] J. Ma, Y. Kamiya, T. Hong, H. B. Cao, G. Ehlers, W. Tian, C. D. Batista, Z. L. Dun, H. D. Zhou, and M. Matsuda: Phys. Rev. Lett. **116** (2016) 087201.

[22] S. Toth, B. Lake, K. Hradil, T. Guidi, K. C. Rule, M. B. Stone, and A. T. M. N. Islam: Phys. Rev. Lett. **109** (2012) 127203.

[23] D. Wulferding, K.-Y. Choi, P. Lemmens, A. N. Ponomaryov, J. van Tol, A. T. M. N. Islam, S. Toth, and B. Lake: J. Phys.: Condens. Matter **24** (2012) 435604.

[24] T. Ono, K. Matan, Y. Nambu, T. J. Sato, K. Katayama, S. Hirata, and H. Tanaka: J. Phys. Soc. Jpn. **83** (2014) 043701.

[25] M. E. Zhitomirsky and T. Nikuni: Phys. Rev. B **57** (1998) 5013.

[26] M. E. Zhitomirsky and A. L. Chernyshev: Phys. Rev. Lett. **82** (1999) 4536.

[27] M. Mourigal, M. E. Zhitomirsky, and A. L. Chernyshev: Phys. Rev. B **82** (2010) 144402.

[28] W. T. Fuhrman, M. Mourigal, M. E. Zhitomirsky, and A. L. Chernyshev: Phys. Rev. B **85** (2012) 184405.

[29] L. Balents: Nature **464** (2010) 199.

[30] B. J. Powell and R. H. McKenzie: Rep. Prog. Phys. **74** (2011) 056501.

[31] A. V. Chubukov and O. A. Starykh: Phys. Rev. Lett. **110** (2013) 217210.

[32] O. A. Starykh: Reports on Progress in Physics **78** (2015) 052502.

[33] S. Nishimoto, N. Shibata, and C. Hotta: Nat. Commun. **4** (2013) 2287.

[34] M. E. Zhitomirsky and H. Tsunetsugu: EPL (Europhysics Letters) **92** (2010) 37001.

[35] T. Ono, H. Tanaka, Y. Shirata, A. Matsuo, K. Kindo, F. Ishikawa, O. Kolomiyets, H. Mitamura, T. Goto, H. Nakano, N. A. Fortune, S. T. Hannahs, Y. Yoshida, and Y. Takano: J. Phys. Conf. Ser. **302** (2011) 012003.

[36] N. A. Fortune, S. T. Hannahs, Y. Yoshida, T. E. Sherline, T. Ono, H. Tanaka, and Y. Takano: Phys. Rev. Lett. **102** (2009) 257201.

[37] M. Kenzelmann, R. Coldea, D. A. Tennant, D. Visser, M. Hofmann, P. Smeibidl, and Z. Tylczynski: Phys. Rev. B **65** (2002) 144432.

[38] O. Breunig, M. Garst, A. Rosch, E. Sela, B. Buldmann, P. Becker, L. Bohatý, R. Müller, and T. Lorenz: Phys. Rev. B **91** (2015) 024423.

[39] R. Coldea, D. A. Tennant, K. Habicht, P. Smeibidl, C. Wolters, and Z. Tylczynski: Phys. Rev. Lett. **88** (2002) 137203.

[40] M. Y. Veillette, J. T. Chalker, and R. Coldea: Phys. Rev. B **71** (2005) 214426.

[41] C. Hotta, S. Nishimoto, and N. Shibata: Phys. Rev. B **87** (2013) 115128.

[42] A. Lüscher and A. M. Läuchli: Phys. Rev. B **79** (2009) 195102.

[43] O. F. Syljuåsen: Phys. Rev. B **78** (2008) 180413.

[44] Y. Kubo and S. Kurihara: Phys. Rev. B **90** (2014) 014421.

[45] Y. Kubo and S. Kurihara: J. Phys. Conf. Ser. **592** (2015) 012116.

[46] W. Kohn: Phys. Rev. Lett. **2** (1959) 393.

[47] D. A. Krueger: Phys. Rev. B **3** (1971) 2348.

[48] D. L. Huber, J. S. Semura, and C. G. Windsor: Phys. Rev. **186** (1969) 534.

[49] D. A. Krueger: Phys. Rev. B **3** (1971) 2348.

[50] R. L. Douglass: Phys. Rev. **129** (1963) 1132.

[51] C. Hess, H. ElHaes, A. Waske, B. Büchner, C. Sekar, G. Krabbes, F. Heidrich-Meisner, and W. Brenig: Phys. Rev. Lett. **98** (2007) 027201.

[52] A. V. Sologubenko, K. Giannò, H. R. Ott, A. Vietkine, and A. Revcolevschi: Phys. Rev. B **64** (2001) 054412.

[53] C. Hess, C. Baumann, U. Ammerahl, B. Büchner, F. Heidrich-Meisner, W. Brenig, and A. Revcolevschi: Phys. Rev. B **64** (2001) 184305.

[54] X. F. Sun, X. G. Liu, L. M. Chen, Z. Y. Zhao, and X. Zhao: J. Appl. Phys. **113** (2013).

[55] K. Kudo, S. Ishikawa, T. Noji, T. Adachi, Y. Koike, K. Maki, S. Tsuji, and K. ichi Kumagai: J. Phys. Soc. Jpn. **70** (2001) 437.

[56] C. Hess: Eur. Phys. J. Special Topics **151** (2007) 73.

[57] A. V. Sologubenko, K. Giannó, H. R. Ott, U. Ammerahl, and A. Revcolevschi: Phys. Rev. Lett. **84** (2000) 2714.

[58] F. Heidrich-Meisner, A. Honecker, and W. Brenig: Eur. Phys. J. Special Topics **151** 135.

[59] F. Heidrich-Meisner: Physica B **378,379,380** (2006) 299 .

[60] F. Heidrich-Meisner, A. Honecker, and W. Brenig: Phys. Rev. B **71** (2005) 184415.

[61] F. Heidrich-Meisner: Dr. Thesis, Technischen Universität Carolo-Wilhelmina (2005).

[62] S. Langer, R. Darradi, F. Heidrich-Meisner, and W. Brenig: Phys. Rev. B **82** (2010) 104424.

[63] F. Heidrich-Meisner, A. Honecker, D. C. Cabra, and W. Brenig: Phys. Rev. B **66** (2002) 140406.

[64] J. V. Alvarez and C. Gros: Phys. Rev. B **66** (2002) 094403.

[65] K. Louis and C. Gros: Phys. Rev. B **67** (2003) 224410.

[66] J. V. Alvarez and C. Gros: Phys. Rev. Lett. **88** (2002) 077203.

[67] S. Furukawa, D. Ikeda, and K. Sakai: Physica B **74** (2005) 3241.

[68] A. Klmper and K. Sakai: J. Phys. A: Math. Gen. **35** (2002) 2173.

[69] K. Sakai: Bussei Kenkyu (Kyoto) **87** (2006) 214.

[70] R. J. B. C. Sales and D. Mandrus: Proceedings of the 27th International Thermal Conductivity Conference And the 15th International Thermal Expansion Symposium (2004) 65.

[71] B. C. Sales, M. D. Lumsden, S. E. Nagler, D. Mandrus, and R. Jin: Phys. Rev. Lett. **88** (2002) 095901.

[72] R. Jin, Y. Onose, Y. Tokura, D. Mandrus, P. Dai, and B. C. Sales: Phys. Rev. Lett. **91** (2003) 146601.

[73] S. Y. Li, L. Taillefer, C. H. Wang, and X. H. Chen: Phys. Rev. Lett. **95** (2005) 156603.

[74] C. Hess, B. Büchner, U. Ammerahl, L. Colonescu, F. Heidrich-Meisner, W. Brenig, and A. Revcolevschi: Phys. Rev. Lett. **90** (2003) 197002.

[75] X. F. Sun, I. Tsukada, T. Suzuki, S. Komiya, and Y. Ando: Phys. Rev. B **72** (2005) 104501.

[76] X. M. Wang, Z. Y. Zhao, C. Fan, X. G. Liu, Q. J. Li, F. B. Zhang, L. M. Chen, X. Zhao, and X. F. Sun: Phys. Rev. B **86** (2012) 174413.

[77] X. M. Wang, C. Fan, Z. Y. Zhao, W. Tao, X. G. Liu, W. P. Ke, X. Zhao, and X. F. Sun: Phys. Rev. B **82** (2010) 094405.

[78] F. B. Zhang, Q. J. Li, Z. Y. Zhao, C. Fan, S. J. Li, X. G. Liu, X. Zhao, and X. F. Sun: Phys. Rev. B **89** (2014) 094403.

[79] S. J. Li, Z. Y. Zhao, C. Fan, B. Tong, F. B. Zhang, J. Shi, J. C. Wu, X. G. Liu, H. D. Zhou, X. Zhao, and X. F. Sun: Phys. Rev. B **92** (2015) 094408.

[80] C. Fan, Z. Y. Zhao, H. D. Zhou, X. M. Wang, Q. J. Li, F. B. Zhang, X. Zhao, and X. F. Sun: Phys. Rev. B **87** (2013) 144404.

[81] M. Hirschberger, J. W. Krizan, R. J. Cava, and N. P. Ong: Science **348** (2015) 106.

[82] S. Scharffe, G. Kolland, M. Valldor, V. Cho, J. Welter, and T. Lorenz: J. Magn. Magn. Mater. **383** (2015) 83 .

[83] Y. Tokiwa, T. Yamashita, M. Udagawa, S. Kittaka, T. Sakakibara, D. Terazawa, Y. Shimoyama, T. Terashima, Y. Yasui, T. Shibauchi, and Y. Matsuda: Nat. Commun. **7** (2016) 10807.

[84] M. Yamashita, N. Nakata, Y. Kasahara, T. Sasaki, N. Yoneyama, N. Kobayashi, S. Fujimoto, T. Shibauchi, and Y. Matsuda: Nat. Phys. **5** (2009) 44.

[85] M. Yamashita, N. Nakata, Y. Senshu, M. Nagata, H. M. Yamamoto, R. Kato, T. Shibauchi, and Y. Matsuda: Science **328** (2010) 1246.

[86] M. Yamashita, T. Shibauchi, and Y. Matsuda: Chem. Phys. Chem. **13** (2012) 74.

[87] M. Sentef, M. Kollar, and A. P. Kampf: Phys. Rev. B **75** (2007) 214403.

[88] M. A. Sentef: Dr. Thesis, University of Augsburg (2006).

[89] A. S. T. Pires and L. S. Lima: Phys. Rev. B **79** (2009) 064401.

[90] Z. Chen, T. Datta, and D.-X. Yao: Eur. Phys. J. B **86** (2013) 63.

[91] L. P. Kadanoff and P. C. Martin: Annals of Physics **24** (1963) 419 .

[92] F. Schütz, P. Kopietz, and M. Kollar: Eur. Phys. J. B **41** (2004) 557.

[93] S. Maekawa, S. O. Valenzuela, E. Saitoh, and T. Kimura: *Spin Current (Semiconductor Science and Technology)* (Oxford Univ Pr (Txt), 9 2012), pp. 136–148.

[94] Y. Kubo and S. Kurihara: J. Phys. Soc. Jpn. **82** (2013) 113601.

[95] Y. Kubo and S. Kurihara: In preparation .

[96] M. E. Zhitomirsky and A. L. Chernyshev: Rev. Mod. Phys. **85** (2013) 219.

[97] M. Zhitomirsky and T. Nikuni: Physica B **241 242 243** (1997) 573. Proceedings of the International Conference on Neutron Scattering.

[98] W. Zheng, J. O. Fjærestad, R. R. P. Singh, R. H. McKenzie, and R. Coldea: Phys. Rev. B **74** (2006) 224420.

[99] A. L. Chernyshev and M. E. Zhitomirsky: Phys. Rev. B **79** (2009) 174402.

[100] T. Masuda, S. Kitaoka, S. Takamizawa, N. Metoki, K. Kaneko, K. C. Rule, K. Kiefer, H. Manaka, and H. Nojiri: Phys. Rev. B **81** (2010) 100402.

[101] H. S. Koichi Osano and Y. Endoh: Prog. Thor. Phys. **67** (1982) 995.

[102] I. U. Heilmann, J. K. Kjems, Y. Endoh, G. F. Reiter, G. Shirane, and R. J. Birgeneau: Phys. Rev. B **24** (1981) 3939.

[103] R. Coldea, S. M. Hayden, G. Aeppli, T. G. Perring, C. D. Frost, T. E. Mason, S.-W. Cheong, and Z. Fisk: Phys. Rev. Lett. **86** (2001) 5377.

[104] K. W. Plumb, A. T. Savici, G. E. Granroth, F. C. Chou, and Y.-J. Kim: Phys. Rev. B **89** (2014) 180410.

[105] H. M. Rønnow, D. F. McMorrow, R. Coldea, A. Harrison, I. D. Youngson, T. G. Perring, G. Aeppli, O. Syljuåsen, K. Lefmann, and C. Rischel: Phys. Rev. Lett. **87** (2001) 037202.

[106] L. P. Pitaevskii and E. Lifshitz: *Statistical Physics, Part 2: Volume 9 (Pt 2)* (Butterworth-Heinemann, 1 1980) 1 ed.

[107] R. A. Cowley and A. D. B. Woods: Can. J. Phys. **49** (1971) 177.

[108] N. Tsyrulin, T. Pardini, R. R. P. Singh, F. Xiao, P. Link, A. Schneidewind, A. Hiess, C. P. Landee, M. M. Turnbull, and M. Kenzelmann: Phys. Rev. Lett. **102** (2009) 197201.

[109] D. S. Greywall: Phys. Rev. B **18** (1978) 2127.

[110] V. Zapf, M. Jaime, and C. D. Batista: Rev. Mod. Phys. **86** (2014) 563.

[111] T. Nikuni and H. Shiba: J. Phys. Soc. Jpn. **64** (1995) 3471.

[112] E. Batyev: Zh. Eksp. Teor. Fiz **62** (1985) 308.

[113] P. A. Goddard, J. Singleton, P. Sengupta, R. D. McDonald, T. Lancaster, S. J. Blundell, F. L. Pratt, S. Cox, N. Harrison, J. L. Manson, H. I. Southerland, and J. A. Schlueter: New J. Phys. **10** (2008) 083025.

[114] V. Selmani, C. P. Landee, M. M. Turnbull, J. L. Wikaira, and F. Xiao: Inorg. Chem. Commun. **13** (2010) 1399 .

[115] P. A. Maksimov and A. L. Chernyshev: Phys. Rev. B **93** (2016) 014418.

[116] G. S. Dixon: Phys. Rev. B **21** (1980) 2851.

[117] K. Kawasaki: Prog. of Theor. Phys. **29** (1963) 801.

[118] E. Shimshoni, N. Andrei, and A. Rosch: Phys. Rev. B **68** (2003) 104401.

[119] S. Maekawa, S. O. Valenzuela, E. Saitoh, and T. Kimura: *Spin Current (Semiconductor Science and Technology)* (Oxford Univ Pr (Txt), 9 2012).

[120] *Recent Advances in Magnetic Insulators - From Spintronics to Microwave Applications, Volume 64 (Solid State Physics)*, ed. M. Wu and A. Hoffmann (Academic Press, 11 2013) 1 ed.

[121] K. Uchida, J. A. H. Xiao, O. J, S. Takahashi, J. Ieda, T. Ota, Y. Kajiwara, H. Umezawa, H. Kawai, G. E. W. Bauer, M. S, and E. Saitoh: Nat. Mater. **9** (2010) 894.

[122] E. S. Gerrit E. W. Bauer and B. J. van Wees: Nat. Mater. **11** (2012) 391.

[123] S. Maekawa, H. Adachi, K. ichi Uchida, J. Ieda, and E. Saitoh: J. Phys. Soc. Jpn. **82** (2013) 102002.

[124] T. Einarsson and H. J. Schulz: Phys. Rev. B **51** (1995) 6151.

[125] D. J. Scalapino, S. R. White, and S. Zhang: Phys. Rev. B **47** (1993) 7995.

[126] B. S. Shastry and B. Sutherland: Phys. Rev. Lett. **65** (1990) 243.

[127] E. Dagotto: Rev. Mod. Phys. **66** (1994) 763.

[128] P. F. Maldague: Phys. Rev. B **16** (1977) 2437.

[129] P. M. Chaikin and T. C. Lubensky: *Principles of Condensed Matter Physics* (Cambridge University Press, 9 2000) reprint ed.

[130] S. R. de Groot, P. Mazur, and J. T. G. Overbeek: J. Chem. Phys. **20** (1952) 1825.

[131] J. M. Luttinger: Phys. Rev. **135** (1964) A1505.

[132] P. Mazur and S. de Groot: Physica **19** (1953) 961 .

[133] K. Nishikawa and H. Mori: in*Stastical Physics*, ed. K. Asakura (Asakura-Butsurigaku-Taikei 10. Asakura Publishing Co., Ltd., 2000), Asakura-Butsurigaku-Taikei 10.

[134] J. Shan, F. K. Dejene, J. C. Leutenantsmeyer, J. Flipse, M. Münzenberg, and B. J. van Wees: Phys. Rev. B **92** (2015) 020414.

[135] S. Geprägs, A. Kehlberger, F. D. Coletta, Z. Qiu, E.-J. Guo, T. Schulz, C. Mix, S. Meyer, A. Kamra, M. Althammer, H. Huebl, G. Jakob, Y. Ohnuma, H. Adachi, J. Barker, S. Maekawa, G. E. W. Bauer, E. Saitoh, R. Gross, S. T. B. Goennenwein, and M. Kläui: Nat. Commun. **7** (2016) 10452.

[136] S. M. Wu, W. Zhang, A. KC, P. Borisov, J. E. Pearson, J. S. Jiang, D. Lederman, A. Hoffmann, and A. Bhattacharya: Phys. Rev. Lett. **116** (2016) 097204.

[137] K. Kudo and T. Deguchi: J. Phys. Soc. Jpn. **74** (2005) 1992.

[138] R. Kubo: J. Phys. Soc. Jpn. **12** (1957) 570.

[139] R. Kubo, H. Hasegawa, and N. Hashitsume: J. Phys. Soc. Jpn. **14** (1959) 56.

[140] B. S. Shastry: Phys. Rev. B **73** (2006) 085117.

[141] F. Naef and X. Zotos: J. Phys.: Condens. Matter **10** (1998) L183.

[142] W. Kohn: Phys. Rev. **133** (1964) A171.

[143] D. J. Scalapino, S. R. White, and S. C. Zhang: Phys. Rev. Lett. **68** (1992) 2830.

[144] X. Zotos, F. Naef, and P. Prelovsek: Phys. Rev. B **55** (1997) 11029.

[145] P. Mazur: Physica **43** (1969) 533 .

[146] M. Suzuki: Physica **51** (1971) 277 .

[147] H. Kawamura: J. Phys. Soc. Jpn. **53** (1984) 2452.

[148] T. Jolicoeur and J. C. Le Guillou: Phys. Rev. B **40** (1989) 2727.

List of Publications

1. ◯ Yurika Kubo and Susumu Kurihara, Tunable rotons in square-lattice antiferromagnets under strong magnetic fields, Physical Review B 90(1), 014421(1)-(8), 17th, July, 2014.

2. ◯ Yurika Kubo and Susumu Kurihara, Spin Conductivity in Two-Dimensional Non-Collinear Antiferromagnets, Journal of the Physical Society of Japan 82(11), 113601(1)-(4), 4th, October, 2013.